

Fundamental Mechanisms and Biological Applications of DNA-Mediated Charge Transport

Thesis by
Katherine Emily Augustyn

In Partial Fulfillment
of the Requirements
for the Degree of Doctor of Philosophy

California Institute of Technology
Pasadena, California

2007

(Defended May 22, 2007)

© 2007

Katherine Emily Augustyn

All Rights Reserved

Acknowledgements

The past five years have marked a period of intense learning coupled with frustrations as well as successes. I am indebted to my friends and family for supporting me through both the hard times and the sporadic moments of bliss. First and foremost, I must thank my advisor, Professor Jacqueline K. Barton, for providing me with a seemingly endless array of exciting and challenging projects. As I once said during Annual Symposium, “There was never a dull moment” and this cannot be emphasized more. In my tenure in the Barton group, I have learned a countless number of techniques and can undoubtedly proclaim myself to be an official molecularbiophysicalinorganic chemist. Moreover, Jackie has been extremely enthusiastic about my research, and I will never forget the day when she told me “I couldn’t sleep last night because I was trying to come up with a mechanism for your reaction.” This clearly underscores her fervor for this research. Jackie has always been incredibly supportive even throughout my initial struggles with the infamous tethered-quencher project. I appreciate her willingness to allow me to explore other research areas so that, in the end, I could be a well-rounded scientist, versed in a variety of techniques.

A great number of Caltech faculty and staff contributed to my growth and well being here at Caltech. Mo Renta has been a tremendous help in running the group. I will miss her no-nonsense sharp sense of humor expressed often in lunch conversations ranging from politics, to diets, to cats. Back in the day, when I first joined the Barton group as a clueless first year, Professor Eric Stemp was a kind mentor whose astute and didactic nature guided me through the world of nanosecond transient absorption and the

enigma of graduate school. Always willing to spend extra time to elucidate abstruse concepts, Eric is truly blessed with a gift for teaching. I will miss our vibrant discussions about electron transfer and deliciously gossipy Barton-group anecdotes over lunch at CPK.

I was incredibly lucky to have such a wonderful thesis committee. Professor Harry Gray is a caring and easy-going charge transfer connoisseur, whose presence always seemed to dampen the stress level and assuage my fear during candidacy and at the proposal defense. I could not have been more relieved when I was told my proposals were so great I could spend the ensuing hour questioning my committee instead! I would also like to thank Professor Patrick Collier and Professor Dianne Newman for reading my proposals and for their insightful comments concerning my research and other scientific endeavors.

Throughout this graduate school journey, I have been fortunate to meet many wonderful people, many of whom I hope to maintain friendships with into the future. I would like to thank Maria DeRosa for being the best roommate ever, as well as a wonderful friend and mentor. How I would have survived my second and third year without her shoulder to cry on, is beyond comprehension. Paul Lee was, and continues to be, a wonderful friend, and our numerous adventures including concocting epicurean delights, laughing at Tyra and predicting who will be eliminated next on the latest episode of ANTM, enjoying soft serve with cloves, and learning very useful Korean phrases bring back fond memories.

Many long days (and nights) in lab were ameliorated by the presence of my intelligent and witty co-workers. Eddie Merino, my biochemist friend, has been an entertaining source of knowledge in science and politics. The north side of Noyes would be a very dull place indeed, if it were not for Eddie's jovial demeanor. Perhaps he thinks I am a crazy health nut but I will always remember when he proclaimed "See, I'm eating healthy, I just had an apple with my pie." He is learning well. I owe tremendous thanks to Anne Petitjean and Eylon Yavin who helped me through the perils of organic synthesis at the beginning when operating the rotovap posed a serious challenge. Now both professors, in Canada and Israel respectively, I know they will be fabulous mentors for their own students. Tadao Takada, Mi Hee Lim, Donato Ceres, Fangwei Shao, and Joey Genereux have also been wonderful lab-mates who have made this arduous experience all the more bearable.

I also cannot forget the "Settlers" crew, including Eylon, Jens Brunner, and Habib Ahmad. Thanks for initiating me into the world of mutton and terrorists (Don't worry Jens, I will always build at the port). Evelyn Khamou, a summer student, was also a source of amusement throughout my time in the Barton group. Thanks for making flavin ice cream, introducing me to the world of Zankou Chicken (mmmm crispy bird), and frequent trips to the Coffee Bean.

Outside of the lab, I thank my running buddies, Jen and Christian Franck, for being wonderful friends and pleasant distractions from the daily research grind. I will miss our annual 5K Tiger Run and delicious dinners. Christian, although I still scoff at your artichoke aversion, you make an awesome choux paste. Let's have a swan-making party after we finish that 10K we're always talking about. Lisa Lee is a deeply caring and

wonderful person who I am so glad to have met. From introducing me to me to the world of LA fashion to making jam and truffles, I truly enjoyed all the excursions and activities we pursued over the years.

I want to thank my food buddies, including Paul, Lisa, Robert Bao, and Jana Monji for nourishment throughout five years of research debauchery. I have come to discover the culinary secrets of the Los Angeles area, and even though some say that Berkeley is considered the “gourmet ghetto” I will very much miss the delightful ethnic cuisines so readily available in SoCal.

Dianah Barrett, although not in Pasadena, has continued to be a caring and empathetic friend. I remember senior year of college when we truly doubted we would ever be accepted to graduate school. It has been a whirlwind five years of insanity, but we made it, and I will always appreciate how we always seemed to share the same graduate school trials and tribulations, even at opposite ends of the continent.

Finally I want to thank my parents, who above all have put up with me for the past five years. You have been so incredibly supportive and understanding; there is absolutely no way that I would have survived graduate school without your caring and love. I regret that I never discovered the “magic fluid” for the future solar power plants (hey, synthetic organic chemistry is not my forte), and I know you will not miss the long phone calls when I was convinced that quitting research and working at Starbucks was the only option, but thanks to your support, I can proudly say I will be the first Augustyn to earn a PhD, and that, I should add, makes it all worthwhile.

To the Barton group members, past and present, perhaps you will miss my myriad edible surprises. To placate your taste buds in my absence, here is my secret scone recipe.

Experimental

2 cups of all purpose flour (Gold Medal) and 1 tablespoon of baking powder (Clabber Girl) were combined by gentle mixing with a wooden spoon in a large bowl. 1/2 cup (1 stick) chilled unsalted butter (Challenge) was cut into 1 tablespoon chunks and incorporated into the flour mixture until a grainy consistency, reminiscent of pebbles, was reached. In a separate bowl, enough milk (2% w/v fat content, Trader Joe's) was added to one extra-large beaten egg (Safeway) to reach a final volume of 2/3 cup. The egg and milk mixture was then added to the flour mixture while stirring constantly with a wooden spoon, resulting in the formation of a sticky dough. At this point, a generous handful of cranberries, chocolate chips, raisins, or currents were added and incorporated into the mixture. The dough was divided into two balls and rolled out on a floured surface to form rounds approximately 5 inches in diameter. Each round was then cut into 6 triangles using a paring knife (Kitchenaid) and placed on a well-greased baking sheet. The triangles were brushed with an egg wash (prepared by beating 1 egg with 1 tablespoon of water or milk) and sprinkled with granulated sugar (C and H). The dough triangles were heated in a conventional oven set at to 425 °F (Frigidaire) for 10-12 minutes until they doubled in volume and reached a light-brown color. The scones were best enjoyed immediately after preparation, but could be stored in a freezer for up to 1 month in an airtight zip-lock bag.

Abstract

The π -stacked array of heterocyclic aromatic DNA base pairs provides an intriguing medium for facilitating the transport of migrating charges. The mechanism of hole transport through this dynamic molecule has been extensively investigated using a wide range of techniques. In particular, our group has taken advantage of the octahedral metal complexes of rhodium (III) and ruthenium (II) to probe charge transport reactions through DNA at long range. These intercalating photooxidants, which are extremely well coupled to the DNA π -stack, can provide us with mechanistic information through a variety of biochemical and spectroscopic techniques. Here we continue to investigate the mechanism of DNA-mediated charge transport on fast time scales using a variety of hole traps and photooxidants and examine this interesting chemistry in a biological context.

DNA-mediated charge transport across three different adenine tracts lengths is monitored using a probe interior to the bridge, N_6 -cyclopropyladenine, ^{CP}A . Upon oxidation, the cyclopropylamine-substituted deoxynucleoside decomposes rapidly, and the efficiency of decomposition can be used as a kinetically fast measurement of hole occupancy. This trap, incorporated serially across the bridge, can be oxidized by a distally bound photooxidant, $[Rh(\phi)_2(bpy')]^{3+}$ ($\phi = 9,10$ -phenanthrenequinone diimine) without significant attenuation in yield over a distance of 5 nm. These results are consistent with complete delocalization across the DNA bridge.

Photooxidation of N_2 -cyclopropylguanine, ^{CP}G , within duplex DNA is used to probe DNA charge transport reactions initiated by the covalently bound photooxidants, $[Rh(\phi)_2(bpy')]^{3+}$ and anthraquinone. Duplexes containing the photooxidant separated from the ^{CP}G trap by an increasing number of intervening bases are examined in order to

probe DNA charge transport reactions with this kinetically fast hole trap as a function of distance and sequence. Charge transport events through sequences containing various length adenine tracts as well as most mixed sequence bridges do not simply decay exponentially nor geometrically as a function of distance. In particular, for variable-length A-tracts, decomposition decreases in a periodic fashion with increasing distance between the photooxidant and the trap; the period is ~4-5 base pairs. Results obtained from charge injection studies using 2-aminopurine as a fluorescent probe have shown a similar periodic distance dependence. These periodicities are not observed in measurements of oxidative DNA damage using double guanine sites as a slow, irreversible hole trap. Thus, CT through DNA must be probed on multiple time scales to provide mechanistic information. These results are consistent with our model for DNA CT through transient delocalized DNA domains defined by sequence-dependent base pair dynamics.

While mechanistic investigations are critical for a fundamental understanding of how charges migrate through DNA, it is important to consider the biological consequences of this process. A biological role for DNA-mediated CT has been investigated in the context of the transcription factor, p53, a tumor suppressor protein involved in myriad cellular pathways such as apoptosis and growth arrest. DNA assemblies containing an anthraquinone photooxidant tethered to the 5' end of sequences containing p53 binding sites were constructed to examine the binding affinity as a function of photooxidation. We demonstrate that through photoinduced DNA-mediated CT, the p53 protein becomes oxidized and exhibits differential binding for various promoter sequence including *Gadd45*, *p21*, and *Mdm2*. Additionally, insertion of a

mismatch intervening between the photooxidant and the p53 binding site serves to attenuate this change in binding affinity associated with photooxidation. MALDI-TOF mass spectrometric analysis of p53 tryptic digests following irradiation of the DNA-bound protein provides further evidence that a chemical change occurs, consistent with oxidation of a cysteine residue in the DNA binding domain.

Dipyridophenazine complexes of ruthenium (II) have been used extensively to spectroscopically investigate DNA-mediated charge transport. A novel tris heteroleptic dipyridophenazine complex of ruthenium (II), $[\{\text{Ru}(\text{phen})(\text{dppz})(\text{bpy}'\text{-his})\}\{\text{Ru}(\text{NH}_3)_5\}]^{5+}$, containing a covalently tethered ruthenium pentaammine quencher coordinated through a bridging histidine has been synthesized and characterized spectroscopically and biochemically in a DNA environment and in organic solvent. Capable of undergoing intramolecular photoinduced electron transfer, the steady-state and time-resolved luminescence measurements indicate that the tethered-quencher complex is quenched relative to the parent complexes $[\text{Ru}(\text{phen})(\text{dppz})(\text{bpy}')^{2+}$ and $[\text{Ru}(\text{phen})(\text{dppz})(\text{bpy}'\text{-his})]^{2+}$ in DNA and acetonitrile. Intercalated into guanine-containing DNA, $[\{\text{Ru}(\text{phen})(\text{dppz})(\text{bpy}'\text{-his})\}\{\text{Ru}(\text{NH}_3)_5\}]^{5+}$, upon excitation and intramolecular quenching, is capable of injecting charge into the duplex as evidenced by EPR detection of guanine radicals. DNA-mediated charge transport is also evidenced using a kinetically fast cyclopropylamine-substituted base as a hole trap that undergoes irreversible oxidative ring opening on the picosecond time scale. Guanine oxidation is not observed in measurements using guanine radical as a slow, irreversible hole trap indicating that back electron transfer reactions are competitive with hole injection into the duplex. Moreover, transient absorption measurements reveal a novel photophysical

reaction pathway for $[\{\text{Ru}(\text{phen})(\text{dppz})(\text{bpy}'\text{-his})\}\{\text{Ru}(\text{NH}_3)_5\}]^{5+}$ in the presence of DNA, competitive with the intermolecular flash-quench process. These results illustrate the remarkable redox chemistry occurring within a bimolecular ruthenium complex intercalated in duplex DNA.

Table of Contents

Acknowledgements	iii
Abstract	viii
Table of Contents	xii
List of Figures and Tables	xvii

Chapter 1: Charge Transport through the DNA Helix

1.1	The DNA π -stack serves as an effective conduit for charge transport	2
1.2	Probes of charge transport	6
1.2.1	Organic photooxidants and modified bases as probes of DNA-mediated charge transport	6
1.2.2	Metallointercalators as probes of DNA-mediated charge transport	7
1.3	Early photophysical studies	13
1.4	Biochemical studies of long-range oxidative charge transport	15
1.4.1	$[\text{Rh}(\text{phi})_2(\text{bpy}')]^{3+}$ and $[\text{Ru}(\text{phen})(\text{dppz})(\text{bpy}')]^{3+}$ can oxidize guanine	15
1.4.2	Distance dependence using metallointercalators	18
1.5	Ultrafast charge transport	20
1.5.1	Charge transport between two intercalators	20
1.5.2	Charge transport between an intercalator and a DNA base	21
1.5.3	Charge transport between DNA bases	21
1.5.4	Cyclopropylamine-modified bases as ultrafast hole traps	23
1.6	Spectroscopy of charge transfer intermediates	25
1.7	Sensitivity of charge transport to DNA conformation and dynamics	27
1.8	Towards a mechanistic understanding of DNA charge transport	29
1.9	Biological opportunities for DNA charge transport	31

1.10	Dissertation overview	35
1.11	References	36
Chapter 2: Distance-Independent DNA Charge Transport across an Adenine Tract		
2.1	Introduction	46
2.2	Experimental	48
2.2.1	Oligonucleotide synthesis	48
2.2.2	Photooxidation experiments	50
2.3	Results and discussion	51
2.3.1	Experimental design	51
2.3.2	Decomposition as a function of bridge position in A-tracts	55
2.3.3	Comparison with other systems	55
2.4	References	59
Chapter 3: Periodicities in DNA Charge Transport probed with <i>N</i>₂-Cyclopropylguanine, a Kinetically Fast Hole Trap		
3.1	Introduction	66
3.2	Experimental	69
3.2.1	Oligonucleotide synthesis	69
3.2.2	Photooxidation experiments	70
3.2.3	Fluorescence-quenching experiments	72
3.3	Results	73
3.3.1	Experimental design	73
3.3.2	^{CP} G decomposition as a probe of photooxidation in DNA duplexes with A-tracts	79
3.3.3	Variations in photooxidation with temperature	84
3.3.4	Photooxidation of the (AT) _n , (ATIC) _n , (AITC) _n , and (AI) _n sequences	86

3.3.5	Photooxidations with guanine as the hole trap	88
3.3.6	Fluorescence quenching of 2-aminopurine through AT-tracts	88
3.4	Discussion	91
3.4.1	Distance dependence of DNA CT through A-tracts using ^{CP} G	91
3.4.2	Conformational gating by base dynamics	92
3.4.3	Effects of base stacking on distance dependent CT	93
3.4.4	The importance of time scale in monitoring CT processes through DNA	94
3.4.5	Comparison with other DNA CT systems	96
3.4.6	Conformational gating through delocalized domains	97
3.4.7	Other theoretical predictions of periodic distance dependences	99
3.4.8	Implications of the periodic distance dependence to mechanisms for DNA-mediated CT	100
3.5	References	102

Chapter 4: A Role for DNA-Mediated Charge Transport in Regulating p53:

Oxidation of the DNA-Bound Protein from a Distance

4.1	Introduction	111
4.2	Experimental	113
4.2.1	DNA synthesis	113
4.2.2	Gel mobility shift assay	116
4.2.3	Mass spectrometry of oxidized p53	117
4.3	Results and discussion	117
4.3.1	DNA-mediated oxidation of p53 bound to a consensus sequence	117
4.3.2	DNA-mediated oxidation of p53 bound to promoter sequences	119
4.3.3	p53 oxidation observed by MALDI-TOF mass spectrometry	123
4.4	References	127

Chapter 5: Charge Separation in Ruthenium-Quencher Conjugates Bound to DNA

5.1	Introduction	132
5.2	Experimental	137
5.2.1	DNA synthesis	137
5.2.2	Synthesis and characterization of $[\text{Ru}(\text{phen})(\text{dppz})(\text{bpy}'\text{-his})]\text{Cl}_2$	138
5.2.3	Synthesis and characterization of $[\{\text{Ru}(\text{phen})(\text{dppz})(\text{bpy}'\text{-his})\}\{\text{Ru}(\text{NH}_3)_5\}]\text{Cl}_5$	139
5.2.4	Steady-state fluorescence	140
5.2.5	Electrochemistry	140
5.2.6	Irradiation experiments and gel electrophoresis	141
5.2.7	Irradiation experiments and analysis of $^{13}\text{C}/^{12}\text{C}$ ring opening	142
5.2.8	EPR spectroscopy	142
5.2.9	Laser spectroscopy	143
5.3	Results	144
5.3.1	Experimental design	144
5.3.2	Synthesis and characterization of $[\text{Ru}(\text{phen})(\text{dppz})(\text{bpy}'\text{-his})]^{2+}$ and $[\{\text{Ru}(\text{phen})(\text{dppz})(\text{bpy}'\text{-his})\}\{\text{Ru}(\text{NH}_3)_5\}]^{5+}$	146
5.3.3	Steady-state luminescence	149
5.3.4	Time-resolved emission	151
5.3.5	Electrochemistry of ruthenium complexes	154
5.3.6	Analysis of oxidative products	157
5.3.7	EPR spectroscopy	163
5.3.8	Nanosecond transient absorption	163
5.3.9	Charge effect on the transient absorption profile of $[\text{Ru}(\text{phen})(\text{dppz})(\text{bpy}'\text{-his})]^{2+}$	168
5.4	Discussion	169
5.4.1	$[\{\text{Ru}(\text{phen})(\text{dppz})(\text{bpy}'\text{-his})\}\{\text{Ru}(\text{NH}_3)_5\}]^{5+}$ is quenched relative to $[\text{Ru}(\text{phen})(\text{dppz})(\text{bpy}'\text{-his})]^{2+}$ and $[\text{Ru}(\text{phen})(\text{dppz})(\text{bpy}')]^{2+}$	169

5.4.2	$[\{\text{Ru}(\text{phen})(\text{dppz})(\text{bpy}'\text{-his})\}\{\text{Ru}(\text{NH}_3)_5\}]^{5+}$ can oxidize guanine	170
5.4.3	Transient species formed in the presence of DNA	171
5.4.4	$[\{\text{Ru}(\text{phen})(\text{dppz})(\text{bpy}'\text{-his})\}\{\text{Ru}(\text{NH}_3)_5\}]^{5+}$ forms a Ru(I)-like species in a DNA environment	173
5.4.5	Mechanistic considerations	174
5.5	References	177

List of Figures and Tables

Chapter 1: Charge Transport through the DNA Helix

Figure 1.1	Illustration of double helical DNA	3
Figure 1.2	Schematic representation of two mechanistic extremes for DNA-mediated charge transport	5
Figure 1.3	Probes used to monitor charge transport through DNA	8
Figure 1.4	Crystal structure of $\Delta\text{-}\alpha\text{-}[\text{Rh}[(\text{R,R})\text{Me}_2\text{trien}]\text{phi}]^{3+}$ intercalated into a DNA duplex	10
Figure 1.5	Flash-quench scheme for generating guanine radicals in DNA	12
Figure 1.6	Schematic representation of a doubly metallated DNA duplex used to probe charge transport in DNA	14
Figure 1.7	Schematic representation of a metallated duplex designed to probe long-range oxidative damage in DNA	17
Figure 1.8	Schematic representation of a rhodium-tethered 63 base-pair duplex containing six sets of guanine doublets	19
Figure 1.9	Cyclopropylamine-modified nucleosides used to probe hole transport through DNA on fast time scales	24
Figure 1.10	Spectroscopic investigation of DNA charge transport using the methylindole probe	26
Figure 1.11	Schematic illustration of DNA-mediated charge transport through conformationally gated domains	30
Figure 1.12	Schematic illustration of DNA-mediated charge transport in a nucleosome core particle	32
Figure 1.13	Schematic illustration depicting how redox-active DNA repair proteins use DNA-mediated charge transport to locate damage	34

Chapter 2: Distance-Independent DNA Charge Transport across an Adenine Tract

Figure 2.1	Representative HPLC chromatograms of rhodium-containing Oligonucleotides	49
Table 2.1	^{CP} A-containing DNA assemblies	52
Figure 2.2	Schematic representation of experimental design	54
Figure 2.3	Decomposition of ^{CP} A as a function of bridge position	56

Chapter 3: Periodicities in DNA Charge Transport Probed with *N*₂-Cyclopropylguanine, a Kinetically Fast Hole Trap

Table 3.1	DNA assemblies used for oxidative decomposition studies	74
Table 3.2	DNA assemblies used for fluorescence-quenching studies	76
Figure 3.1	Photooxidants, modified bases, and assemblies used to probe CT events in DNA	77
Figure 3.2	^{CP} G decomposition as a function of irradiation time for duplexes containing rhodium and anthraquinone photooxidants	78
Figure 3.3	CT decays in yield as a function of A-tract bridge length using rhodium and anthraquinone photooxidants	80
Figure 3.4	Selected fits of A-tract decomposition profiles	81
Table 3.3	Equations for fitting Rh-A _n decomposition data	82
Figure 3.5	^{CP} G decomposition as a function of temperature in the Rh-A _n series	85
Figure 3.6	Semilog plots showing the distance dependence of CT yield through sequences containing various bridging bases	87
Figure 3.7	Semilog plot of the distance dependence of CT yield in the AQ-A _n series revealed with two oxidative traps, ^{CP} G and guanine	89
Figure 3.8	Comparison of distance dependence of charge injection into A and AT-tracts using aminopurine fluorescence quenching	90

Chapter 4: A Role for DNA-Mediated Charge Transport in Regulating p53: Oxidation of the DNA-Bound Protein from a Distance

Figure 4.1	Schematic illustration of photoinduced DNA-mediated charge transport to promote oxidation and dissociation of bound p53	114
Figure 4.2	Oxidation of p53 bound to a consensus sequence as monitored by gel mobility shift assay	118
Figure 4.3	Oxidation of p53 bound to natural promoter sequences as monitored by gel mobility shift assay	120
Figure 4.4	Oxidation of p53 bound to the <i>Mdm2</i> promoter as monitored by gel mobility shift assay	122
Figure 4.5	MALDI-TOF mass spectrometric analysis of p53 tryptic digests following photoinduced oxidation of the DNA-bound protein	124

Chapter 5: Charge Separation in Ruthenium-Quencher Conjugates Bound to DNA

Figure 5.1	Representation of a modified flash-quench scheme for a ruthenium (II) complex with a tethered quencher	135
Figure 5.2	Structures of tris heteroleptic dipyrrophenazine complexes of ruthenium (II)	136
Figure 5.3	Schematic illustration of solid-phase chemistry used to generate $[\{\text{Ru}(\text{phen})(\text{dppz})(\text{bpy}'\text{-his})\}\{\text{Ru}(\text{NH}_3)_5\}]^{5+}$ and $[\text{Ru}(\text{phen})(\text{dppz})(\text{bpy}'\text{-his})]^{2+}$	145
Figure 5.4	HPLC and UV-Vis absorbance characterization of the ruthenium complexes	147
Figure 5.5	Effect of irradiation on the stability of $[\{\text{Ru}(\text{phen})(\text{dppz})(\text{bpy}'\text{-his})\}\{\text{Ru}(\text{NH}_3)_5\}]^{5+}$	148
Table 5.1	Steady-state quantum yields of ruthenium complexes	150
Table 5.2	Excited state lifetimes of ruthenium complexes	153
Figure 5.6	Electrochemical profiles of ruthenium complex reduction	155
Table 5.3	Electrochemical potentials for ruthenium complexes	156

Figure 5.7	Guanine oxidation by ruthenium complexes as monitored by gel electrophoresis	158
Table 5.4	% of ^{CP} C and ^{CP} G decomposition with noncovalently bound ruthenium and rhodium complexes	160
Figure 5.8	Decomposition of ^{CP} G and ^{CP} C using ruthenium complexes	162
Figure 5.9	EPR spectroscopy of guanine radical formation induced by photooxidation of $[\{\text{Ru}(\text{phen})(\text{dppz})(\text{bpy}'\text{-his})\}\{\text{Ru}(\text{NH}_3)_5\}]^{5+}$	164
Figure 5.10	Transient absorption spectroscopy at 440 nm for ruthenium complexes	166
Figure 5.11	Transient absorption difference spectra for $[\{\text{Ru}(\text{phen})(\text{dppz})(\text{bpy}'\text{-his})\}\{\text{Ru}(\text{NH}_3)_5\}]^{5+}$ and reductive quenching of $[\text{Ru}(\text{phen})(\text{dppz})(\text{bpy}'\text{-his})]^{2+}$ with ascorbate	167
Figure 5.12	Schematic illustration of various photophysical pathways for $[\{\text{Ru}(\text{phen})(\text{dppz})(\text{bpy}'\text{-his})\}\{\text{Ru}(\text{NH}_3)_5\}]^{5+}$ bound to DNA	176

Chapter 1

Charge Transport through the DNA Helix

Adapted from Augustyn, K.E.; Pierre, V.C.; Barton, J.K. “Metallointercalators as probes of DNA recognition and reaction” in *Wiley Encyclopedia of Chemistry and Biology* 2007.

1.1 The DNA π -stack serves as an effective conduit for charge transport

DNA is widely viewed in terms of its ability to encode genetic information through noncovalent interactions with proteins and nucleic acids [1-3]. The myriad cellular reactions involving DNA depend on its well-defined double helical structure comprised of a polyanionic sugar phosphate backbone encasing an extended π -stacked array of heterocyclic aromatic bases (Figure 1.1). It was not long after the elucidation of the double helical structure of DNA [4] that Eley and Spivy, noting the striking similarity between the π -stacked bases of the helix and a highly conductive one-dimensional aromatic crystal, posed the question asking whether the electronically coupled π -stacked bases might also provide an effective medium for charge separation [5]. A plethora of ensuing work has shown undeniably that due to inherent stacking of the aromatic base pairs, charges can indeed migrate through DNA [6-8]. However, the heterogeneity of DNA that allows it to store requisite information for cellular functions in a four-base code presents a challenge for those researchers attempting to elucidate the mechanism of charge migration through this dynamic molecule. In contrast to a homogeneous solid state π -stack, electron and hole transport through DNA is inevitably complicated due to the different redox potentials and stacking capabilities of the bases, which lead to variations in electronic coupling along the helix.

The dynamic nature and heterogeneity of the double helix has resulted in many models ranging from hopping to superexchange in order to mechanistically characterize DNA charge transport [9, 10]. In these models, a donor and acceptor are separated by an intervening DNA base pair bridge (Figure 1.2). In a case of pure superexchange, the

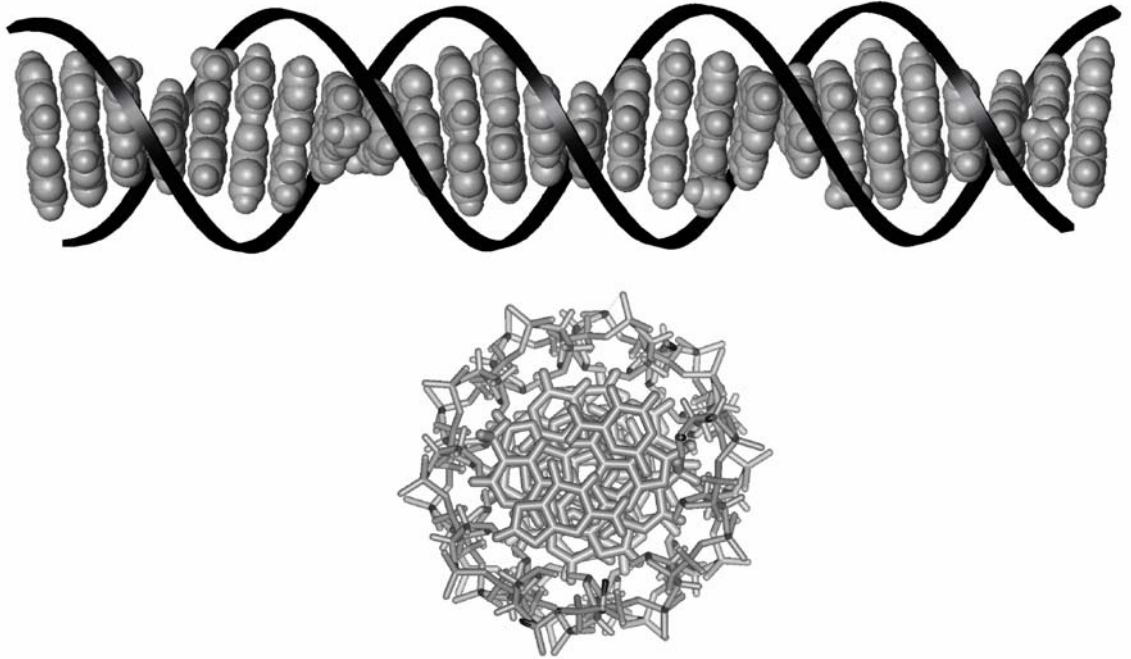


Figure 1.1. The structure of the DNA double helix (top). The polyanionic sugar phosphate backbone is indicated in black, while the inner core of stacked aromatic bases is delineated in grey. A view perpendicular to the helical axis highlights the degree of overlap between the stacked bases (bottom). Adapted from reference 19.

donor is lower in energy than the intervening bridge, and charge tunnels through the bases to reach the acceptor without actually occupying base pair orbitals. These systems show an exponential decrease in rate as a function of distance between the donor and acceptor and can be quantified by the parameter β , a measurement of exponential decay with increasing distance between the donor and acceptor [11]. In contrast, a hopping mechanism occurs when the donor is higher in energy than the bridging bases and the charge hops between low energy sites from the donor to the acceptor resulting in a geometric as opposed to exponential distance dependence [9]. In the context of hopping, the power parameter η is used instead of β and indicates the degree of variance from an ideal random walk. Rates of charge transport in proteins have found β values on the order of 1.1 \AA^{-1} which is characteristic of purely σ -bonded systems [12]. Interestingly, experimentally determined β values for DNA have ranged from 1.5 - 0.03 \AA^{-1} indicating that in certain cases, charge transport through DNA is effectively distance-independent [13-16]. This wide range of values arises due to differences in stacking between the donor, acceptor, and the bridge in the systems used, and the resulting variations in electronic coupling. More importantly, the nonlinearity often observed in rate as a function of distance for well coupled donor-acceptor-bridge systems clearly suggests that pure superexchange, and hence measurements of β , may not be an adequate description of DNA-mediated charge transport. Conversely, a purely hopping mechanism cannot account for the fact that charge transport is exquisitely sensitive to distortions in local base stacking such as mismatches and bulges [17, 18]. Undoubtedly then, charge transport through DNA does not follow a strictly superexchange or hopping mechanism

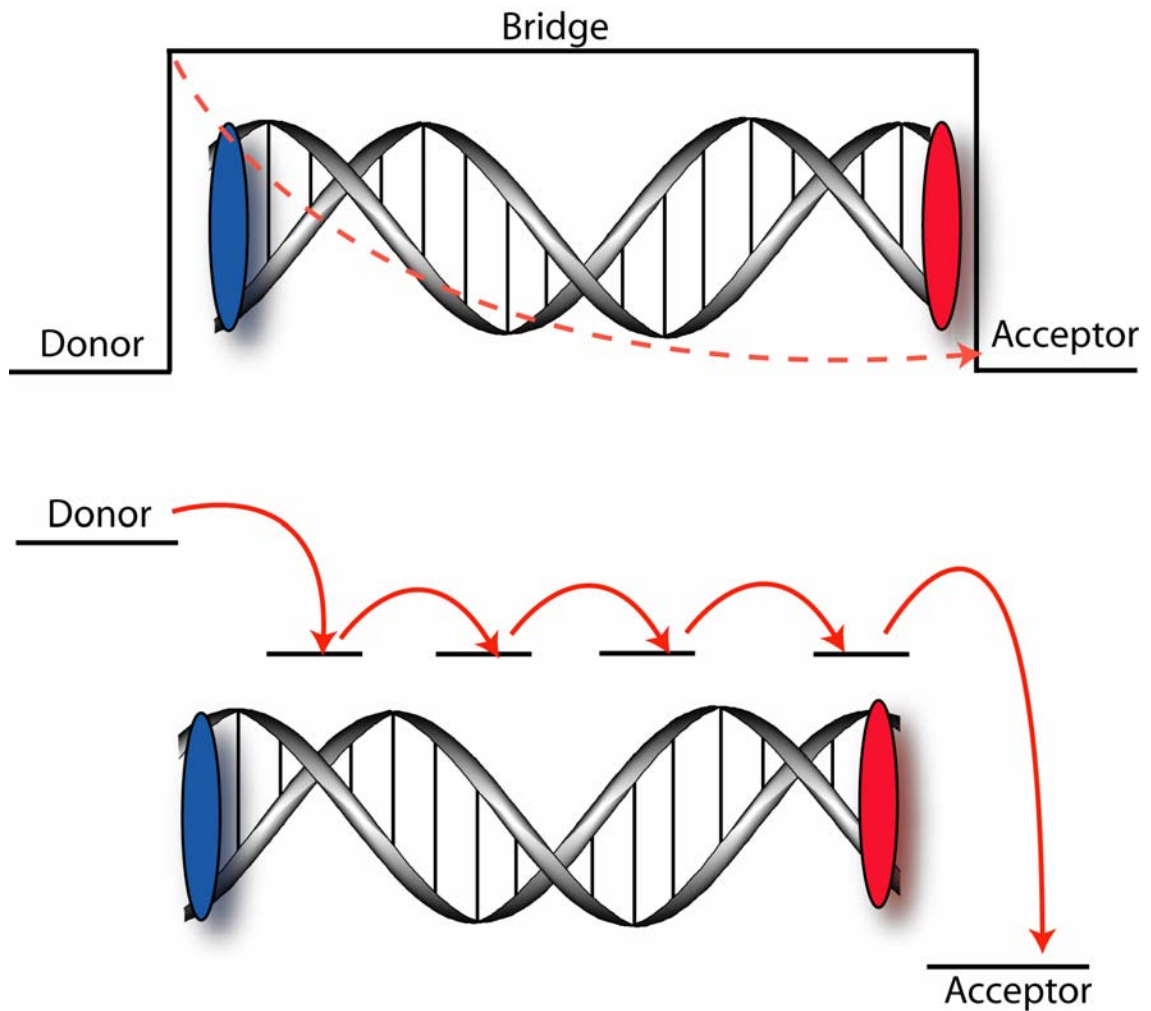


Figure 1.2. Schematic representation of two mechanistic extremes used to describe DNA charge transport. Superexchange occurs when the donor and acceptor are lower in energy than the intervening DNA base pair bridge and the charge tunnels from the donor to the acceptor without occupying the orbitals of the individual bases (top). Conversely, hopping occurs when the donor is higher in energy than the intervening base pair bridge and the charge hops from the donor to the acceptor transiently occupying low energy sites on the individual bridging bases (bottom).

as evidenced by the complexity in experimentally determined β values and the inherent sensitivity to structural perturbations in the base pair stack.

1.2 Probes of charge transport

A large assortment of metallointercalators, organic photooxidants, and modified bases with varied redox potentials and photophysical properties have been used as probes of charge transport through DNA (Figure 1.3). Ultimately, successful systems incorporate donors and acceptors that are well electronically coupled to the intervening base pair stack. Donor-bridge-acceptor systems using combinations of these probes have led to measurements of charge transport over distances ranging from 3.4 to 200 Å and with charge separation driving forces as large as 2 V [19].

1.2.1 Organic photooxidants and modified bases as probes of DNA-mediated charge transport

There are several organic photooxidants amenable to monitoring charge transport reactions through DNA. These molecules can be covalently appended to DNA such that distance dependences of charge transport can be determined. The classic example of an organic DNA intercalator is ethidium which avidly binds to DNA with a dissociation constant on the order of 10^6 M^{-1} [20]. Ethidium exhibits increased fluorescence when intercalated into DNA but its excited state potential of 1.2 V vs. NHE is too low to oxidize the natural DNA bases [21]. Consequently, this probe can serve as a photooxidant only in the presence of a modified base or acceptor with a suitably low oxidation potential such as deazaguanine. Anthraquinone has also been widely used for initiating charge injection into DNA [22]. However, unlike ethidium, this photooxidant interacts

with DNA through end capping as opposed to intercalation. Other nonintercalating photooxidants such as naphthalene diimide, cyanobenzophenone-modified deoxyuridine, and 4-pivaloyl thymidine have also been used to investigate charge transport through DNA [23-26]. In addition to the organic photooxidants, several modified bases exist that can act either as photooxidants or hole acceptors. These modified bases are often excellent probes of DNA CT because they are inherent to the DNA duplex. The fluorescent adenine analogues, 2-aminopurine (2-AP) and 1-*N*₆-ethenoadenine (ϵ A), have excited state potentials of 1.5 and 1.4 V respectively and are thus capable of oxidizing guanine [27]. However, 2-AP is a more effective probe than ϵ A, due to its ability to stack well with neighboring bases. Modified bases can also function as hole acceptors. Cyclopropylamine-substituted bases such as ^{CP}G, ^{CP}A, and ^{CP}C have provided very fast traps for DNA charge transport utilizing an irreversible ring opening reaction associated with oxidation and are particularly useful for monitoring charge transport processes on faster time scales than would be possible by trapping of the long-lived guanine radical [28].

1.2.2 Metallointercalators as probes of DNA-mediated charge transport

Octahedral rhodium and ruthenium complexes with intercalating ligands have served as powerful probes of DNA-mediated charge transport. Since DNA-mediated charge transport depends so sensitively upon π -stacking, it is reasonable that a probe that intercalates into DNA, with optimum π -stacking, might also serve as a powerful probe of this chemistry. The dipyrrophenazine complexes of ruthenium (II) such as [Ru(phen)(dppz)(bpy')]²⁺, and the phenanthrenequinone diimine complexes of rhodium (III) such as [Rh(phi)₂(bpy')]³⁺ have proven as useful probes of charge transport

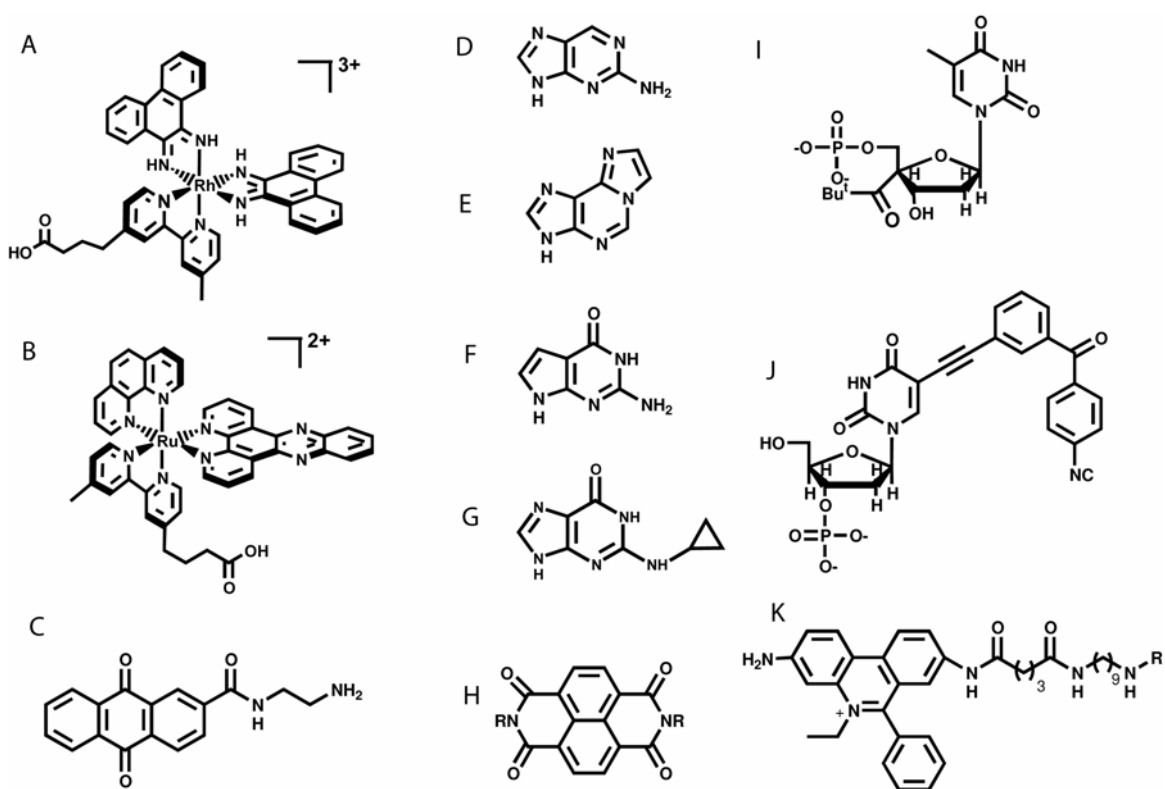


Figure 1.3. Probes used to monitor charge transport through DNA. $[\text{Rh}(\text{phi})_2(\text{bpy}')^3]^3+$ (A), $[\text{Ru}(\text{phen})(\text{dppz})(\text{bpy}')^2]^2+$ (B), a modified anthraquinone (C), 2-aminopurine (D), 1- N_6 -ethenoadenine (E), deazaguanine (F), N_2 -cyclopropylguanine (G), naphthalene diimide (H), 4-pivaloyl thymidine (I), a cyanobenzophenone-modified deoxyuridine (J), and a modified ethidium (K) [18, 21-27, 49, 55-57].

owing to the ability of the intercalating ligand to electronically couple with the DNA base pairs. These complexes bind DNA via intercalation into the major groove with high affinity ($K_a > 10^6 \text{ M}^{-1}$) and in some cases, high sequence specificity [29]. Indeed, an extended aromatic system on the ligand outward from the metal center, as in the case of the phi or dppz ligands, favors its intercalative stacking between the base pairs of the double helix. The intercalating ligand of these complexes thus behaves as a stable anchor in the major groove, oriented parallel to the base pairs, and directing the orientation of functionalized ancillary ligands with respect to the DNA duplex. Photophysical studies first provided support for intercalation [30]. Extensive NMR studies and a crystal structure detailed the nature of the snug intercalation for the metal complexes via the major groove of the DNA [31-33, Figure 1.4].

Importantly, these complexes possess rich photochemical and photophysical characteristics that have been exploited advantageously both to probe interactions with DNA and subsequent charge transport reactions. The phi complexes of rhodium (III) have proven to be efficient agents for biochemically probing DNA charge transport chemistry [34]. Irradiation at 365 nm of 5' radioactively labeled DNA duplexes containing the tethered rhodium intercalator generates a potent photooxidant with a potential greater than 2.0 V vs. NHE capable of inducing oxidative damage through long-range hole transport that can be revealed by gel electrophoresis following treatment in hot piperidine [35]. If these same duplexes are irradiated at a shorter wavelength (313 nm), hydrogen abstraction leads to direct scission of the DNA backbone, indicating the exact position of intercalation. Thus the dual functionality of these complexes can delineate their intercalation site as well as inducing charge injection into the DNA.

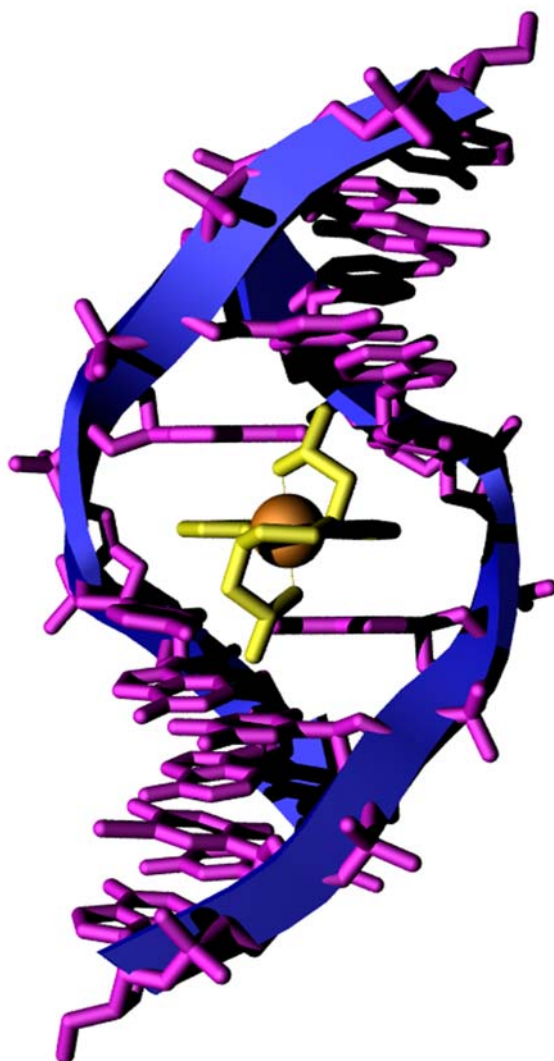


Figure 1.4. Crystal structure of intercalated $\Delta\text{-}\alpha\text{-}[\text{Rh}[(\text{R,R})\text{Me}_2\text{trien}]\text{phi}]^{3+}$ in the major groove of 5'-G-dIU-TGCAAC-3'. The phi ligand is well stacked with the DNA bases effectively acting as an additional base pair with minimal perturbation to the overall structure [33].

Dppz complexes of ruthenium (II) serve as light switches for DNA. A well studied example is $[\text{Ru}(\text{bpy})_2(\text{dppz})]^{2+}$ which, when excited in organic solvents, leads to a direct charge transfer from the metal to the intercalating ligand with a lifetime on the order of 270 ns [36, 37]. In aqueous solution, however, its emission is quenched due to the ability of water to deactivate the excited state through hydrogen bonding with the phenazine nitrogen atoms of the intercalating ligand. Upon intercalation in DNA in aqueous solution, it luminesces again, reflecting the shielding of the intercalating ligand from bulk solvent by the stacked bases of the double helix. This is akin to introducing the complex into a local organic solvent that shields the ring nitrogens on the intercalating ligand from protonation. Thus the luminescence properties of these complexes can reflect the degree of intercalation into the DNA π -stack. In the context of charge transport, these complexes have the unique ability to directly inject charge into the π -stack as the excited state is localized on the intercalating ligand. Quenching of the Ru(II) excited state via the flash-quench technique by agents such as $[\text{Co}(\text{NH}_3)_5\text{Cl}]^{2+}$, $[\text{Ru}(\text{NH}_3)_6]^{3+}$, and methyl viologen generate *in situ*, a powerful Ru(III) ground state oxidant capable of oxidizing guanine [38]. Thus the flash-quench technique, originally developed by Gray and co-workers to investigate charge transport reactions in proteins [39], can be used to monitor analogous reactions through DNA (Figure 1.5).

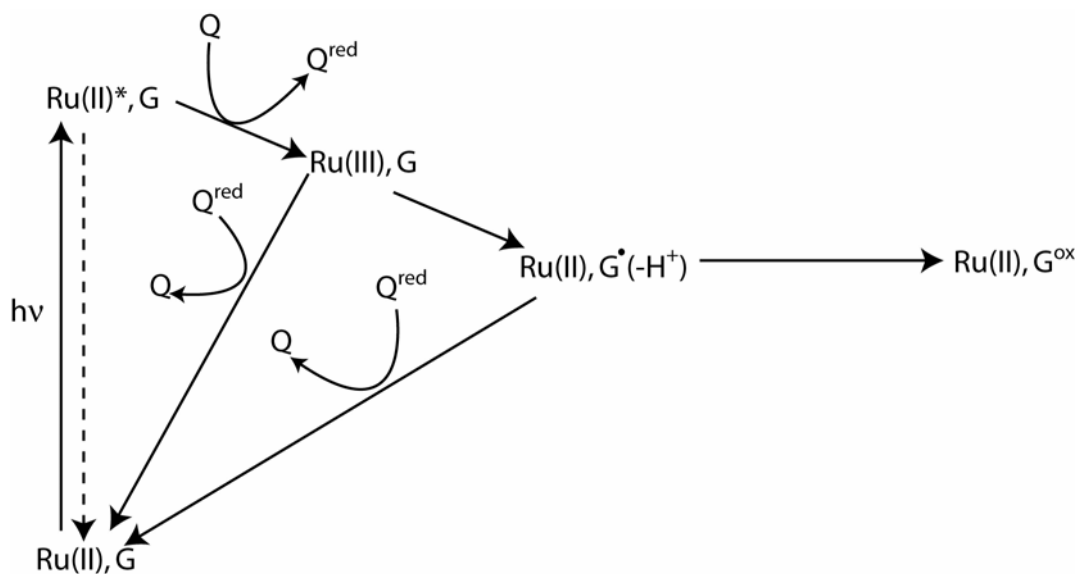


Figure 1.5. Flash-quench scheme for generating guanine radicals. A ground state Ru(II) complex in the presence of guanine containing DNA is excited into its MLCT band to generate the Ru(II) excited state. A diffusible quencher (Q) such as methyl viologen, $[\text{Co}(\text{NH}_3)_5\text{Cl}]^{2+}$, or $[\text{Ru}(\text{NH}_3)_6]^{3+}$ can abstract an electron from the Ru(II) excited state to generate *in situ*, the potent ground state oxidant Ru(III) which is capable of oxidizing guanine. Once oxidized, the guanine radical cation rapidly deprotonates to form the neutral guanine radical, which can react with water to form permanently damaged products. Conversely, back electron transfer can occur between the oxidized ruthenium and the reduced quencher, or between the oxidized guanine and the reduced quencher to regenerate the initial reactants.

1.3 Early photophysical studies

The earliest studies of DNA-mediated charge transport employed a dppz-containing ruthenium complex as the photooxidant and a phi-containing rhodium complex as the electron acceptor (Figure 1.6). Assemblies containing 5'-tethered $[\text{Ru}(\text{phen}')_2(\text{dppz})]^{2+}$ ($\text{phen}'=5\text{-amido-glutarate-1,10-phenanthroline}$) with and without 5'-tethered $[\text{Rh}(\text{phi})_2(\text{phen}')]^{3+}$ were designed where fluorescence quenching of the photooxidant was observed only in the presence of the electron acceptor [13]. Given a 0.75 V driving force, little spectral overlap between the excited state of ruthenium and the ground state of rhodium, and the fact that the tethered complexes are well separated on a 15-mer duplex, the observed results are consistent with DNA-mediated charge transfer. This work set the stage for many varied experiments using metallointercalators to characterize this interesting chemistry.

Further experiments spectrally identifying the ruthenium (III) intermediate confirmed that the quenching mechanism was due to charge transfer [40]. When bound to DNA, $[\text{Ru}(\text{DMP})_2(\text{dppz})]^{2+}$ decays with two lifetimes corresponding to the two orientations of the intercalating dppz ligand. Following excitation at 480 nm of intercalating $[\text{Ru}(\text{DMP})_2(\text{dppz})]^{2+}$ ($\text{DMP}= 4,7\text{-dimethylphenanthroline}$) in the presence of $[\text{Rh}(\text{phi})_2(\text{bpy})]^{3+}$, a negative transient was observed on the microsecond time scale at 440 nm following the initial bleach corresponding to the decay of the ruthenium excited state. As the rhodium concentration was increased, the observed decrease in luminescence intensity but not in lifetime of the ruthenium excited state indicated that the quenching and hence rate of charge transport was fast relative to the measurement. The same

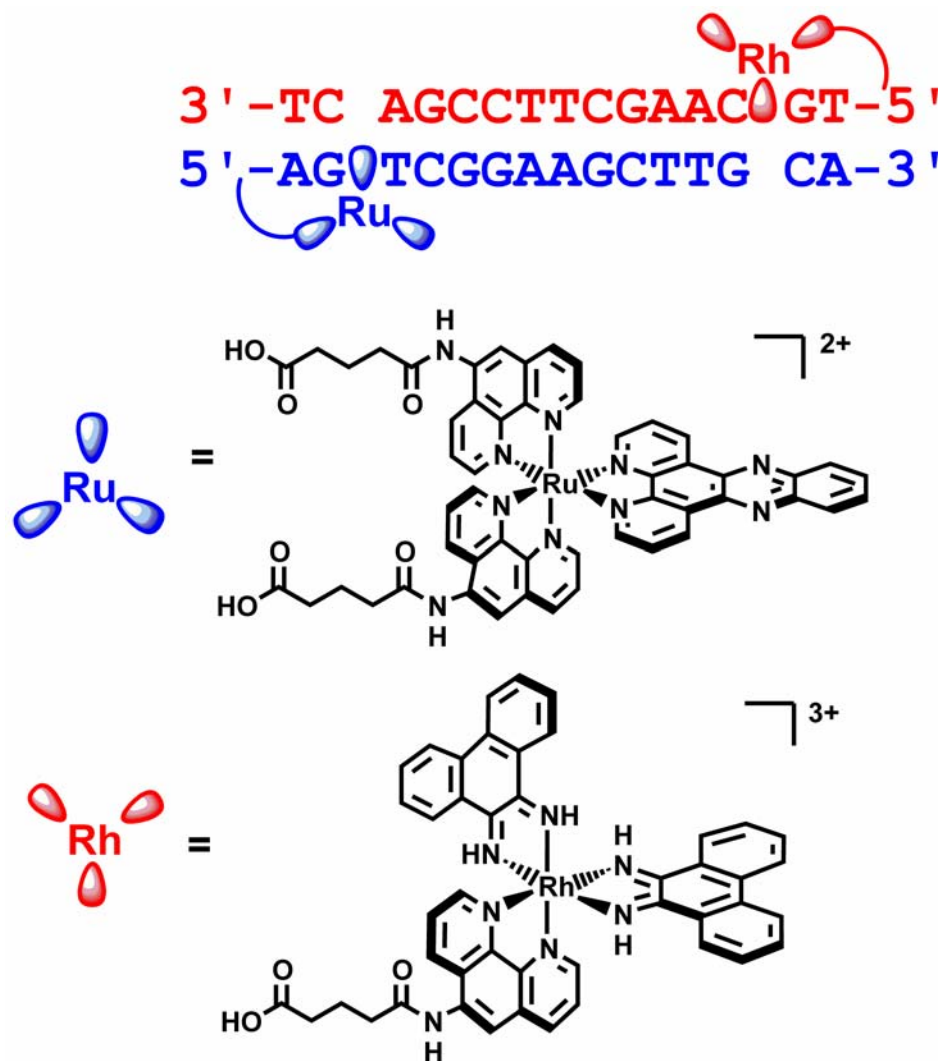


Figure 1.6. Schematic representation of a doubly metallated DNA duplex used to probe photoinduced electron transfer in DNA [13].

transient was also observed when $[\text{Ru}(\text{NH}_3)_6]^{3+}$ was used as the quencher, albeit with a slower rate of formation. As expected, the decay kinetics of the transient were similar for both quenchers. Differences in quenching kinetics between $[\text{Rh}(\text{phi})_2(\text{bpy})]^{3+}$ and $[\text{Ru}(\text{NH}_3)_6]^{3+}$ are attributed to intercalation: the intercalative $[\text{Rh}(\text{phi})_2(\text{bpy})]^{3+}$ exhibits static quenching while the diffusional $[\text{Ru}(\text{NH}_3)_6]^{3+}$ shows dynamic quenching.

1.4 Biochemical studies of long-range oxidative charge transport

Oxidative conditions within the cell can lead to damage of the DNA bases. Guanine, experimentally determined to have the lowest oxidation potential of the naturally occurring bases, is the most easily damaged [41]. Upon oxidation, the neutral guanine radical can react with water or oxygen to form permanently damaged products such as 8-oxo-G, oxazolone, or imidazolone [42]. Many organic photooxidants such as anthraquinone, riboflavin, and naphthalimide have been shown to specifically damage the 5' guanine of a guanine doublet [43-46].

1.4.1 $[\text{Rh}(\text{phi})_2(\text{bpy}')]^{3+}$ and $[\text{Ru}(\text{phen})(\text{dppz})(\text{bpy}')]^{3+}$ can oxidize guanine

The rhodium intercalator, tethered to the terminus of an oligonucleotide, was first employed to demonstrate oxidative damage to DNA from a distance through DNA charge transport [48, 49, Figure 1.7]. Comparison of the irradiation products of 15-mer oligonucleotides containing two sets of guanine doublets with a 5'-tethered rhodium intercalator vs. one where the photooxidant is intercalated noncovalently reveals that the

damage patterns show little distinction in oxidation of the proximal and distal guanine doublets. However, the 5' guanines in both doublets were more susceptible to damage than the 3' guanine consistent with *ab initio* molecular orbital calculations that have indicated that the HOMO is localized on the 5' guanine of a guanine doublet [47]. This preferential reaction at the 5'-G of guanine doublets has become a signature for one-electron DNA oxidation [48]. Irradiation at 313 nm reveals that the covalently tethered rhodium intercalates three bases from the tethered end while the noncovalent complex intercalates throughout the duplex. As the covalently bound rhodium intercalates far away from the observed damaged guanines, oxidation must therefore occur through long-range DNA-mediated charge transport. Further analysis of the damaged products by HPLC following enzymatic digestion showed that the primary damage product is 8-oxo-G.

Oxidative DNA damage has also been studied using the ruthenium intercalator, $[\text{Ru}(\text{phen})(\text{dppz})(\text{bpy}')]^{2+}$. DNA duplexes containing 5' tethered $[\text{Ru}(\text{phen})(\text{dppz})(\text{bpy}')]^{2+}$ were irradiated at 442 nm in the presence of either methyl viologen or $[\text{Ru}(\text{NH}_3)_6]^{3+}$ [18], and preferential damage was observed at the 5' guanine of a guanine doublet, consistent with one-electron oxidation chemistry. HPLC analysis showed 8-oxo guanine also as a primary oxidation product. In order to rule out guanine damage due to singlet oxygen sensitization, duplexes containing tethered ruthenium were irradiated in the absence of quencher. Damage was only observed at guanines near the ruthenium intercalation site, and was not 5' specific. Furthermore this damage without quencher increased when the experiments were performed in D_2O , a characteristic of singlet oxygen chemistry.

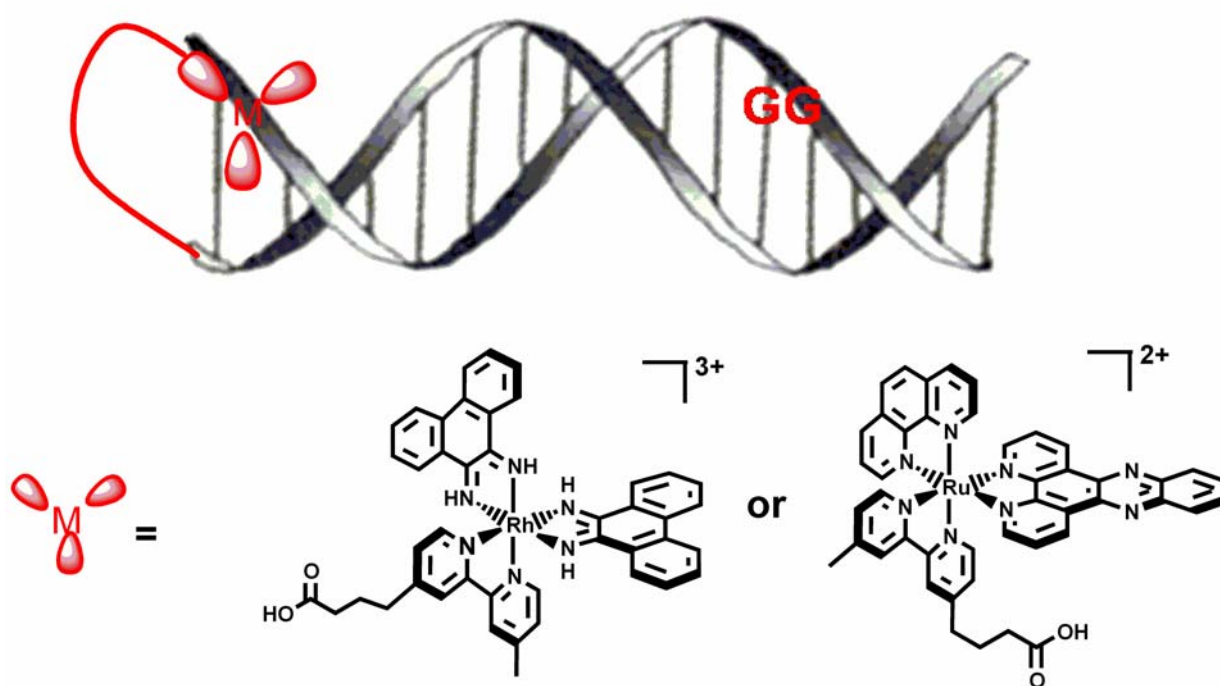


Figure 1.7. Schematic representation of a metallated duplex designed to probe long-range oxidative damage in DNA. Oxidative damage is found at the 5'-G of the guanine doublets [18, 48, 49].

1.4.2 Distance dependence using metallointercalators

The previous results utilizing the tethered rhodium and ruthenium photooxidants indicate that DNA charge transport might be significant over long molecular distances and certainly over longer distances than had been demonstrated in studies of protein electron transfer. The tethered rhodium intercalator was employed in the design of assemblies to examine relative oxidative damage at two guanine doublets within a 28-mer duplex [50]. The proximal guanine doublet was kept at a constant distance from the rhodium intercalator while the distal doublet was placed in 2 base pair increments at increasing distances from the photooxidant. The damage ratio between the proximal and distal double guanine sites then serves as an indicator of charge transport efficiency. Remarkably the damage ratio did not show significant diminution as a function of distance over 75 Å. DNA charge transport thus shows a very shallow distance dependence that is not a result of helical phasing.

Similar studies were also carried out using the ruthenium intercalator, $[\text{Ru}(\text{phen})(\text{dppz})(\text{bpy}')]^{2+}$. Comparison of oxidative damage with the rhodium and ruthenium photooxidants was carried out in a 63 base pair duplex containing 6 sets of guanine doublets arranged at 10 base pair increments [50, Figure 1.8]. Both complexes are able to oxidize all 6 sets of double guanines indicating that DNA charge transport chemistry can be observed at distances up to 197 Å away from the intercalation site! Oxidative damage to DNA, in fact, can arise over biologically significant distances.

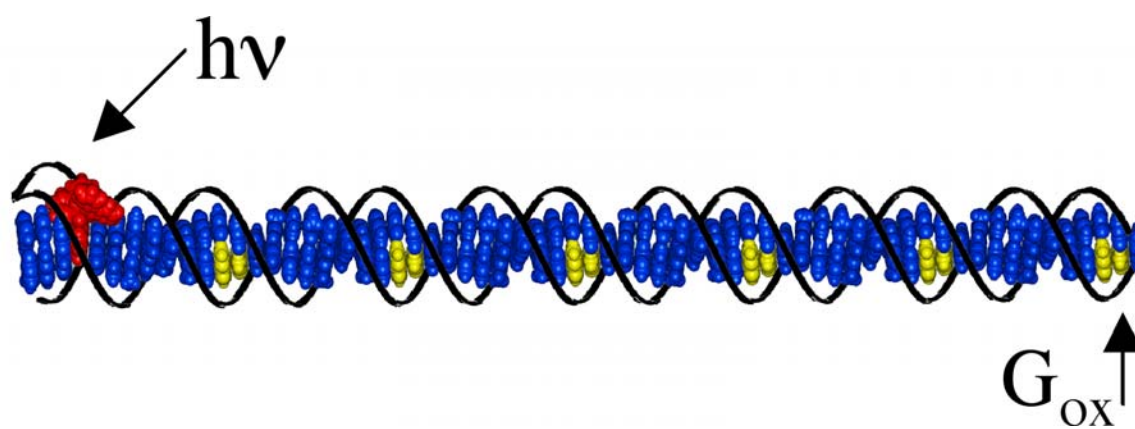


Figure 1.8. Schematic representation of a rhodium-tethered 63 base-pair DNA duplex containing six sets of guanine doublets. Charge injected at the rhodium intercalation site can travel ~ 200 Å resulting in oxidative damage at all low-energy double guanine sites [50].

1.5 Ultrafast charge transport

1.5.1 Charge transport between two intercalators

While the distance dependence of charge transport has been characterized biochemically through yields of guanine damage measured by gel electrophoresis, this technique cannot reveal charge transport events occurring on fast time scales owing to the millisecond lifetime of the guanine radical [51]. Thus, not long after charge transport between two covalently tethered metallointercalators was demonstrated, a systematic distance dependence of charge transport through DNA was investigated using an ethidium photooxidant and a rhodium acceptor [14]. DNA assemblies containing a covalently tethered intercalating ethidium photooxidant separated from an intercalated rhodium quencher by increasing distances were excited to inject a charge into the duplex. Yields of charge transfer quenching of the ethidium excited state by rhodium suggested a weak distance dependence over the 24-38 Å regime. Interestingly, the excited state lifetime of ethidium is unaffected by increasing distance from the rhodium quencher indicating that the charge transport rate is faster than the instrument response time (10^{-10} s). Therefore it was suggested that the weak distance dependence in charge transport yield is governed by base stacking rather than rate. This led to experiments probing the sensitivity of charge transport to stacking by introducing a CA mismatch intervening between the photooxidant and the rhodium hole trap. Remarkably, the presence of a single mismatch, capable of locally disrupting the π -stack, results in significant attenuation of charge transport further underscoring the importance of a well-stacked π -system for efficient reaction.

1.5.2 Charge transport between an intercalator and a DNA base

In order to further probe the distance dependence of charge transport through DNA on a faster time scale, duplex assemblies containing the tethered ethidium photooxidant separated from a deazaguanine hole trap by a series of increasing base pairs were prepared [21]. Similarly to the ethidium-rhodium experiment, the yield of charge transport monitored by the quenching of ethidium by deazaguanine shows a shallow distance dependence over 6-24 Å, yet the rates, even when monitored on a femtosecond time scale, show little variation with distance. Two lifetimes of 5 and 75 picoseconds are observed with the shorter lifetime reflecting the rate of charge transfer between deazaguanine and ethidium and the longer lifetime reflecting the dynamics of ethidium within its binding site. Thus, this slower lifetime suggests the ethidium must reorient itself prior to charge injection to adopt a suitable conformation for efficient transport. These studies indicate that conformational gating by the motions of ethidium can govern the charge transport process and initiated a series of photophysical experiments investigating the role of base dynamics on the distance dependence of charge transport.

1.5.3 Charge transport between DNA bases

The fluorescent adenine analogues 2-aminopurine (AP) and N_6 -ethenoadenine (ϵA) have provided a means to investigate charge transport between bases in a DNA duplex. In these systems, charge transport can be monitored by redox probes inherent to

the DNA bases thus directly probing the stacking required for an efficient process. These two probes have sufficient potential to selectively oxidize guanine yet their stacking within duplex DNA differs dramatically. While AP can base pair with thymine in a similar fashion as adenine, the sterically bulky ϵ A cannot hydrogen bond with thymine and thus exhibits impaired stacking in DNA [52, 53]. These differences in stacking are remarkably apparent in charge transport yields as measured by emission quenching by guanine and rates monitored by probe lifetime. The AP probe shows a shallow distance dependence over 3.4-13.6 Å with an ultrafast rate constant (10^{10} - 10^{11} s⁻¹) while the ϵ A probe exhibits a steep distance dependence with a slower rate constant over the same regime [27].

More recently, AP was used to investigate the distance dependence of charge transport through longer DNA bridges [54]. A series of AP containing duplexes separated from guanine by an increasing number of adenine base pairs was synthesized to probe charge transport through bridges spanning 3.4-35 Å. Similarly to the aforementioned experiment, a shallow distance dependence is observed for charge transport yield with β values on the order of 0.1-0.2 Å⁻¹. Moreover, increasing the temperature has a significant effect on the charge transport yield as a function of bridge length. Duplexes containing the AP probe in direct contact with guanine show a decreased yield in charge transport with increased temperature. Conversely, duplexes containing the AP probe spaced farther away from guanine have increased yields of charge transport at higher temperatures. These results suggest that base motions, facilitated by an increase in temperature, are required for the DNA bridge to reach a charge transport active conformation. Shorter bridges, already in charge transport active conformations, do not yield enhanced charge

transport at higher temperatures. Longer bridges however, require activation energy facilitated by increased temperature to achieve the optimal conformation for efficient charge transport.

1.5.4 Cyclopropylamine-modified bases as ultrafast kinetic hole traps

Cyclopropylamine-substituted bases have provided very fast traps for DNA charge transport utilizing an irreversible ring opening reaction associated with oxidation [55, Figure 1.9]. Guanine is, in fact, a rather poor oxidative trap, since the guanine radical reacts only on the microsecond to millisecond time scale with water and oxygen to form irreversible products; model studies suggest that irreversible ring opening of the N_2 -cyclopropylguanine radical occurs on the picosecond time scale. Recently our lab has designed a series of rhodium-tethered duplexes, in which the oxidative trap is N_2 -cyclopropylguanine [56]. With intervening adenine tracts bridging the intercalator and trap, a shallow distance dependence is observed, now with prominent periodic features. Interestingly, if the same experiments are repeated monitoring guanine damage, the periodicities are not apparent. These periodicities are also absent in assemblies containing AT base pair bridges, and are less pronounced when the intervening bridge consists of AI, ATIC, or AITC repeats.

An analogous hole trap, N_4 -cyclopropylcytosine, has also been used to monitor charge transport through the higher energy pyrimidine bases [57]. When rhodium-tethered duplexes containing a distally placed cyclopropylcytosine are irradiated, ring opening is observed. This striking result indicates that rhodium-induced charge

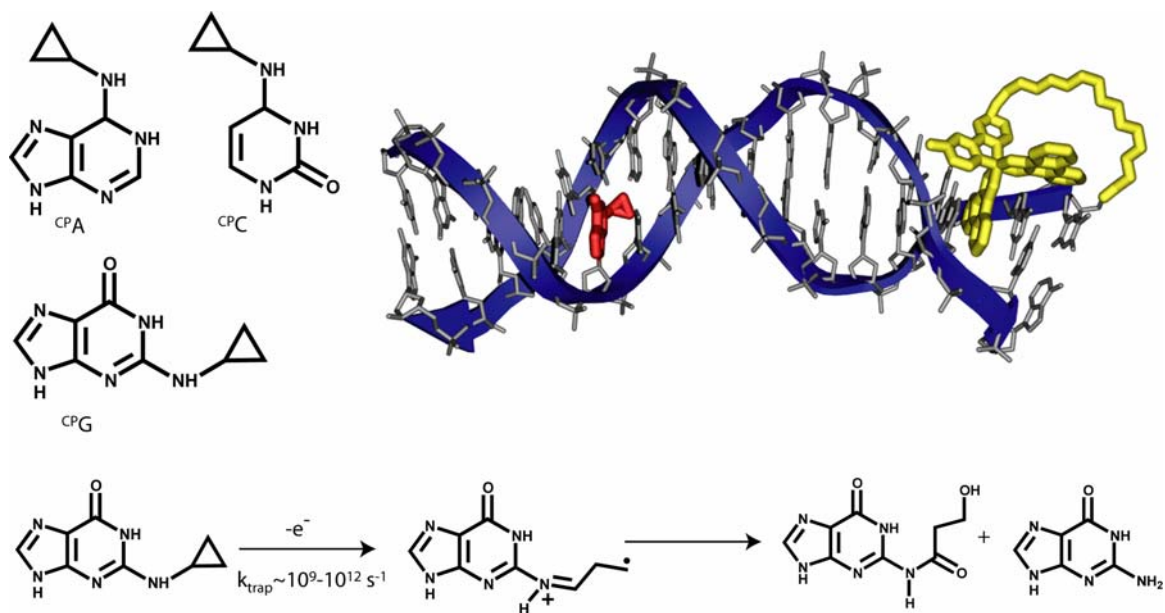


Figure 1.9. The cyclopropylamine-modified nucleosides ^{CP}A, ^{CP}G, and ^{CP}C are used as kinetically fast reporters of hole density over the DNA duplex. Upon oxidation, the cyclopropyl ring opens irreversibly on a picosecond time scale. A schematic representation of a rhodium tethered duplex containing the modified ^{CP}G base is shown (top right).

transport can not only oxidize guanine bases but also cytosines. These findings indicate that charge transport through DNA must involve all the DNA bases, not only the low energy guanines we observe using gel electrophoresis.

1.6 Spectroscopy of charge transfer intermediates

Spectroscopic studies provide a means to characterize DNA-mediated charge transport in more detail and to provide a link to biochemical observations. The flash-quench technique was first used in experiments involving the synthetic oligonucleotide poly d(GC) [38]. In the presence of poly d(GC), the negative absorbance at 440 nm, due to excited state quenching of intercalated $[\text{Ru}(\text{phen})_2\text{dppz}]^{2+}$ by nonintercalating $[\text{Ru}(\text{NH}_3)_6]^{3+}$, disappears concomitantly with a rise in a positive signal at 390 nm, consistent with the formation of the guanine radical. A difference spectrum of this species was obtained with strong positive features at 390 and 550 nm, indicative of the deprotonated neutral guanine radical. Importantly, this signal is not observed in the presence of the synthetic oligomer poly d(AT) nor in the absence of quencher in poly d(GC). Formation of the radical occurs in less than 10^{-7} s, or within the time scale of quenching of the ruthenium excited state.

Spectroscopic studies of long-range DNA charge transport were next carried out on assemblies containing tethered $[\text{Ru}(\text{phen})(\text{dppz})(\text{bpy}')]^{2+}$ as the oxidant and the artificial base 4-methylindole as a guanine analogue [58]. The oxidation potential of 4-methylindole is lower than that of guanine, and the higher extinction coefficient of its radical at 600 nm renders it particularly amenable to spectroscopic studies of

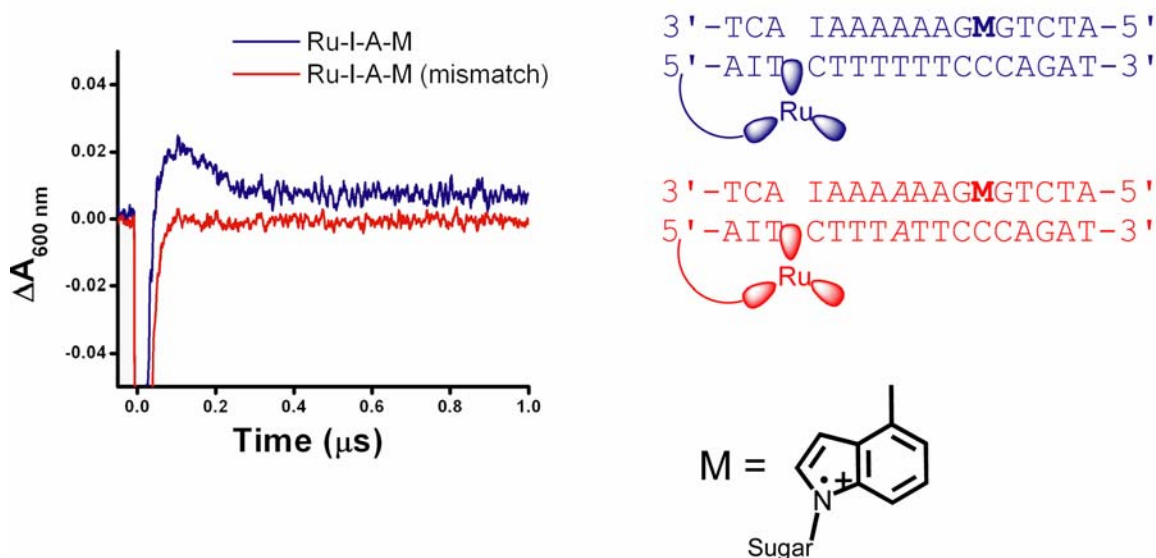


Figure 1.10. Charge transport through a DNA duplex can be observed spectroscopically using the highly absorbing methylindole (M) radical as a probe [58]. A ruthenium photooxidant initiates charge injection into the duplex via the flash-quench technique. Charge transport through a well stacked duplex (Ru-I-A-M) leads to formation of the methylindole radical, which absorbs at 600 nm (blue trace). However, a mismatch (Ru-I-A-M mismatch) perturbs the integrity of the base pair stack, resulting in complete attenuation of charge transport evidenced by a lack of methylindole radical formation (red trace).

DNA-mediated charge transport. Excitation of ruthenium followed by oxidative quenching induces charge injection into the duplex. Hole migration to the methylindole base gives rise to a positive absorbance at 600 nm. However, if a mismatch is introduced into the intervening π -stack of the duplex, DNA-mediated charge transport is disrupted, leading to a complete attenuation of methylindole radical formation (Figure 1.10).

The effect of sequence on charge transfer rate was assessed with assemblies containing a tethered ruthenium photooxidant separated from the methylindole hole trap by a series of A-T base pairs of increasing length. Over distances of 17-37 Å, methylindole radical formation is found to occur concomitantly with quenching of the Ru(II) excited state. Thus the rate of radical formation over this distance through A-tracts is greater than 10^7 s^{-1} and over these distances, charge transport through the DNA is not rate limiting. Furthermore, guanine radical formation can compete with that of the methylindole radical as charge equilibrates across the duplex [59].

1.7 Sensitivity of charge transport to DNA conformation and dynamics

The importance of DNA conformation to DNA-mediated charge transport is evident also in many of the earlier photophysical studies. In fluorescence quenching experiments using assemblies containing the organic intercalator ethidium tethered to one end of the duplex, and the rhodium intercalator tethered to the other end, quenching by photoinduced electron transfer is found with a well-matched duplex, but no significant quenching is seen when a CA mismatch intervenes [14]. A well π -stacked array of heterocyclic aromatic bases is essential to the efficient transport of charge over a duplex. Perturbations in the intervening π -stack inhibit long-range oxidative damage. Assemblies

containing a series of single base mismatches located between a proximal and distal guanine doublet sites relative to a tethered ruthenium photooxidant were designed to explore the effect of stacking disruption on charge transport yield [60]. These studies show the dependence of charge transport efficiency on the dynamics of a mismatch; those mismatches which are relatively well stacked, as in purine-purine mismatches, cause only small attenuations in charge transport yield, while disruptive mismatches cause significant attenuations. In addition to mismatches, bulges can also disrupt the integrity of charge transport [17]. Duplexes containing a tethered rhodium photooxidant and an ATA bulge positioned in between a proximal and distal double guanine site show a drastic diminution in damage at the distal guanine doublet site, again underscoring the necessity of a well-stacked duplex. Indeed, the sensitivity in charge transport yield to intervening perturbations in base stacking has two important consequences: (i) the path of charge transport must be through the bases rather than through the sugar-phosphate backbone; (ii) the reaction can report sensitively upon the integrity of the DNA duplex.

An interesting study using the base flipping enzyme Methyltransferase HhaI (M.HhaI) indicates that disruption of the π -stack by protein binding with insertion of a non-aromatic amino acid side chain, can also significantly attenuate charge transport [61]. M.HhaI performs its alkylation reaction on DNA after flipping out the central cytosine in the 5'-GCGC-3' sequence and inserting a glutamine residue in its place. An assembly containing a covalently tethered rhodium photooxidant and proximal and distal 5'-GG-3' doublets separated by the M.HhaI target site was used to investigate charge transport yield in the presence versus absence of the enzyme. Site-specific binding of the

enzyme to its target sequence is effective in eliminating oxidation at the distal double guanine site. Moreover, when a mutant enzyme containing a tryptophan in place of glutamine in the wild type was used instead, insertion of the aromatic amino acid serves to restore the base pair stack, leading to extensive damage at the distal site. Hence from these studies it appears that the binding of DNA-binding proteins can both inhibit and activate long-range DNA charge transport.

1.8 Towards a mechanistic understanding of DNA charge transport

Taken together, results from fluorescence quenching, gel electrophoresis, and cyclopropylamine ring opening can be rationalized by considering a novel mechanism for DNA-mediated charge transport: conformationally gated domain hopping. While these results cannot be explained by either superexchange or hopping alone, a mechanism has been proposed in which the charge migrates through the DNA by transport between transiently generated delocalized domains, defined by base sequence and dynamics [62, Figure 1.11]. Here, a domain is described as a series of 4 to 5 bases acting in concert, over which a charge can delocalize. As the gel electrophoresis experiments measure guanine radical trapping on the millisecond time scale, contributions from base dynamics are not easily revealed. However, when the faster assay of oxidation-induced ring opening is used, additional effects due to base dynamics can be discerned. Base motions, occurring on picosecond time scales contribute to conformational gating of the charge transfer events, both limiting and facilitating the migration of charge between domains [54].

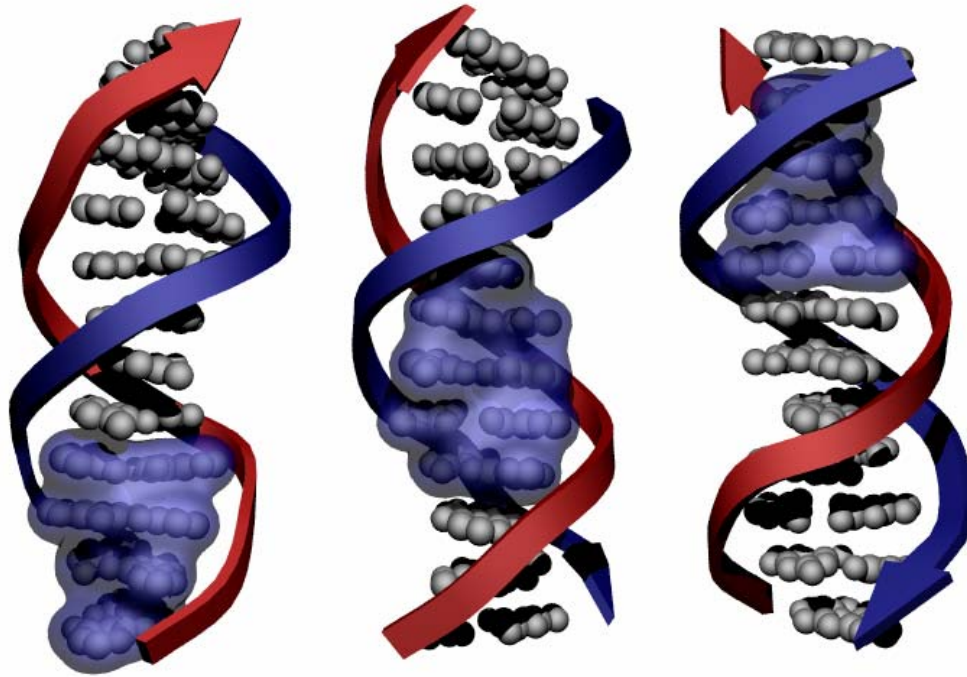


Figure 1.11. DNA charge transport can be explained mechanistically by conformationally gated domain hopping. Here a charge migrates between transiently formed delocalized DNA domains, a series of four to five consecutive bases over which a charge can delocalize. Domains can form and dissolve by base dynamics resulting in either charge transfer active or inactive conformations.

1.9 Biological opportunities for DNA charge transport

The effect of sequence, structure, and distance dependence of DNA-mediated charge transport has been extensively studied. However, the ultimate question still remains, is DNA-mediated charge transport an issue, indeed perhaps even a useful reaction, within the cell? It is well established that charge transport chemistry can occur over long enough distances to be biologically relevant, and that DNA-binding proteins can modulate the chemistry, but whether this transport chemistry can occur within the tightly packed nucleosome structures found in cells remained elusive. Within these structures, the DNA is highly bent, wrapped around a positively charged histone core. A nucleosome core particle, containing a 5' tethered rhodium was therefore constructed; upon photoactivation of the tethered rhodium, oxidative damage at a distance to guanines within the core particle is observed [63, 64, Figure 1.12]. In fact, the efficiency of damage is quite similar to that seen on the same DNA in the absence of bound histones. Interestingly, experiments have also shown that rhodium can induce DNA damage in the nucleus of HeLa cells [65]. If the sites of rhodium binding are compared to those of strong oxidative damage, it becomes apparent that oxidative damage can occur *at a distance* within the cell nucleus. Moreover, it was recently determined that rhodium-induced oxidative damage at guanine sites can occur in mitochondrial DNA [66]. Thus, long-range charge transport through DNA does arise within the cell.

Further evidence indicating that DNA charge transport may be biologically relevant comes from studies with iron-sulfur cluster containing DNA repair proteins such as MutY and EndoIII [67]. Bound to DNA, the redox potential of the [4Fe-4S] cluster in these proteins is found to be shifted so that the protein is more easily oxidized. By

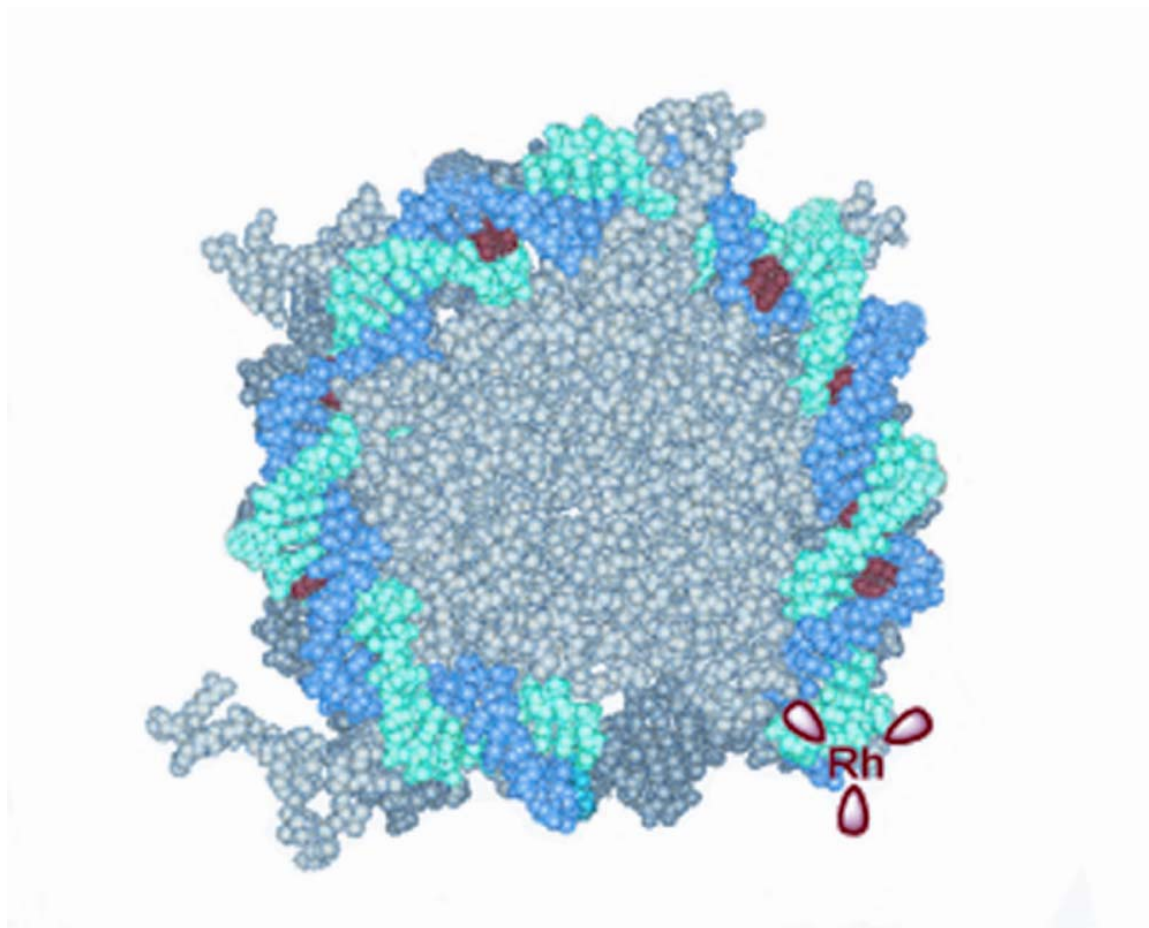


Figure 1.12. Shown is a nucleosome core particle containing a 146 base pair DNA duplex wrapped around a histone octamer with a rhodium intercalating photooxidant tethered to the DNA terminus. This particle was constructed to probe DNA charge transport through a nucleosome. Seven sets of guanine doublets are located at the red positions along the duplex. Oxidative damage initiated by rhodium photoactivation is observed at the guanine doublets, demonstrating long-range oxidation within the nucleosome [63].

comparing potentials bound to DNA and free, the binding affinity of the oxidized form is estimated to be at least three orders of magnitude higher than that of the reduced form. Based on these studies, a model has been proposed in which BER enzymes can locate damaged DNA using DNA-mediated charge transport (Figure 1.13). A repair protein in its reduced state can bind to DNA, becoming more easily oxidized so as to transfer an electron to another DNA repair protein bound at a distal site, reducing the distally bound protein and promoting its dissociation. But this DNA-mediated reaction can only occur if the intervening DNA base stack is intact and well stacked; if not, the protein remains associated with the DNA and on a slower time scale can processively migrate to the damaged site. DNA-mediated charge transport thus serves to redistribute the repair proteins in regions of the genome near damage. The redistribution of repair proteins to a damage site using DNA-mediated charge transport essentially provides a way for the proteins to scan large regions of DNA without physically binding to each base. Significantly this scanning for damage is particularly important under conditions of oxidative stress, when guanine radicals are generated. The flash-quench method with ruthenium intercalators was utilized to show that guanine radicals can provide the first signal for repair, also promoting the oxidation of the DNA repair proteins in a DNA-mediated reaction [68].

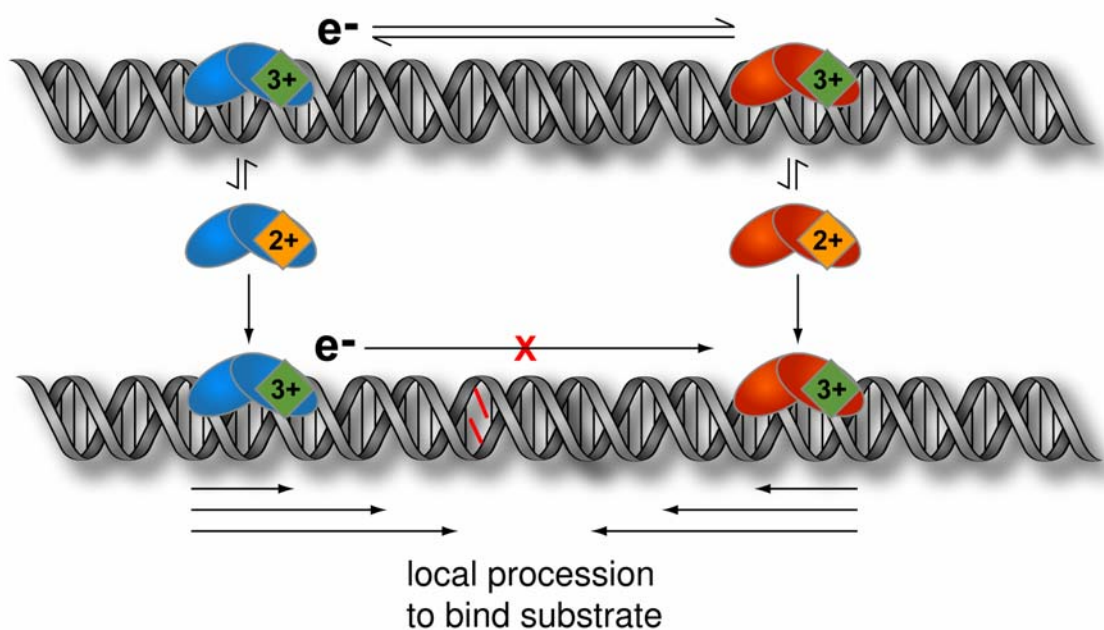


Figure 1.13. A model for understanding how redox active DNA repair proteins communicate to search for damaged bases. Upon binding to DNA, a repair protein in the reduced form undergoes a potential shift such that it can easily give up an electron and thus become oxidized and gain a higher affinity for DNA. The electron can be transferred through the base stack to a distally bound repair protein in the oxidized state, thus promoting its dissociation. This process can occur only if the intervening DNA base pair stack is well coupled. However, if a mismatch disrupts the integrity of the π -stack, the electron will not reach the distally bound protein which will remain in the reduced state with high affinity for DNA. Thus, charge transport, relying on a well coupled π -stack, can serve to redistribute proteins to sites of damage [68].

1.10 Dissertation overview

The work presented in this thesis builds on our expanding knowledge of DNA-mediated charge transport in terms of mechanistic considerations and biological consequences. We continue to refine our model of charge transport through transiently formed DNA domains as a function of distance and sequence using ultrafast hole traps. Chapter 2 describes work investigating the distance independence of charge transport through a fixed length A-tract while in Chapter 3, the distance dependence of charge transport through A-tracts and mixed-sequence bridges is explored using a variety of hole traps and photooxidants. We also examine charge transport in a biological context by investigating its role in the regulation of p53, a transcription factor involved in controlling cellular growth, differentiation, and apoptosis as detailed in Chapter 4. Finally, Chapter 5 describes the synthesis and characterization of a novel tethered ruthenium-quencher conjugate designed to spectroscopically probe DNA charge transport on fast time scales.

1.11 References

- [1] Schleif, R. DNA binding by proteins. *Science* **241**, 1182-1187 (1988).
- [2] Ollis, D.L.; White, S.W. Structural basis of protein-nucleic acid interactions. *Chem. Rev.* **87**, 981-995 (1987).
- [3] Travers, A.A. DNA conformation and protein binding. *Annu. Rev. Biochem.* **58**, 427-452 (1989).
- [4] Watson, J.D.; Crick, F.C.H. A structure for deoxyribonucleic acid. *Nature* **171**, 737 (1953).
- [5] Eley, D.D.; Spivey, D.I. Semiconductivity of organic substances: Nucleic acids in the dry state. *Trans. Faraday Soc.* **58**, 411 (1962).
- [6] Nuñez, M.E.; Barton, J.K. Probing DNA charge transport with metallointercalators. *Curr. Opin. Chem. Biol.* **4**, 199-206 (2000).
- [7] Schuster, G.B. Long-range charge transfer in DNA: Transient structural distortions control the distance dependence. *Acc. Chem. Res.* **33**, 253-260 (2000).
- [8] Giese, B. Long-distance electron transfer through DNA. *Ann. Rev. Biochem.* **71**, 51-70 (2002).
- [9] Voityuk, A.A.; Rösch, N.; Bixon, M.; Jortner, J. Electronic coupling for charge transfer and transport in DNA. *J. Phys. Chem. B.* **104**, 9740-9745 (2000).
- [10] Berlin, Y.A.; Burin, A.L.; Ratner, M.A. Charge hopping in DNA. *J. Am. Chem. Soc.* **123**, 260-268 (2001).
- [11] Marcus, R.A.; Sutin, N. Electron transfers in chemistry and biology. *Biochim. Biophys. Acta.* **811**, 265-322 (1985).

- [12] Gray, H.B.; Winkler, J.R. Electron transfer in proteins. *Annu. Rev. Biochem.* **65**, 573-561 (1996).
- [13] Murphy, C.J.; Arkin, M.R.; Jenkins, Y.; Ghatlia, N.D.; Bossmann, S.H.; Turro, N.J.; Barton, J.K. Long-range photoinduced electron transfer through a DNA helix. *Science* **262**, 1025-1029 (1993).
- [14] Kelley, S.O.; Holmlin, R.E.; Stemp, E.D.A.; Barton, J.K. Photoinduced electron transfer in ethidium-modified DNA duplexes: dependence on distance and base stacking. *J. Am. Chem. Soc.* **119**, 9861-9870 (1997).
- [15] Lewis, F.D.; Wu, T.; Zhang, Y.; Lesting, R.L.; Greenfield, S.R.; Wasielewski, M.R. Distance dependent electron transfer in DNA hairpins. *Science* **277**, 673-676 (1997).
- [16] Augustyn, K.E.; Genereux, J.C.; Barton, J.K. Distance-independent DNA charge transport across an adenine tract. *Angew. Chem. Int. Ed.* In press (2007).
- [17] Hall, D.B.; Barton, J.K. Sensitivity of DNA-mediated electron transfer to the intervening π -stack: a probe for the integrity of the DNA-base stack. *J. Am. Chem. Soc.* **119**, 5045-5046 (1997).
- [18] Arkin, M.R.; Stemp, E.D.A.; Pulver, S.C.; Barton, J.K. Long-range oxidation of guanine by Ru(III) in duplex DNA. *Chem. Biol.* **4**, 389-400 (1997).
- [19] O'Neill, M.A.; Barton, J.K. DNA-mediated charge transport in chemistry and biology. *Top. Curr. Chem.* **236**, 67-115 (2004).
- [20] Waring, M.J. Complex formation between ethidium bromide and nucleic acids. *J. Mol. Biol.* **13**, 269-282 (1965).

- [21] Kelley, S.O.; Barton, J.K. DNA-mediated electron transfer from a modified base to ethidium: π -stacking as modulator of reactivity. *Chem. Biol.* **5**, 413-425 (1998).
- [22] Gasper, S.M.; Schuster, G.B. Intramolecular photoinduced electron transfer to anthraquinones linked to duplex DNA: the effect on gaps and traps on long-range radical cation migration. *J. Am. Chem. Soc.* **119**, 12762-12771 (1997).
- [23] Nakatani, K.; Dohno, C.; Saito, I. Chemistry of sequence-dependent remote guanine oxidation: photoreaction of duplex DNA containing cyanobenzophenone-substituted uridine. *J. Am. Chem. Soc.* **121**, 10854-10855 (1999).
- [24] Giese, B. Long-distance charge transport in DNA: the hopping mechanism. *Acc. Chem. Res.* **33**, 631-636 (2000).
- [25] Matsugo, S.; Kawanishi, S.; Yamamoto, K.; Sugiyama, H.; Matura, T.; Saito, I. Bis(hydroperoxy)naphthaldiiimide as photo-Fenton-reagent: Sequence-specific photochemical DNA cleavage. *Angew. Chem. Int. Ed.* **30**, 1351-1353 (1991).
- [26] Nuñez, M.E.; Noyes, K.T.; Gianolio, D.A.; McLaughlin, L.W.; Barton, J.K. Long-range guanine oxidation in DNA restriction fragments by a triplex-directed naphthalene diimide intercalator. *Biochemistry* **39**, 6190-6199 (2000).
- [27] Kelley, S.O.; Barton, J.K. Electron transfer between bases in double helical DNA. *Science* **283**, 375-381 (1999).
- [28] Musa, O. M.; Horner, J. H.; Shahin, H.; Newcomb, M. Direct measurements of unimolecular radical kinetics employing ultrafast radical rearrangements as reporters. *J. Am. Chem. Soc.* **118**, 3862-3868 (1996).
- [29] Erkkila, K.E.; Odom, D.T.; Barton, J.K. Recognition and reaction of metallointercalators with DNA. *Chem. Rev.* **99**, 2777-2795 (1999).

- [30] Pyle, A.M.; Rehmann, J.P.; Meshoyrer, R.; Kumar, C.V.; Turro, N.J.; Barton, J.K. Mixed ligand complexes of ruthenium(II) – factors governing binding to DNA. *J. Am. Chem. Soc.* **111**, 3051-3058 (1989).
- [31] David, S.S.; Barton, J.K. NMR Evidence for Specific Intercalation of Δ -Rh(phen)₂phi³⁺ in [d(GTCGAC)]₂. *J. Am. Chem. Soc.* **115**, 2984-2985 (1993).
- [32] Hudson, B.P.; Barton, J.K. Solution structure of a metallointercalator bound site specifically to DNA. *J. Am. Chem. Soc.* **120**, 6877-6888 (1998).
- [33] Kielkopf, C.L.; Erkkila, K.E.; Hudson, B.P.; Barton, J.K.; Rees, D.C. Structure of a photoactive rhodium complex intercalated into DNA. *Nat. Struct. Biol.* **7**, 117-121 (2000).
- [34] Turro, C.; Hall, D.B.; Chen, W.; Zuilhof, H.; Barton, J.K. Turro, N.J. Solution photoreactivity of phenanthrenequinone diimine complexes of rhodium and correlations with DNA photocleavage and photooxidation. *J. Phys. Chem. A.* **102**, 5708-5715 (1998).
- [35] Arkin, M.R.; Stemp, E.D.A.; Holmlin, R.E.; Barton, J.K.; Hormann, A.; Olson, E.J.C.; Barbara, P.F. Rates of DNA-mediated electron transfer between metallointercalators. *Science* **273**, 475-480 (1996).
- [36] Friedman, A.E.; Chambron, J.C.; Sauvage, J.P.; Turro, N.J.; Barton, J.K. A molecular light switch for DNA: Ru(bpy)₂(dppz)²⁺. *J. Am. Chem. Soc.* **112**, 4960-4962 (1990).
- [37] Jenkins, Y.; Friedman, A.E.; Turro, N.J.; Barton, J.K. Characterization of dipyridophenazine complexes of ruthenium(II): the light switch effect as a

- function of nucleic acid sequence and conformation. *Biochemistry* **31**, 10809-10816 (1992).
- [38] Stemp, E.D.A.; Arkin, M.R.; Barton, J.K. Oxidation of guanine in DNA by Ru(phen)₂(dppz)³⁺ using the flash quench technique. *J. Am. Chem. Soc.* **119**, 2921-2925 (1997).
- [39] Chang, I.J.; Gray, H.B.; Winkler, J.R. High-driving-force electron transfer in metalloproteins: intramolecular oxidation of ferrocycochrome c by Ru(2,2'-bpy)₂(im)(his-33)³⁺. *J. Am. Chem. Soc.* **113**, 7056-7057 (1991).
- [40] Stemp, E.D.A.; Arkin, M.R.; Barton, J.K. Electron-transfer between metallointercalators bound to DNA: Spectral identification of the transient intermediate. *J. Am. Chem. Soc.* **117**, 2375-2376 (1995).
- [41] Steenken, S.; Jovanovic, S.V. How easily oxidizable is DNA? One-electron reduction potentials of adenosine and guanosine radicals in aqueous solution. *J. Am. Chem. Soc.* **119**, 617-618 (1997).
- [42] Burrows, C.J.; Muller, J.G. Oxidative nucleobase modifications leading to strand scission. *Chem. Rev.* **98**, 1109-1151 (1998).
- [43] Breslin, D.T.; Schuster, G.B. Anthraquinone photoreases: mechanisms for GG-selective and nonselective cleavage of double-stranded DNA. *J. Am. Chem. Soc.* **118**, 2311-2319 (1996).
- [44] Saito, I.; Takayama, M.; Sugiyama, H.; Nakatani, K. Photoinduced DNA cleavage via electron transfer: demonstration that guanine residues located 5' to guanine are the most electron donating sites. *J. Am. Chem. Soc.* **117**, 6406-6407 (1995).

- [45] Kasai, H.; Yamaizumi, Z.; Berger, M.; Cadet, J. Photosensitized formation of 7,8-dihydro-8-oxo-2'-deoxyguanosine (8-hydroxy-2'-deoxyguanosine) in DNA by riboflavin: a nonsinglet oxygen-mediated reaction. *J. Am. Chem. Soc.* **114**, 9692-9694 (1992).
- [46] Ito, K.; Inoue, S.; Yamamoto, K.; Kawanishi, S. 8-Hydroxydeoxyguanosine formation at the 5' site of 5'-GG-3' sequences in double-stranded DNA by UV radiation with riboflavin. *J. Biol. Chem.* **268**, 13221-13227 (1993).
- [47] Sugiyama, H.; Saito, I. Theoretical studies of GG-specific photocleavage of DNA via electron transfer: significant lowering of ionization potential and 5'-localization of HOMO of stacked GG bases in B-Form DNA. *J. Am. Chem. Soc.* **118**, 7063-7068 (1996).
- [48] Holmlin, R.E.; Dandliker, P.J.; Barton, J.K. Charge transfer through the DNA base stack. *Angew. Chem. Int. Ed.* **36**, 2714-2730 (1997).
- [49] Hall, D.B.; Holmlin, R.E.; Barton, J.K. Oxidative DNA damage through long-range electron transfer. *Nature* **382**, 731-735 (1996).
- [50] Nuñez, M.E.; Hall, D.B.; Barton, J.K. Long-range oxidative damage to DNA: effects of distance and sequence. *Chem. Biol.* **6**, 85-97 (1999).
- [51] Nguyen, K.; Steryo, M.; Kurbanyan, K.; Nowitzki, K.M.; Butterfield, S.M.; Ward, S.R.; Stemp, E.D.A. DNA-protein cross-linking from oxidation of guanine via the flash-quench technique. *J. Am. Chem. Soc.* **122**, 3585-3594 (2000).
- [52] Kouchakdijian, M.; Eisenberg, M.; Yarema, K.; Basu, A.; Essigmann, J.; Patel, D.J. NMR studies of the exocyclic 1,N₆-ethenodeoxyadenosine adduct (ϵ DA)

- opposite thymidine in a DNA duplex. Nonplanar alignment of ϵ dA(anti) and dT(anti) at the lesion site. *Biochemistry* **30**, 1820-1828 (1991).
- [53] Nordlund, T.M.; Andersson, S.; Nilsson, L.; Rigler, R.; Graslud, A.; McLaughlin, L.W. Structure and dynamics of a fluorescent DNA oligomer containing the EcoRI recognition sequence: fluorescence, molecular dynamics, and NMR studies. *Biochemistry* **28**, 9095-9103 (1989).
- [54] O'Neill, M.A.; Barton, J.K. DNA charge transport: conformationally gated hopping through stacked domains. *J. Am. Chem. Soc.* **126**, 11471-11483 (2004).
- [55] Nakatani, K.; Dohno, C.; Saito, I. Design of a hole-trapping nucleobase: termination of DNA-mediated hole transport at N₂-cyclopropyldeoxyguanosine. *J. Am. Chem. Soc.* **123**, 9681-9682 (2001).
- [56] Augustyn, K.E.; Shao, F.; Genereux, J.C.; Barton, J.K. Periodicities in DNA charge transport probed with N₂-cyclopropylamine guanine, a kinetically fast hole trap. Submitted.
- [57] Shao, F.; O'Neill, M.A.; Barton, J.K. Long-range oxidative damage to cytosines in duplex DNA. *Proc. Natl. Acad. Sci. USA.* **101**, 17914-17919 (2004).
- [58] Pascaly, M.; Yoo, J.; Barton, J.K. DNA-mediated charge transport: characterization of a DNA radical localized at an artificial nucleic acid base. *J. Am. Chem. Soc.* **124**, 9083-9092 (2002).
- [59] Yoo, J.; Delaney, S.; Stemp, E.D.A.; Barton, J.K. Rapid radical formation by DNA charge transport through sequences lacking intervening guanines. *J. Am. Chem. Soc.* **125**, 6640-6641 (2003).

- [60] Bhattacharya, P.K.; Barton, J.K. Influence of intervening mismatches on long-range guanine oxidation in DNA duplexes. *J. Am. Chem. Soc.* **123**, 8649-8656 (2001).
- [61] Wagenknecht, H.A.; Rajsiki, S.R.; Pascaly, M.; Stemp, E.D.A.; Barton, J.K. Direct observation of radical intermediates in protein-dependent DNA charge transport. *J. Am. Chem. Soc.* **123**, 4400-4407 (2001).
- [62] Shao, F.; Augustyn, K.E.; Barton, J.K. Sequence dependence of charge transport through DNA domains. *J. Am. Chem. Soc.* **127**, 17445-17452 (2005).
- [63] Nuñez, M.E.; Noyes, K.T.; Barton, J.K. Oxidative charge transport through DNA in nucleosome core particles. *Chem. Biol.* **9**, 403-415 (2002).
- [64] Bjorklund, C.C.; Davis, W.B. Attenuation of DNA charge transport by compaction into a nucleosome core particle. *Nucleic Acids Res.* **34**, 1836-1846 (2006).
- [65] Nuñez, M.E.; Holmquist, G.P.; Barton, J.K. Evidence for DNA charge transport in the nucleus. *Biochemistry* **40**, 12465-12471 (2001).
- [66] Merino, E.J.; Barton, J.K. Oxidation by DNA charge transport damages conserved sequence block II, a regulatory element in mitochondrial DNA. *Biochemistry* **46**, 2805-2811 (2007).
- [67] Boal, A.K.; Yavin, E.; Lukianova, O.A.; O'Shea, V.L.; David, S.S.; Barton, J.K. DNA-bound redox activity of DNA repair glycosylases containing [4Fe-4S] clusters. *Biochemistry* **44**, 8397-8407 (2005).
- [68] Yavin, E.; Boal, A.K.; Stemp, E.D.A.; Boon, E.M.; Livingston, A.L.; O'Shea, V.L.; David, S.S.; Barton, J.K. Protein-DNA charge transport: redox activation of

a DNA repair protein by guanine radical. *Proc. Natl. Acad. Sci. USA.* **102**, 3546-3551 (2005).

Chapter 2

Distance-Independent DNA Charge Transport across an Adenine Tract

Adapted from Augustyn, K.E.; Genereux, J.C.; Barton, J.K. *Angew. Chem. Int. Ed.* In press (2007).

2.1 Introduction

The exquisite sensitivity of DNA-mediated charge transport (CT) to the intervening π -stack has been extensively studied using a wide variety of photooxidants and hole traps [1]. A well coupled π -stack facilitates efficient charge transport and exhibits a relatively weak distance dependence rendering this process useful in applications such as nanotechnology and sensing [2-5]. We have proposed a conformationally gated mechanism, governed by base sequence and dynamics [6]. Increasingly, it has become apparent that some form of charge delocalization with a characteristic domain length of 4 bases may occur during this process [6, 7].

Adenine tracts are particularly interesting as a medium for CT due to their resistance to inherent charge trapping, structural homogeneity, and established efficient CT [1, 6, 8-13]. To examine the distance dependence through A-tracts, various donors and acceptors have been employed. Yields of CT from sugar radicals to triple guanine sites were found to decrease exponentially with increasing A-tract length up to three adenine base pairs, but yields through longer A-tracts followed a weaker distance dependence [8]. A thermally activated localized hopping model was developed to explain this weak distance dependence [9]. A later model allowing delocalized states through A-tracts generated yields that were more consistent with the experimental data, and a delocalized polaron model also successfully fit these data [10, 11]. The kinetics of CT through A-tracts were examined later by transient absorption of stilbene capped hairpins; rates with increasingly weak distance dependences were attributed to superexchange, localized hopping, and delocalized hopping with limiting $\beta \sim 0.1 \text{ \AA}^{-1}$ [12]. Studies to examine injection yields of CT through A-tracts have also been performed with

phenothiazine as the hole acceptor and naphthalddiimide as the hole donor, with $\beta = 0.08 \text{ \AA}^{-1}$ [13]. With phenothiazine as the hole donor and 8-oxo guanine as the hole acceptor, a β value of 0.2 \AA^{-1} is observed. Interestingly, when the A-tract was disrupted by insertion of a double guanine site, CT is attenuated. We have investigated charge injection through increasing length A-tracts by monitoring the quenching of photoexcited 2-aminopurine by guanine and also observe a shallow distance dependence ($\beta \sim 0.1 \text{ \AA}^{-1}$) [6].

Significantly, these studies all incorporate hole acceptors external to the A-tract, inherently convoluting transport within the bridge and transport from the bridge to the trap. Here we report the first study of DNA-mediated CT using a probe *interior* to the bridge so as to monitor hole occupation at all positions within the tract. Using N_6 -cyclopropyladenine ($^{\text{CP}}\text{A}$) as the hole acceptor gives us the unique ability to monitor CT to each position on the bridge itself, without modifying the sequence of the duplex.

Cyclopropylamine substituted nucleosides provide an intrinsic DNA base to monitor CT on the picosecond time scale, at guanine (N_2 -cyclopropylguanine, $^{\text{CP}}\text{G}$), adenine, or cytosine (N_4 -cyclopropylcytosine, $^{\text{CP}}\text{C}$) [14-16]. Model studies of a cyclopropylaminium ion show a ring opening rate of $7 \times 10^{11} \text{ s}^{-1}$. This trap is fast enough to compete with back electron transfer (BET) and charge equilibration over the duplex, allowing events that are suppressed on the slower time scale of trapping at double guanine sites to be revealed [8-13]. Given the sensitivity of CT to the integrity of the π -stack, the cyclopropyl modification allows transport to be probed using an endogenous base with minimal perturbation to the duplex. It should be noted that $^{\text{CP}}\text{A}$ -containing duplexes have slightly lower melting temperatures than analogous duplexes without the cyclopropyl modification. The % change in hyperchromicity as a function of temperature however, is

unchanged between the ^{CP}A and unmodified duplexes indicating that stacking is not disrupted. The ^{CP}A probe was first used to demonstrate charge occupation on, rather than tunneling through, adenines [15]. Similarly, our ^{CP}C trap allows observation of hole occupancy on pyrimidines in direct competition with guanine oxidation [16]. These experiments underscore the utility of the kinetic traps in probing preequilibrium CT dynamics.

2.2 Experimental

2.2.1 Oligonucleotide synthesis

Strands containing covalently tethered $[\text{Rh}(\text{phi})_2(\text{bpy}')]^{3+}$ were synthesized using standard phosphoramidite chemistry with a final cleavage of the dimethoxytrityl group. The DNA-bound resin was reacted with carbonyldiimidazole and diammonononane in dioxane resulting in addition of a 5' nine carbon amine linker. The amine-modified resin-bound strands (2 μmol) were added to a solution containing 10 mg of $[\text{Rh}(\text{phi})_2(\text{bpy}')]\text{Cl}_3$ ($\text{bpy}' = 4\text{-(4'-methyl-2,2'-bipyridyl)}$) valerate, the synthesis of which has been described [17], 1.9 mg of N-hydroxybenzotriazole (HOBT), 4.4 mg of O-benzotriazole-N,N,N',N'-tetramethyluronium-hexafluorophosphate (HBTU) in 1 mL dry dimethylformamide (DMF). 4 μL of diisopropylethylamine was added and the reaction was allowed to proceed by gently stirring for 6 hours at ambient temperature. Following reaction, the yellowish resin was washed three times with 5 mL of DMF, acetonile, and MeOH. Rhodium-tethered strands were simultaneously deprotected and cleaved from the resin by incubation in NH_4OH at 60 °C for 6 hours. Strands were purified by reverse-phase HPLC using a Varian C4 column (Figure 2.1). The two diastereomeric conjugates

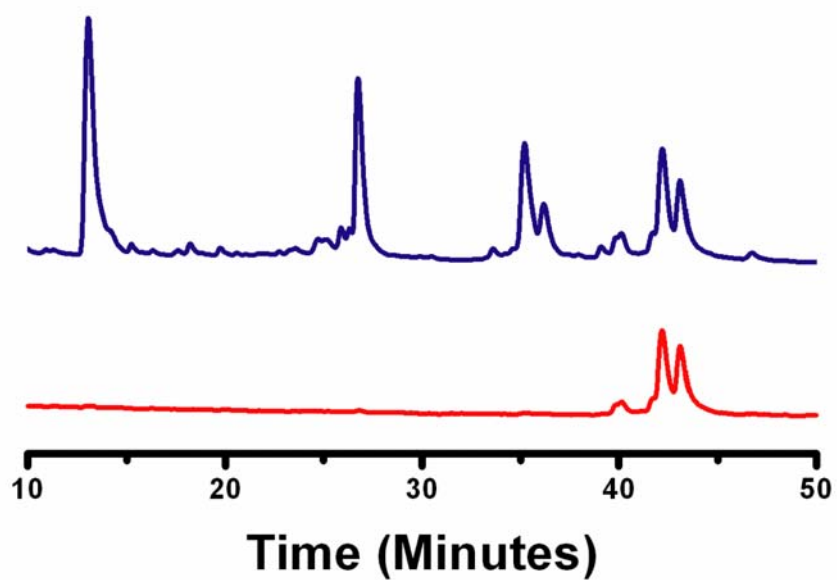


Figure 2.1. Representative reverse-phase HPLC chromatogram monitoring at 260 nm (blue trace, top) and 365 nm (red trace, bottom) for the purification of rhodium-tethered DNA. The two diastereomeric conjugates elute using a gradient of 5-15% acetonitrile against 50 mM ammonium acetate over 45 minutes followed by increasing the acetonitrile percentage to 50 over 5 minutes using a C4 column.

eluted with different retention times but were collected together and used for subsequent experiments. The rhodium-tethered DNA conjugates were characterized by MALDI-TOF mass spectrometry.

Strands containing ^{CP}A were synthesized using standard phosphoramidite chemistry by placing O₆-phenylinosine at the target ^{CP}A site and leaving the 5' trityl group intact. Following overnight incubation at 60 °C in aqueous 6 M cyclopropylamine, resulting in simultaneous cyclopropyl substitution, cleavage, and deprotection, the strands were purified by reverse-phase HPLC. The trityl group was removed by treatment in 80% acetic acid for 15 minutes, repurified by reverse-phase HPLC, and characterized by MALDI-TOF mass spectrometry.

2.2.2 Photooxidation experiments

Duplexes (30 µl aliquots, 10 µM in 20 mM sodium phosphate, 50 mM NaCl, pH 7) were irradiated for various times at 365 nm using a 1000 W Hg/Xe lamp equipped with a 320 nm long-pass filter and monochromator. Decomposition was found to be linear at 30 seconds and all subsequent experiments were carried out with a 30 second irradiation. To assay for ^{CP}A decomposition following irradiation, the samples were subsequently digested into deoxynucleosides by incubating with phosphodiesterase I (USB) and alkaline phosphatase (Roche) overnight at 37 °C. The resulting deoxynucleosides were analyzed by reverse-phase HPLC using a Chemocobond 5-ODS-H, 4.6 mm x 100 mm column. The amount of ^{CP}A decomposition (Y) was determined by subtracting the ratio of the area under the ^{CP}A peak in an irradiated sample over that in a nonirradiated sample from one using inosine as an internal standard for all HPLC traces. Irradiations were

repeated three times and the results averaged. Data are reported with 2 standard errors for a 95% confidence level.

2.3 Results and Discussion

2.3.1 Experimental design

In the present study we constructed three sets of duplexes containing either a 14, 6, or 4 base pair A-tract and a covalently attached $[\text{Rh}(\text{phi})_2(\text{bpy}')]^{3+}$ serving as the intercalating photooxidant (Table 2.1, Figure 2.2). $^{\text{CP}}\text{A}$ was serially substituted at each site of the A-tract by reacting the commercially available O₆-phenylinosine precursor with aqueous cyclopropylamine. For all assemblies, there is a constant 4 base pair segment surrounding the rhodium binding site for optimal intercalation of the photooxidant. Figure 2.2 shows a schematic illustration of the three sets of duplexes with an arrow over the A-tract indicating all possible positions of $^{\text{CP}}\text{A}$ substitution. Here, the assemblies are depicted with rhodium intercalating between the third and fourth base pairs from the 5' terminus although intercalation between the second and third base pairs is equally probable due to the diastereomeric nature of the conjugates. Although the trapping rate of guanine is slow on the time scale of $^{\text{CP}}\text{A}$ ring opening, back electron transfer to rhodium is fast so inosine was used in place of guanine in positions proximal to the hole trap to eliminate possibilities of back electron. The duplexes were subsequently irradiated at 365 nm for 30 seconds to induce hole injection into the DNA. Following enzymatic digestion with phosphodiesterase I and alkaline phosphatase, the resulting deoxynucleosides were analyzed by reverse-phase HPLC to quantify the amount

Table 2.1. ^{CP}**A-containing DNA assemblies**

DNA #	Sequence ^a
Rh-A4-1	3' -TICTI X AAAGGTCTAATCTG-5' 5' -Rh-ACIACTTTTCCAGATTAGAC-3'
Rh-A4-2	3' -TICTIA X AAGGTCTAATCTG-5' 5' -Rh-ACIACTTTTCCAGATTAGAC-3'
Rh-A4-3	3' -TICTIAA X AGGTCTAATCTG-5' 5' -Rh-ACIACTTTTCCAGATTAGAC-3'
Rh-A4-4	3' -TICTIAAA X GGTCTAATCTG-5' 5' -Rh-ACIACTTTTCCAGATTAGAC-3'
Rh-A6-1	3' -TICTI X AAAAAGGTCTTCTG-5' 5' -Rh-ACIACTTTTTTCCAGAAGAC-3'
Rh-A6-2	3' -TICTIA X AAAAGGTCTTCTG-5' 5' -Rh-ACIACTTTTTTCCAGAAGAC-3'
Rh-A6-3	3' -TICTIAA X AAAGGTCTTCTG-5' 5' -Rh-ACIACTTTTTTCCAGAAGAC-3'
Rh-A6-4	3' -TICTIAAA X AAGGTCTTCTG-5' 5' -Rh-ACIACTTTTTTCCAGAAGAC-3'
Rh-A6-5	3' -TICTIAAAA X AGGTCTTCTG-5' 5' -Rh-ACIACTTTTTTCCAGAAGAC-3'
Rh-A6-6	3' -TICTIAAAAA X GGTCTTCTG-5' 5' -Rh-ACIACTTTTTTCCAGAAGAC-3'
Rh-A14-1	3' -TICTI X AAAAAAAAAAAAAGGTCTTG-5' 5' -Rh-ACIACTTTTTTTTTTTTTTTTCCAGAAC-3'
Rh-A14-2	3' -TICTIA X AAAAAAAAAAAAAGGTCTTG-5' 5' -Rh-ACIACTTTTTTTTTTTTTTTTCCAGAAC-3'
Rh-A14-3	3' -TICTIAA X AAAAAAAAAAAAAGGTCTTG-5' 5' -Rh-ACIACTTTTTTTTTTTTTTTTCCAGAAC-3'
Rh-A14-4	3' -TICTIAAA X AAAAAAAAAAAAAGGTCTTG-5' 5' -Rh-ACIACTTTTTTTTTTTTTTTTCCAGAAC-3'
Rh-A14-5	3' -TICTIAAAA X AAAAAAAAAAAAAGGTCTTG-5' 5' -Rh-ACIACTTTTTTTTTTTTTTTTCCAGAAC-3'

Rh-A14-6	3' -TICTIAAAAAA X AAAAAAAGGTCTTG-5' 5' -Rh-ACIACTTTTTTTTTTTTTTTTCCAGAAC-3'
Rh-A14-7	3' -TICTIAAAAAA X AAAAAAAGGTCTTG-5' 5' -Rh-ACIACTTTTTTTTTTTTTTTTCCAGAAC-3'
Rh-A14-8	3' -TICTIAAAAAA X AAAAAAAGGTCTTG-5' 5' -Rh-ACIACTTTTTTTTTTTTTTTTCCAGAAC-3'
Rh-A14-9	3' -TICTIAAAAAA X AAAAAGGTCTTG-5' 5' -Rh-ACIACTTTTTTTTTTTTTTTTCCAGAAC-3'
Rh-A14-10	3' -TICTIAAAAAA X AAAAGGTCTTG-5' 5' -Rh-ACIACTTTTTTTTTTTTTTTTCCAGAAC-3'
Rh-A14-11	3' -TICTIAAAAAA X AAAGGTCTTG-5' 5' -Rh-ACIACTTTTTTTTTTTTTTTTCCAGAAC-3'
Rh-A14-12	3' -TICTIAAAAAA X AAGGTCTTG-5' 5' -Rh-ACIACTTTTTTTTTTTTTTTTCCAGAAC-3'
Rh-A14-13	3' -TICTIAAAAAA X AGGTCTTG-5' 5' -Rh-ACIACTTTTTTTTTTTTTTTTCCAGAAC-3'
Rh-A14-14	3' -TICTIAAAAAA X GGTCTTG-5' 5' -Rh-ACIACTTTTTTTTTTTTTTTTCCAGAAC-3'

a. X = N_6 -cyclopropyladenine, ^{CP}A

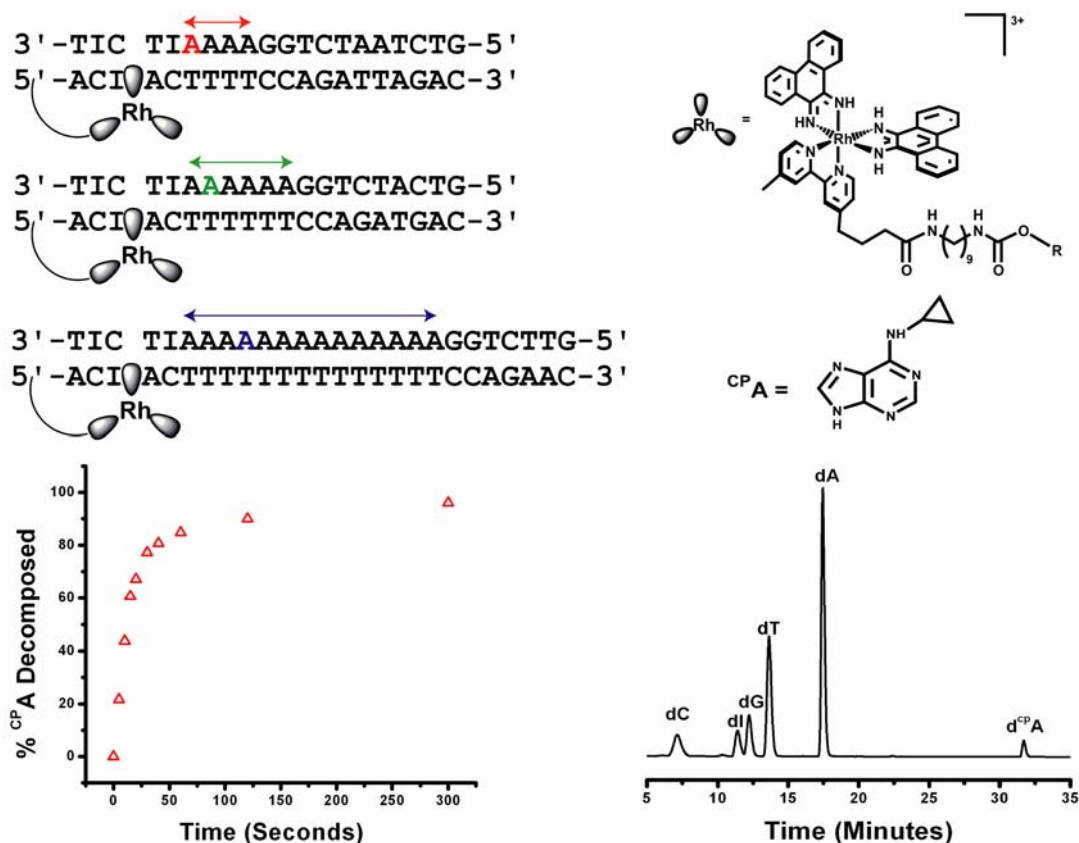


Figure 2.2. Examples of duplexes used in this study for the ^{CP}A4, 6, and 14 series. One position of ^{CP}A is indicated in color with an arrow spanning the A-tract indicating all employed positions of substitution. Also shown is the structure of the rhodium photooxidant, $[Rh(\phi)_2(bpy')]^{3+}$, and the ^{CP}A nucleoside. A representative HPLC trace monitoring at 260 nm shows the relative retention times of the various nucleosides. A plot of ^{CP}A decomposition as a function of irradiation time as determined by HPLC for the 14 base pair adenine tract in which ^{CP}A is substituted at the first position is also shown.

of ^{CP}A decomposition relative to a non-irradiated standard [7, 15]. As shown in Figure 2.2, irradiation time courses confirm that ^{CP}A decomposition is not saturating at 30 seconds. Prior experiments with both ^{CP}C and ^{CP}G showed variation in decomposition as a function of sequence indicating that ring opening is not rate limiting [7].

2.3.2 Decomposition as a function of bridge position in A-tracts

Figure 2.3 shows the decomposition yield (Y) as a function of ^{CP}A bridge position. Y is determined by calculating the fraction of ^{CP}A -containing duplexes undergoing ring opening. Remarkably, over the 14 base pair A-tract, we find essentially no decay, $\beta = 0.0013(3) \text{ \AA}^{-1}$. This result markedly contrasts with the larger values found using acceptors external to the bridge [8-13]. The flatness implies that all holes reach the A-tract terminus following injection. Thus, the time scale for transport over the entire 48 \AA A-tract must be faster than BET from the first bridge position [14, 18]. A range of experiments have found that BET over several base pairs can occur on the picosecond time scale [19]. The inclusion of inosines near the rhodium binding site also retards competing back electron transfer processes. CT across the A-tract must be faster. These data cannot be accounted for by a localized hopping mechanism through the 14 bases of the A-tract.

2.3.3 Comparison with other systems

For hole acceptors external to the bridge there is consensus in the current literature that the distance dependence is characterized by a β value of $\sim 0.1\text{-}0.2 \text{ \AA}^{-1}$. Guanine damage experiments result in a shallow distance dependence, but this can be

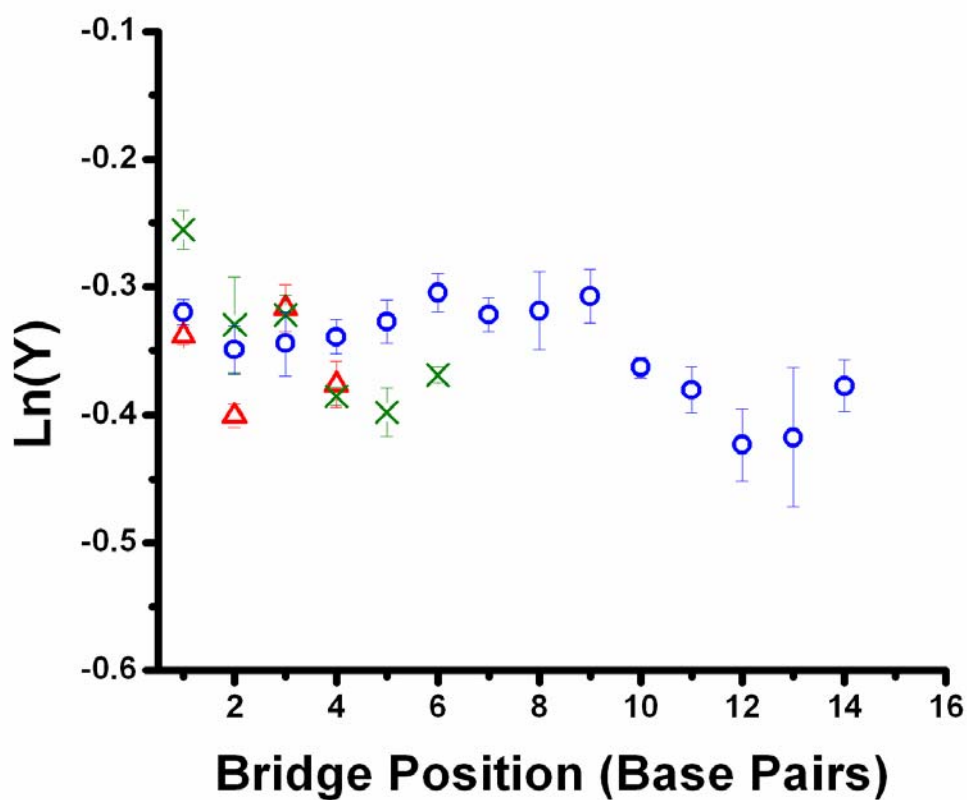


Figure 2.3. Decomposition (Y), as a function of bridge position for the ${}^{\text{CP}}\text{A-4}$ (red triangles), 6 (green Xs), and 14 (blue circles) series following a 30 second irradiation at 365 nm. Decomposition was determined by integrating the HPLC peak corresponding to ${}^{\text{CP}}\text{A}$ in an irradiated sample relative to a non-irradiated sample. Each HPLC trace was normalized to an internal inosine standard. The bars correspond to two standard errors for a 95% confidence level (see Experimental).

attributed to charge equilibration prior to the millisecond trapping event [5, 8, 20]. Our present result is not subject to this problem as the cyclopropylamine ring opening occurs faster than charge equilibration. We previously found that the stacking of the donor and acceptor with the DNA bases has a dramatic effect on the distance dependence of CT through A-tracts [5]. When ethenoadenine, a poorly stacked adenine analogue, was used as the photooxidant, a steeper β value of 1.0 \AA^{-1} is found, consistent with poorly coupled superexchange. This is a characteristic value found for purely σ -bonded systems [21]. With the well-stacked adenine analogue, 2-aminopurine, as photooxidant, the distance dependence is that expected in well-stacked systems. Note that there is only a 200 mV potential difference between ethenoadenine and 2-aminopurine. The marked difference in distance dependences found for these two systems therefore cannot be due to energetics alone. In this context, the present results are not surprising. Our trap is well coupled with and isoenergetic to the bridge, and thus we observe distance-independent CT. Interestingly, when a G intervenes within an A-tract, CT is attenuated [5, 7, 13].

This dramatic difference in distance dependence found using a trap endogenous to the bridge underscores the importance of coupling to the trap. In a variety of conductivity experiments, it has been found that poor coupling between the probe and the bridge can dominate the measured response [22]. By employing such a well-coupled system, we are able to observe the inherent distance independence of CT through the A-tract. These results are completely consistent with a fully delocalized transport model.

Thus, a well-coupled trap incorporated into an A-tract bridge can be oxidized through DNA-mediated CT without significant attenuation over 5 nm. This result

highlights the importance of the coupling of the acceptor to the bridge and further validates the widespread interest in DNA as a charge conduit in nanotechnology.

2.4 References

- [1] (a) Hall, D.B.; Holmlin, E.R.; Barton, J.K. Oxidative DNA damage through long-range electron transfer *Nature* **382**, 731-735 (1996). (b) Nuñez, M.E.; Hall, D.B.; Barton, J.K. Long-range oxidative damage to DNA: Effects of distance and sequence. *Chem. Biol.* **6**, 85-97 (1999). (c) Henderson, P.T.; Jones, D.; Hampikian, G.; Kan, Y.Z.; Schuster, G.B. Long-distance charge transport in duplex DNA: the phonon-assisted polaron-like hopping mechanism. *Proc. Natl. Acad. Sci. USA.* **96**, 8353-8358 (1999). (d) Bixon, M.; Giese, B.; Wessely, S.; Langenbacher, T.; Michel-Beyerle, M.E.; Jortner, J. Long-range charge hopping in DNA. *Proc. Natl. Acad. Sci. USA.* **96**, 11713-11716 (1999). (e) Kawai, K.; Takada, T.; Tojo, S.; Ichinose, N.; Majima, T. Observation of hole transfer through DNA by monitoring the transient absorption of pyrene radical cation. *J. Am. Chem. Soc.* **123**, 12688-12689 (2001). (f) Lewis, F.D.; Letsinger, R.L.; Wasielewski, M.R. Dynamics of photoinduced charge transfer and hole transport in synthetic DNA hairpins. *Acc. Chem. Res.* **34**, 159-170 (2001).
- [2] (a) Kelley, S.O.; Jackson, N.M.; Hill, M.G.; Barton, J.K. Long-range electron transfer through DNA films. *Angew. Chem. Int. Ed.* **38**, 941-945 (1999). (b) Boon, E.M.; Ceres, D.M.; Drummond, T.G.; Hill, M.G.; Barton, J.K. Mutation detection by electrocatalysis at DNA-modified electrodes. *Nat. Biotechnol.* **18**, 1096-1100 (2000). (c) Boon, E.M.; Salas, J.E.; Barton, J.K. An electrical probe of protein-DNA interactions on DNA-modified surfaces. *Nat. Biotechnol.* **20**, 282-286 (2002).

- [3] (a) Boon, E.M.; Livingston, A.L.; Chmiel, N.H.; David, S.S.; Barton, J.K. DNA-mediated charge transport for DNA repair. *Proc. Natl. Acad. Sci. USA*. **100**, 12543-12547 (2003). (b) Boal, A.K.; Yavin, E.; Lukianova, O.A.; O'Shea, V.L.; David, S.S.; Barton, J.K. DNA-bound redox activity of DNA repair glycosylases containing [4Fe-4S] clusters. *Biochemistry* **44**, 8397-8407 (2005).
- [4] (a) Kelley, S.O.; Holmlin, E.R.; Stemp, E.D.A.; Barton, J.K. Photoinduced electron transfer in ethidium-modified DNA duplexes: dependence on distance and base stacking. *J. Am. Chem. Soc.* **199**, 9861-9870 (1997). (b) Bhattacharya, P.K.; Barton, J.K. The influence of intervening mismatches on long-range guanine oxidation in DNA duplexes. *J. Am. Chem. Soc.* **123**, 8649-8656 (2001). (c) Hall, D.B.; Barton, J.K. Sensitivity of DNA-mediated electron transfer to the intervening π -stack: a probe for the integrity of the DNA base stack. *J. Am. Chem. Soc.* **119**, 5045-5046 (1997).
- [5] (a) Kelley, S.O.; Barton, J.K. Electron transfer between bases in double helical DNA. *Science* **283**, 375-381 (1999). (b) O'Neill, M.A.; Barton, J.K. DNA-mediated charge transport chemistry and biology. *Top. Curr. Chem.* **236**, 67-115 (2004). (c) Williams, T.T.; Odom, D.T.; Barton, J.K. Variations in DNA charge transport with nucleotide composition and sequence. *J. Am. Chem. Soc.* **122**, 9048-9049 (2000).
- [6] (a) O'Neill, M.A.; Barton, J.K. DNA charge transport: conformationally gated hopping through stacked domains. *J. Am. Chem. Soc.* **126**, 11471-11483 (2004). (b) Wan, C.Z.; Fiebig, T.; Kelley, S.O.; Treadway, C.R.; Barton, J.K.; Zewail, A.H. Femtosecond dynamics of the DNA intercalator ethidium and electron

- transfer with mononucleotides in water. *Proc. Natl. Acad. Sci. USA.* **96**, 6014-6019 (1999). (c) O'Neill, M.A.; Becker, H.C.; Wan, C.Z.; Barton, J.K.; Zewail, A.H. Ultrafast dynamics in DNA-mediated electron transfer: base gating and the role of temperature. *Angew. Chem. Int. Ed.* **42**, 5896-5900 (2003). (d) O'Neill, M.A.; Barton, J.K. DNA-mediated charge transport requires conformational motion of the DNA bases: elimination of charge transport in rigid glasses at 77 K. *J. Am. Chem. Soc.* **126**, 13234-13235 (2004).
- [7] (a) Shao, F.; Augustyn, K.E.; Barton, J.K. Sequence dependence of charge transport through DNA domains. *J. Am. Chem. Soc.* **127**, 17445-17452 (2005). (b) Conwell, E.M.; Rakhmanova, S.V. Polarons in DNA. *Proc. Natl. Acad. Sci. USA.* **97**, 4556-4560 (2000). (c) Kendrick, T.; Giese, B. Charge transfer through DNA triggered by site selective charge injection into adenine. *Chem. Comm.* 2016-2017 (2002). (d) Barnett, R.N.; Cleveland, C.L.; Joy, A.; Landman, U.; Schuster, G.B. Charge migration in DNA: ion-gated transport. *Science* **294**, 567-571 (2001).
- [8] Giese, B.; Amaudrut, J.; Kohler, A.; Spormann, M.; Wessely, S. Direct observation of hole transfer through DNA by hopping between adenine bases and by tunneling. *Nature* **412**, 318-320 (2001).
- [9] (a) Jortner, J.; Bixon, M.; Langenbacher, T.; Michel-Beyerle, M.E. Charge transfer and transport in DNA. *Proc. Natl. Acad. Sci. USA.* **95**, 12759-12765 (1998). (b) Bixon, M.; Jortner, J. Long-range and very long-range charge transport in DNA. *Chem. Phys.* **281**, 393-408 (2002).

- [10] Renger, T.; Marcus, R.A. Variable-range hopping electron transfer through disordered bridge states: applications to DNA. *J. Phys. Chem. A.* **107**, 8404-8419 (2003).
- [11] (a) Basko, D.M.; Conwell, E.M. Effect of salvation on hole motion in DNA. *Phys. Rev. Lett.* **88**, 98-102 (2002). (b) Conwell, E.M.; Park, J.H.; Choi, H.Y. Polarons in DNA: transition from guanine to adenine transport. *J. Phys. Chem. B.* **109**, 9760-9763 (2005).
- [12] (a) Lewis, F.D.; Zhu, H.; Daublain, P.; Cohen, B.; Wasielewski, M.R. Hole mobility in DNA A-tracts. *Angew. Chem. Int. Ed.* **45**, 7982-7985 (2006). (b) Lewis, F.D.; Zhu, H.; Daublain, P.; Fiebig, T.; Raytchev, M.; Wang, Q.; Shafirovich, V. Crossover from superexchange to hopping as the mechanism for photoinduced charge transfer in DNA hairpin conjugates. *J. Am. Chem. Soc.* **128**, 791-800 (2006).
- [13] (a) Kawai, K.; Takada, T.; Tojo, S.; Majima, T. Kinetics of weak distance-dependent hole transfer in DNA by adenine-hopping mechanism. *J. Am. Chem. Soc.* **125**, 6842-6843 (2003). (b) Takada, T.; Kawai, K.; Cai, X.; Sugimoto, A.; Fujitsuka, M.; Majima, T. Charge separation in DNA via consecutive adenine hopping. *J. Am. Chem. Soc.* **126**, 1225-1129 (2004). (c) Takada, T.; Kawai, K.; Fujitsuka, M.; Majima, T. Rapid long-distance hole transfer through consecutive adenine sequence. *J. Am. Chem. Soc.* **128**, 11012-11013 (2006).
- [14] (a) Nakatani, K.; Dohno, C.; Saito, I. Design of a hole-trapping nucleobase: termination of DNA-mediated hole transport at N₂-cyclopropyldeoxyguanosine. *J. Am. Chem. Soc.* **123**, 9681-9682 (2001). (b) O'Neill, M.A.; Dohno, C.; Barton,

- J.K. Direct chemical evidence for charge transfer between photoexcited 2-aminopurine and guanine in duplex DNA. *J. Am. Chem. Soc.* **126**, 1316-1317 (2004). (c) Musa, O.M.; Horner, J.H.; Shahin, H.; Newcomb, M. A kinetic scale for dialkylaminy radical reactions. *J. Am. Chem. Soc.* **118**, 3862-3868 (1996).
- [15] Dohno, C.; Ogawa, A.; Nakatani, K.; Saito, I. Hole trapping at N₆-cyclopropyldeoxyadenosine suggests a direct contribution of adenine bases to hole transport through DNA. *J. Am. Chem. Soc.* **125**, 10154-10155 (2003).
- [16] Shao, F.; O'Neill, M.A.; Barton, J.K. Long-range oxidative damage to cytosines in duplex DNA. *Proc. Natl. Acad. Sci. USA.* **101**, 17914-17919 (2004).
- [17] Sitlani, A.; Long, E.C.; Pyle, A.M.; Barton, J.K. DNA photocleavage by phenanthrenequinone diimine complexes of rhodium(III): shape-selective recognition and reaction. *J. Am. Chem. Soc.* **114**, 2303-2311 (1992).
- [18] Williams, T.T.; Dohno, C.; Stemp E.D.A.; Barton, J.K. Effects of the photooxidant on DNA-mediated charge transport. *J. Am. Chem. Soc.* **126**, 8148-8158 (2004).
- [19] (a) Arkin, M.R.; Stemp, E.D.A.; Holmlin, R.E.; Barton, J.K.; Hormann, A; Olson, E.J.C.; Barbara, P.F. Rates of DNA-mediated electron transfer between metallointercalators. *Science* **273**, 475-480 (1996). (b) Reid, G.D.; Whittaker, D.J.; Day, M.A.; Turton, D.A.; Kayser, V.; Kelly, J.M.; Beddard, G.S. Femtosecond electron-transfer reactions in mono- and polynucleotides and in DNA. *J. Am. Chem. Soc.* **124**, 5518-5527 (2002).

- [20] Delaney, S.; Yoo, J.; Stemp, E.D.A.; Barton, J.K. Charge equilibration between two distinct sites in double helical DNA. *Proc. Natl. Acad. Sci. USA*. **101**, 10511-10516 (2004).
- [21] Gray, H.B.; Winkler, J.R. Electron transfer in proteins. *Annu. Rev. Biochem.* **65**, 573-561 (1996).
- [22] (a) Nitzan, A.; Ratner, M.A. Electron transport in molecular wire junctions. *Science* **300**, 1384-1389 (2003). (b) Cui, X.D.; Primak, A.; Zarate, X.; Tomfohr, J.; Sankey, O.F.; Moore, L.; Moore, T.A.; Gust, D.; Harris, G.; Lindsay, S.M. Reproducible measurement of single-molecule conductivity. *Science* **294**, 571-574 (2001) (c) Ceres, D.M.; Udit, A.K.; Hill, H.D.; Hill, M.G.; Barton, J.K. Differential ionic permeation of DNA-modified electrodes. *J. Phys. Chem. B*. **111**, 663-668 (2007).

Chapter 3

Periodicities in DNA Charge Transport Probed with N_2 -Cyclopropylguanine, a Kinetically Fast Hole Trap

*Adapted from Augustyn, K.E.; Shao, F.; Genereux, J.C.; Barton, J.K. Submitted for publication in 2007.

** Dr. Fangwei Shao synthesized the Ap and AQ- containing strands and performed the fluorescence and gel electrophoresis experiments whereas Dr. Katherine Augustyn synthesized the remaining sequences and carried out the ^{CP}G decomposition studies. Joseph Genereux performed the data fitting analyses.

3.1 Introduction

Charge transport (CT) through the DNA double helix has been extensively studied over a wide range of distances using various pendant photooxidants and hole acceptors [1-9]. CT through the π -stacked array of bases can proceed over distances of 200 Å with a shallow distance dependence [10, 11]. This shallow distance dependence coupled with a sensitivity to perturbations in base pair stacking has led to the development of acute DNA-based diagnostic sensors [12]. This chemistry has further prompted the consideration of biological roles for CT in the context of how DNA is damaged and repaired in the cell [13, 14].

Despite a wide range of measurements of DNA CT using a variety of techniques, there is still debate over the mechanistic description of this phenomenon [15-23]. Models for CT commonly fall within two extremes, tunneling, where the charge only virtually occupies the DNA bridge, and hopping, where, in an incoherent process, discrete radicals occupy and migrate across the bridge. An interesting proposal was made to account for the varied behavior of DNA CT by including both components of hopping among low energy guanine sites and tunneling through higher energy bases [24]. Many studies showing significant oxidative guanine damage across long tracts of adenines, however, sharply contrasted this model [4, 25, 26]. More recently we have found that discrete radical density also arises on intervening pyrimidines and with occupancies quite comparable to neighboring guanine sites [27]. We have also seen that DNA CT is conformationally gated by motions of the hole donor and bases within the bridge [28-30]. We have therefore developed a model in which four to five neighboring bases act in concert to form an extended π -orbital that can accept a migrating charge [27, 31]. These

delocalized domains, forming and dissolving as a function of sequence-dependent dynamics, facilitate hole transport through the DNA duplex.

The fast cyclopropylamine radical trap has been used effectively in a variety of studies to probe the mechanism of DNA CT [27, 32-36]. Model studies suggest that the oxidative ring opening occurs on a time scale of $\sim 10^{-12}$ s [37]. The ring opening reaction of cyclopropylamine-substituted bases upon oxidation is conveniently monitored by enzymatic DNA digestion followed by HPLC analysis of the resulting deoxynucleosides. Moreover, this hole is trapped is much more rapidly than on the guanine radical, which decays in aerated aqueous solution in $10^{-4} - 10^{-3}$ s [38]. While biochemical studies of guanine damage have been fruitful in establishing that the reaction occurs at long range and is sensitive to mismatches and protein binding, studies of mechanism and inferences of relative CT rates cannot be reliably made with such a slow radical trap. Indeed, biochemical measurements actually monitor the formation of irreversible products of guanine oxidation several steps removed from the formation of its radical [39].

Saito and co-workers first examined long-range DNA CT using *N*₂-cyclopropylguanine (^{CP}G) to provide a faster hole trap for mechanistic investigations [32]. They went on to show definitively that the charge does not tunnel through adenines in studies using *N*₆-cyclopropyladenine (^{CP}A) to trap radicals in the bridge [33]. In our laboratory, we first applied ^{CP}G in DNA CT studies to show chemically that the photoinduced quenching of 2-aminopurine (Ap) by guanine in DNA duplexes is the result of DNA CT [34]. We then utilized ^{CP}G to compare DNA CT with different photooxidants [35]. We demonstrated that some potent photooxidants, including thionine and our rhodium intercalator, which give low yields in guanine damage due to

competitive back electron transfer (BET) relative to radical trapping, exhibit higher CT yields with the fast ^{CP}G trap. Most importantly, in the context of mechanism, we recently carried out DNA CT studies using *N*₄-cyclopropylcytosine (^{CP}C). In this work, it was evident that in DNA CT, not only does the charge occupy low energy purines, but a comparable amount of hole density is found on pyrimidines [27, 36].

Given the utility of the fast cyclopropylamine-substituted base trap in mechanistic studies, we have now reinvestigated DNA CT as a function of sequence and distance using ^{CP}G. For repetitive adenine tracts, we find a remarkable periodic dependence in the decay with distance, and for most other repetitive sequences, the decay is not monotonic. It is worthwhile noting that a periodic decay with distance has been seen previously in studies of DNA CT using fluorescence quenching of Ap by guanine to determine CT yield reporting on a subnanosecond time scale [31]. Here a period of 4-5 bases was observed. This assay of fluorescence quenching, like ^{CP}G ring opening, provides a measurement of CT on a fast time scale, but unlike ^{CP}G ring opening, Ap quenching measures charge injection into the DNA bridge. When normalized to duplexes with inosine replacing guanine, coherent CT events are revealed. Using ^{CP}G as the hole trap, we find a periodicity of 4-5 bases, consistent with CT through delocalized domains.

3.2 Experimental

3.2.1 Oligonucleotide synthesis

DNA oligonucleotides were synthesized using standard phosphoramidite chemistry on an ABI DNA synthesizer. Cyclopropylamine-substituted sequences were prepared by incorporating the precursor base, 2-fluorinosine at the desired position for substitution and, during synthesis, leaving the trityl group intact. The resin was then reacted with 1 M diaza(1,3)bicyclo[5.4.0]undecane (DBU) in acetonitrile to effectively remove the oxygen protecting group. The oligonucleotides were subsequently incubated overnight in 6 M aqueous cyclopropylamine at 60 °C, resulting in substitution and simultaneous cleavage from the resin. The cleaved strands were dried *in vacuo* and purified by reverse-phase HPLC. The trityl group was then removed by treatment in 80% acetic acid for 15 minutes. The detritylated strands were repurified by reverse-phase HPLC. Oligonucleotides were characterized by MALDI-TOF mass spectrometry.

Rhodium-modified oligonucleotides were synthesized as described previously [40]. The detritylated resin-bound oligonucleotides were first modified with a nine-carbon amine linker by reaction with carbonyldiimidazole and diamnononane in dioxane. The amine-modified strands were then reacted with $[\text{Rh}(\text{phi})_2(\text{bpy}')]\text{Cl}_3$ ($\text{bpy}' = 4\text{-(4'-methyl-2,2'-bipyridyl) valerate}$) in 1:1:1 methanol:acetonitrile:isopropanol using O-(N-succinimidyl)-1,1,3,3-tetramethyl uranium tetrafluoroborate (TSTU) as the coupling reagent. Cleavage from the resin was accomplished by incubation in NH_4OH at 60 °C for 6 hours. Strands were HPLC-purified using a Varian C4 reverse-phase column. The two diastereomeric conjugates, differing in configuration at the metal center, have different retention times. However, both isomers were collected together and used for

subsequent experiments. MALDI-TOF mass spectrometry was used to characterize the metallated DNA conjugates.

Anthraquinone (AQ)-tethered oligonucleotides were synthesized as described previously by incorporating an anthraquinone phosphoramidite at the 5' end of the oligonucleotide [41]. The DNA was deprotected in NH_4OH at 60 °C overnight. The resulting oligonucleotides were purified once by reverse-phase HPLC and characterized by MALDI-TOF mass spectrometry.

Oligonucleotides containing 2-Aminopurine were synthesized on the DNA synthesizer using an aminopurine phosphoramidite (Glen Research). Ap-containing strands were synthesized leaving the trityl group intact, and purified twice by reverse-phase HPLC. The strands were characterized by MALDI-TOF mass spectrometry.

All oligonucleotides were suspended in a buffer containing 20 mM sodium phosphate, 50 mM NaCl, pH 7 and quantified using UV-visible spectroscopy. Duplexes were prepared by heating equal concentrations of complementary strands to 90 °C for 5 minutes and slow cooling to ambient temperature. Melting temperatures (T_m) were obtained for all duplexes. All duplexes melted between 55-60 °C at a 1.5 μM concentration in 20 mM sodium phosphate, 50 mM NaCl, pH 7.

3.2.2 Photooxidation experiments

Photooxidations of Rh-tethered oligonucleotides were carried out by irradiating 30 μL aliquots of 10 μM duplex in a buffer containing 20 mM sodium phosphate, 50 mM NaCl, pH 7, for 30 seconds at 365 nm on a 1000 W Hg/Xe lamp equipped with a 320 nm

long pass filter and monochromator. AQ-containing duplexes in the same buffer (30 μ l, 10 μ M) were irradiated at 350 nm using the same apparatus for 5 minutes. Irradiation times were varied and the decomposition was linear over the times used as shown in Figure 3.2. Samples were irradiated at various temperatures ranging from 20 to 80 °C.

To analyze for ^{CP}G ring opening following irradiation, the samples were digested by phosphodiesterase I (USB) and alkaline phosphatase (Roche) at 37 °C for 24 hours. The resulting deoxynucleosides were analyzed by reverse-phase HPLC using a Chemcobond 5-ODS-H, 4.6 mm \times 100 mm column. The amount of ^{CP}G decomposition (Y) was determined by subtracting the ratio of the area under the ^{CP}G peak in an irradiated sample over that in a non irradiated sample from one using thymidine as an internal standard for all HPLC traces. Irradiations were repeated three times and the results averaged.

To analyze for guanine oxidation, reactions were carried out analogously to those previously described [1, 10, 35]. DNA strands were first labeled at the 5' end with [³²P] γ -ATP using polynucleotide kinase and purified on a 20% denaturing polyacrylamide gel (Sequagel). The desired band was identified by autoradiography, excised from the gel and eluted into 500 mM ammonium acetate. Labeled DNA was isolated using Micro Bio-Spin 6 columns (BioRad) and hybridized to complementary strands in a buffer containing 20 mM sodium phosphate, 50 mM NaCl, pH 7. AQ-containing duplexes (4 μ M) were irradiated for 1 hour at 350 nm using a 1000 W Hg/Xe lamp containing a 320 nm long-pass filter and monochromator. Following irradiation, samples were treated with 10% piperidine, heated to 90 °C for 30 minutes, and dried *in vacuo*. Samples were eluted through a 20% denaturing polyacrylimide gel for 1.5 hours at 90 W and imaged on a Storm 820 phosphoimager (Molecular Dynamics/ GE Healthcare). Oxidative damage

products were quantified by phosphoimagery using Image Quant 5.2 (Molecular Dynamics).

3.2.3 Fluorescence-quenching experiments

Steady-state fluorescence measurements of Ap containing DNA oligonucleotides were conducted using an ISS K2 spectrofluorimeter (5 mm path length) equipped with a Peltier-controlled thermostated sample holder (Quantum Northwest). Aliquots (300 μ L) were prepared by annealing Ap-containing DNA strands (50 μ M) and their complements in 100 mM sodium phosphate, pH 7. Emission spectra were obtained by exciting at 325 nm and monitoring the integrated emission between 340 and 500 nm. Temperature fluctuations during spectral acquisition were less than \pm 0.02 $^{\circ}$ C. CT yields were obtained from emission spectra by comparing the observed fluorescence intensity of the redox-active duplexes containing guanine to that of the redox-inactive duplexes containing inosine [31, 42]. The redox-inactive reference was employed to delineate CT from other modes of quenching. The fraction of fluorescence quenching, F_q , due to CT was quantified as $F_q = 1 - (\Phi_G/\Phi_I)$. Relative quantum yields (Φ_G and Φ_I) at each temperature were determined from the ratio of the integrated emission of the Ap-containing DNA to 50 mM free Ap in 100 mM sodium phosphate, pH 7 in at least three trials.

3.3 Results

3.3.1 Experimental design

These studies utilize a variety of modified oligonucleotides and techniques to probe CT through DNA. Figure 3.1 illustrates some of the assemblies we have synthesized. For the ${}^{\text{CP}}\text{G}$ decomposition studies, six sets of duplexes were prepared. The Rh- A_n and AQ- A_n series contain rhodium or anthraquinone separated from ${}^{\text{CP}}\text{G}$ by a bridge containing increasing numbers of adenine base pairs (Table 3.1). For all Rh-modified assemblies there is a four base pair segment surrounding the rhodium binding site to provide optimum intercalation for the photooxidant. In Figure 3.1, the rhodium is shown intercalated two base pairs from the terminus but likely a mixture of binding sites are available to the diastereomers. On the side distal to the hole trap, there is a constant three base sequence so that fraying ends do not interfere with the results. Guanine can serve as a thermodynamic well if placed near the rhodium intercalation site and although the trapping rate is slow, back electron transfer to rhodium is fast. Therefore, inosine was employed as a substitute for guanine to enhance ${}^{\text{CP}}\text{G}$ decomposition [36]. Note that the first four adenine tract sequences, Rh- A_2 through Rh- A_8 are composed of 20 base pairs, while that of Rh- A_8' through Rh- A_{14} are slightly longer, with 26 base pairs. Rh- A_8 and Rh- A_8' , both containing the 8 base pair long adenine tract but differing in length, yield equivalent decomposition profiles, and in subsequent results and figures, the data from Rh- A_8' are presented. In the Rh-(AT) $_n$ and Rh-(AI) $_n$ series, the repetitive bridge is composed of varying length alternating AT or AI base pairs, respectively. In the Rh-(ATIC) $_n$ series, the repetitive bridge consists of ATIC repeats, and the Rh-(AITC) $_n$

Table 3.1. DNA assemblies used for oxidative decomposition studies

DNA #^a	Sequence^b
PhO-A ₂	3' - TICTI - AA - GXTCTAATAACTG - 5' 5' - PhO - ACIAC - TT - CCAGATTATTGAC - 3'
PhO-A ₄	3' - TICTI - AAAA - GXTCTAATCTG - 5' 5' - PhO - ACIAC - TTTT - CCAGATTAGAC - 3'
PhO-A ₆	3' - TICTI - AAAAA - GXTCTTCTG - 5' 5' - PhO - ACIAC - TTTTTT - CCAGAAGAC - 3'
PhO-A ₈	3' - TICTI - AAAAAAAA - GXTCTTG - 5' 5' - PhO - ACIAC - TTTTTTTT - CCAGAAC - 3'
PhO-A ₈ '	3' - TICTI - AAAAAAAA - GXTCTCTATCTTG - 5' 5' - PhO - ACIAC - TTTTTTTT - CCAGAGATAGAAC - 3'
PhO-A ₁₀	3' - TICTI - AAAAAAAAAA - GXTCTATCTTG - 5' 5' - PhO - ACIAC - TTTTTTTTTT - CCAGATAGAAC - 3'
PhO-A ₁₂	3' - TICTI - AAAAAAAAAAAA - GXTCTCTTG - 5' 5' - PhO - ACIAC - TTTTTTTTTTTT - CCAGAGAAC - 3'
PhO-A ₁₄	3' - TICTI - AAAAAAAAAAAAAA - GXTCTTG - 5' 5' - PhO - ACIAC - TTTTTTTTTTTTTT - CCAGAAC - 3'
Rh-AT ₂	3' - TICTI - AT - GXTCTAATAACTG - 5' 5' - Rh - ACIAC - TA - CCAGATTATTGAC - 3'
Rh-AT ₄	3' - TICTI - ATAT - GXTCTAATCTG - 5' 5' - Rh - ACIAC - TATA - CCAGATTAGAC - 3'
Rh-AT ₆	3' - TICTI - ATATAT - GXTCTTCTG - 5' 5' - Rh - ACIAC - TATATA - CCAGAAGAC - 3'
Rh-AT ₈	3' - TICTI - ATATATAT - GXTCTTG - 5' 5' - Rh - ACIAC - TATATATA - CCAGAAC - 3'
Rh-ATIC ₂	3' - TICTI - AT - GXTCTAATAATCTATCTTG - 5' 5' - Rh - ACIAC - TA - CCAGATTATTAGATAGAAC - 3'
Rh-ATIC ₄	3' - TICTI - ATIC - GXTAATAATCTATCTTG - 5' 5' - Rh - ACIAC - TACG - CCATTATTAGATAGAAC - 3'
Rh-ATIC ₆	3' - TICTI - ATICAT - GXATAATCTATCTTG - 5' 5' - Rh - ACIAC - TACGTA - CCTATTAGATAGAAC - 3'

Rh-ATIC ₈	3' -TICTI-ATICATIC-GXAATCTATCTTG-5' 5' -Rh-ACIAC-TACGTACG-CCTTAGATAGAAC-3'
Rh-ATIC ₁₀	3' -TICTI-ATICATICAT-GXTCTATCTTG-5' 5' -Rh-ACIAC-TACGTACGTA-CCAGATAGAAC-3'
Rh-ATIC ₁₂	3' -TICTI-ATICATICATIC-GXTATCTTG-3' 5' -Rh-ACIAC-TACGTACGTACG-CCATAGAAC-5'
Rh-AITC ₂	3' -TICTI-AI-GXTCTAATAATCTATCTTG-5' 5' -Rh-ACIAC-TC-CCAGATTATTAGATAGAAC-3'
Rh-AITC ₄	3' -TICTI-AITC-GXTAATAATCTATCTTG-5' 5' -Rh-ACIAC-TCAG-CCATTATTAGATAGAAC-3'
Rh-AITC ₆	3' -TICTI-AITCAI-GXATAATCTATCTTG-5' 5' -Rh-ACIAC-TCAGTC-CCTATTAGATAGAAC-3'
Rh-AITC ₈	3' -TICTI-AITCAITC-GXAATCTATCTTG-5' 5' -Rh-ACIAC-TCAGTCAG-CCTTAGATAGAAC-3'
Rh-AITC ₁₀	3' -TICTI-AITCAITCAI-GXTCTATCTTG-5' 5' -Rh-ACIAC-TCAGTCAGTC-CCAGATAGAAC-3'
Rh-AITC ₁₂	3' -TICTI-AITCAITCAITC-GXTATCTTG-5' 5' -Rh-ACIAC-TCAGTCAGTCAG-CCATAGAAC-3'
Rh-AI ₂	3' -TICTI-AI-GXTCTAATAATCTATCTTG-5' 5' -Rh-ACIAC-TC-CCAGATTATTAGATAGAAC-3'
Rh-AI ₄	3' -TICTI-AIAI-GXTAATAATCTATCTTG-5' 5' -Rh-ACIAC-TCTC-CCATTATTAGATAGAAC-3'
Rh-AI ₆	3' -TICTI-AIAIAI-GXATAATCTATCTTG-5' 5' -Rh-ACIAC-TCTCTC-CCTATTAGATAGAAC-3'
Rh-AI ₈	3' -TICTI-AIAIAIAI-GXAATCTATCTTG-5' 5' -Rh-ACIAC-TCTCTCTC-CCTTAGATAGAAC-3'
Rh-AI ₁₀	3' -TICTI-AIAIAIAIAI-GXTCTATCTTG-5' 5' -Rh-ACIAC-TCTCTCTC-CCAGATAGAAC-3'
Rh-AI ₁₂	3' -TICTI-AIAIAIAIAIAI-GXTATCTTG-5' 5' -Rh-ACIAC-TCTCTCTCTC-CCATAGAAC-3'

- a. PhO= Anthraquinone or $[\text{Rh}(\text{phi})_2(\text{bpy}')]^{3+}$ tethered as in Figure 3.1.
b. X= ^{CP}G or guanine.

Table 3.2. DNA assemblies used for fluorescence-quenching studies ^a

DNA #	Sequence
Ap (AT) ₁ Y3	5' -GTAATATCTTGATAAC T-TA-CCATAACTTATGTAATC-3' 3' -CATTATAGAACTATTI _{Ap} -AT-YITATTGAATACATTAG-5'
Ap (AT) ₂ Y3	5' -GAATATCATGATAAC T-TATA-CCATAACAATGTAATC-3' 3' -CTTATAGTACTATTI _{Ap} -ATAT-YITATTGTTACATTAG-5'
Ap (AT) ₃ Y3	5' -GAATATCTGATAAC T-TATATA-CCATAACAAGTAATC-3' 3' -CTTATAGACTATTI _{Ap} -ATATAT-YITATTGTTACATTAG-5'
Ap (AT) ₄ Y3	5' -GAATCTGATAAC T-TATATATA-CCATAACATGTAATC-3' 3' -CTTAGACTATTI _{Ap} -ATATATAT-YITATTGTACATTAG-5'
Ap (AT) ₅ Y3	5' -GAATCTGATAAC T-TATATATATA-CCATAACTGAATC-3' 3' -CTTAGACTATTI _{Ap} -ATATATATAT-YITATTGACTTAG-5'
Ap (AT) ₁ Y5	3' -GTAATATCTTGATAAC T-TA-CCATAACTTATGTAATC-5' 5' -CATTATAGAACTATTI _{Ap} -AT-YITATTGAATACATTAG-3'
Ap (AT) ₂ Y5	3' -GAATATCATGATAAC T-TATA-CCATAACAATGTAATC-5' 5' -CTTATAGTACTATTI _{Ap} -ATAT-YITATTGTTRCATTAG-3'
Ap (AT) ₃ Y5	3' -GAATATCTGATAAC T-TATATA-CCATAACAAGTAATC-5' 5' -CTTATAGACTATTI _{Ap} -ATATAT-YITATTGTTACATTAG-3'
Ap (AT) ₄ Y5	3' -GAATCTGATAAC T-TATATATA-CCATAACATGTAATC-5' 5' -CTTAGACTATTI _{Ap} -ATATATAT-YITATTGTACATTAG-3'
Ap (AT) ₅ Y5	3' -GAATCTGATAAC T-TATATATATA-CCATAACTGAATC-5' 5' -CTTAGACTATTI _{Ap} -ATATATATAT-YITATTGACTTAG-3'

a. Duplexes contain an aminopurine (Ap) base and either an inosine or guanine (Y) on one strand, separated by a bridge of increasing length AT base pairs. Fluorescence experiments were carried out using 50 μ M duplex in 100 mM sodium phosphate, pH 7.

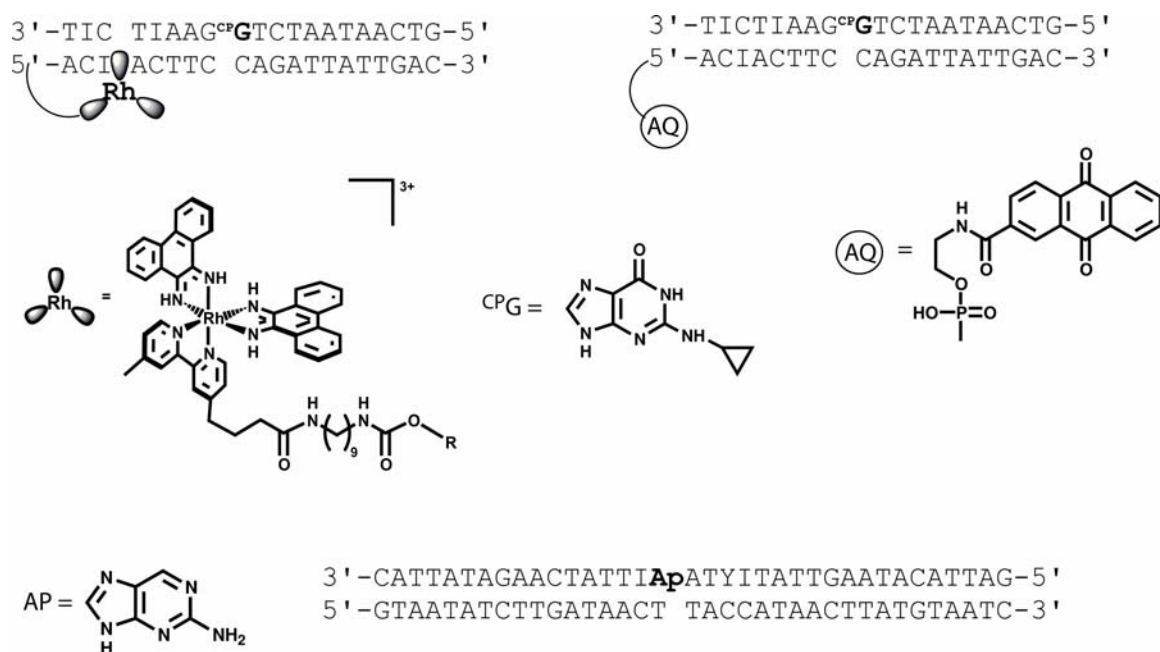


Figure 3.1. Photooxidants, modified bases, and assemblies used to probe CT events in DNA. Shown on the top are representative assemblies containing either rhodium (top left) or anthraquinone (top right) as the photooxidant and ^{CPG} as the trap. The rhodium complex is tethered to the 5' end of amino-modified DNA by a nine carbon linker as represented in the center left and the anthraquinone is capped on the 5' end through the phosphate. A representative aminopurine assembly is shown on the bottom.

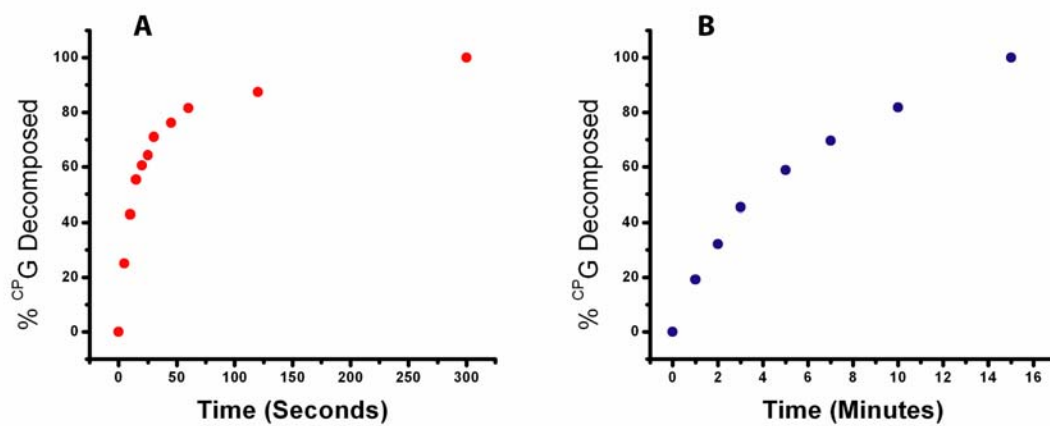


Figure 3.2. ^{CP}G decomposition as a function of irradiation time for Rh-A2 (A) and AQ-A2 (B). 10 μ M duplexes were irradiated at 365 nm (Rh) or 350 nm (AQ).

series contains duplexes with bridging AITC repeats. Derivatives of the AQ-A_n series with G replacing ^{CP}G were used for the gel electrophoresis experiments monitoring damage at double guanine sites.

For the fluorescence quenching studies, as shown in Table 3.2, the Ap(AT)_nY series was synthesized in which Y is either guanine or inosine, and is separated from the Ap photooxidant by a variable number of ATs. The bases flanking Ap are kept constant throughout the series and on either side of the repetitive bridge, six bases of random but constant sequence have been employed to ensure stability.

3.3.2 ^{CP}G Decomposition as a probe of photooxidation in DNA duplexes with A-tracts

Figure 3.3A shows the variation in the decomposition yield (Y) as a function of bridge length for the Rh-A_n series. Y is determined by calculating the fraction of ^{CP}G-containing duplexes undergoing ring opening. The data were fit to an equation combining geometric and periodic terms as shown:

$$\ln Y = A - \gamma \ln(d) + B \sin(2\pi/p*d) \quad (1)$$

where d is the distance between the photooxidant and the trap, γ is a monotonic fall-off parameter, and B and p are the amplitude and period respectively. The first term describes the logarithmic distance dependence that is expected for any incoherent process, with γ analogous to η , the hopping parameter [16, 24]. The sinusoidal term is included to describe the observed periodicities.

The Rh-A_n series were also fit to a series of equations including an exponential decay, an exponential decay with a sinusoidal term, a geometric decay, a geometric decay with a sinusoidal term, a fourth-order polynomial spline, and a four-parameter step

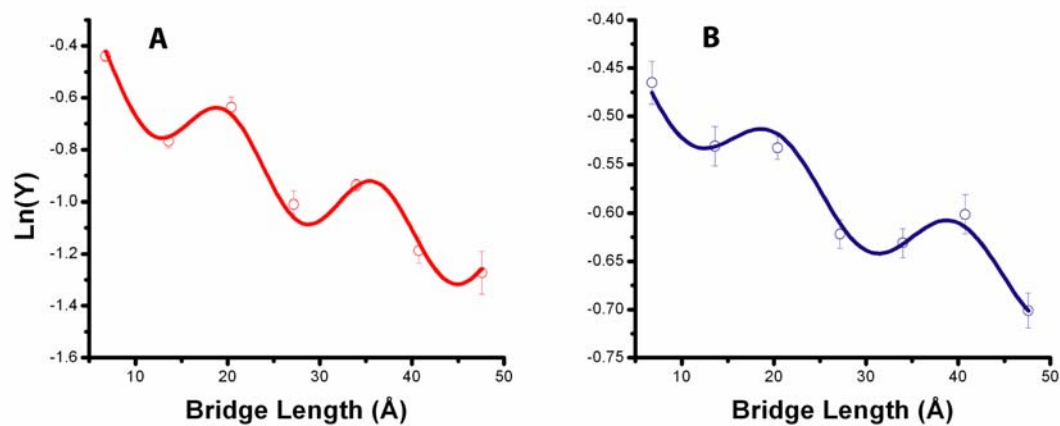


Figure 3.3. CT decays in yield as a function of bridge length for two photooxidants in the Rh-A_n series (**A**) and AQ-A_n series (**B**). Duplexes (10 μM) were irradiated at 365 nm in 20 mM sodium phosphate, 50 mM NaCl, pH 7 at 25 °C as described in the text. The bridge length is defined as the length of the repeating bases between the photooxidant and the trap. The experiments were repeated three times and the results averaged. The curves shown here and for all figures represent the best fit to the exponential decay with a sinusoidal term (equation 1), with correlation coefficients ≥ 0.99 . The error bars are a result of three trials and represent 2 standard deviations from the mean for a 95% confidence level.

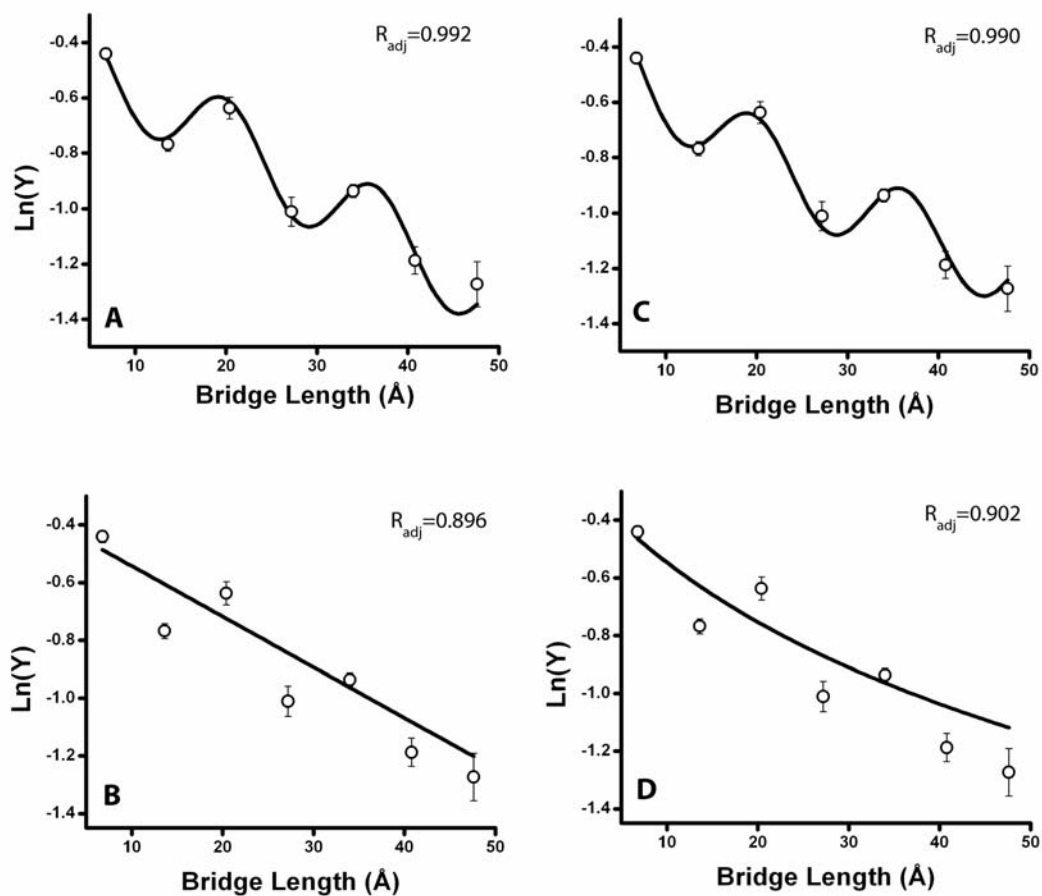


Figure 3.4. Selected fits of data from Figure 3.3A and corresponding R values, adjusted for the number of parameters. Fits include exponential decay with a sinusoidal term (A), exponential decay (B), geometric decay with a sinusoidal term (C), and geometric decay (D). Data were also fit to a four-parameter step function and a fourth-order polynomial spline with R values less than 0.99. See Table 3.3 for equations.

Table 3.3. Equations for fitting Rh-A_n decomposition data

Model	Equation
Exponential decay	$\ln Y = m_1 - m_2[(x/3.4) + 5]$
Exponential decay with a sinusoidal term	$\ln Y = m_1 - m_2[(x/3.4) + 5] - m_3 \sin[2\pi((x/3.4) + 5)/m_4]$
Geometric decay	$\ln Y = m_1 - m_2 \ln[(x/3.4) + 5]$
Geometric decay with a sinusoidal term	$\ln Y = m_1 - m_2 \ln[(x/3.4) + 5] - m_3 \sin[2\pi((x/3.4) + 5)/m_4]$

function as shown in Figure 3.4 and Table 3.3. None of the four fits that do not include a sinusoidal term have R values above 0.99. To account for the degrees of freedom, the R values are adjusted by

$$R_{adj} = \sqrt{1 - (1 - R^2) \left(\frac{n-1}{n-k-1} \right)} \quad (2)$$

where n is the number of data points (7) and k is the number of parameters of a given fit.

For a superexchange mechanism, one expects an exponential decay with a slope = β . For a hopping mechanism, the distance dependence is expected to decay geometrically, be more shallow, but certainly monotonic [24]. As is evident in Figure 3.3A, measurements of decomposition with distance of ^{CP}G in Rh-tethered assemblies exhibit non-monotonic periodic decays. The amplitude of the periodicities exceeds significantly that of the uncertainty in the measurement. When the data are fit to equation 1, a period of 4.8 bases, γ value of 0.72 (0.02), and a $\beta = 0.0191$ (0.0006) \AA^{-1} results from the exponential fit.

It is noteworthy that this periodic decay with distance resembles that seen earlier in fluorescence quenching studies using Ap as the photooxidant and guanine as the trap separated by a bridge of increasing adenine base pairs [31]. In those measurements we found a period of 4-5 bases and $\gamma = 2$ where the data were fit to equation 1.

In order to investigate whether this periodic distance dependence is specific to rhodium, we also synthesized the AQ-A_n series, which is identical to the Rh-A_n series but uses anthraquinone instead as the pendant photooxidant. Irradiations for the AQ-A_n series were carried out at ambient temperature. Semilog plots showing ^{CP}G decomposition as a function of the length of the adenine bridge can be seen in Figure

3.3B. As with the Rh-A_n series, photooxidation of the AQ-A_n assemblies shows a shallow, non-monotonic periodic distance dependence in yield. Decay parameters are comparable. In the case of AQ-A_n, the β value is 0.005 (0.003) Å⁻¹, $\gamma = 0.25$ (0.02) and the period is 5-6 bases. The periodic behavior we observe is therefore independent of the photooxidant.

3.3.3 Variations in photooxidation with temperature

In the Rh-A_n duplexes, we also examined how the decomposition varies with temperature. As can be seen in Figure 3.5A, increasing the temperature below the T_m of the duplex leads to increased ^{CP}G decomposition. Once the duplex begins to melt, thus unstacking the base pairs, the decomposition efficiencies sharply drop to zero. This decrease in decomposition occurs between 50-60 °C, fully consistent with the T_m found for the duplexes at the equivalent concentration.

These data may also be examined by plotting the decay in efficiency as a function of distance at several temperatures (Figure 3.5B). Again periodicities are consistently apparent with amplitudes exceeding the uncertainty in the measurement. It is furthermore evident that below the melting temperature, the periods remain essentially constant over the temperature range. These results also compare closely to those examined earlier by fluorescence quenching of Ap in A-tracts [31].

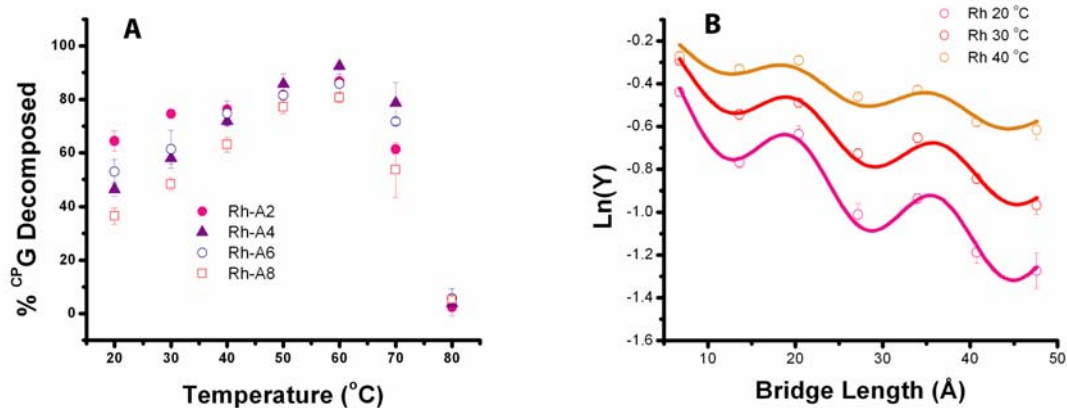


Figure 3.5. ^{CPG} decomposition as a function of temperature. For the Rh-A_n series, shown in (A) is the %^{CPG} decomposition as a function of temperature and in (B) is the semilog plot of decomposition yield (Y) as a function of the length of the bridging adenine tract separating the photooxidant from the ^{CPG} trap. Conditions for these experiments are as in Figure 3.3. Note for these duplexes the melting temperatures determined by UV-visible spectroscopy are 55- 60 °C.

3.3.4 Photooxidation of the $(AT)_n$, $(ATIC)_n$, $(AITC)_n$, and $(AI)_n$ sequences

We were interested in determining whether the periodic decay with distance was a phenomenon unique to A-tracts. Therefore, the Rh- $(ATIC)_n$, Rh- $(AITC)_n$, Rh- $(AT)_n$, and Rh- $(AI)_n$ duplex series containing mixed or alternating base sequences were investigated. The Rh- $(ATIC)_n$ series contains a bridge comprised of four different bases alternating evenly between purines and pyrimidines. The Rh- $(AITC)_n$ series contains a bridge comprised of the same four bases as in the Rh- $(ATIC)_n$ series, but with alternating purine-purine pyrimidine-pyrimidine repeats. The Rh- $(AT)_n$ series and Rh- $(AI)_n$ series contain bridges composed of alternating adenines and thymines or alternating adenines and inosines respectively. Distance dependent CT reactions for these duplexes were carried out at ambient temperature.

Inspection of the data in Figure 3.6 shows that for the Rh- $(AT)_n$ series, periodicities are not apparent. In contrast, the Rh- $(AI)_n$, Rh- $(ATIC)_n$ and Rh- $(AITC)_n$ assemblies show non-monotonic variations with periodicities less obvious than for the Rh- A_n series. In particular, for the Rh- $(AITC)_n$ series there is an initial increase in decomposition followed by a sharp decrease when the bridge is extended from 4-6 bases. This non-monotonic behavior is again greater than the uncertainty in the measurement. If one fits the data for the Rh- $(AI)_n$, Rh- $(ATIC)_n$ and Rh- $(AITC)_n$ assemblies to equation 1, periods of 4-7 base pairs are obtained. If the data for all the sequences are plotted on the same graph, simulating a random sequence, the decomposition behavior is very scattered, with an exponential decay fit equal to 0.05 \AA^{-1} .

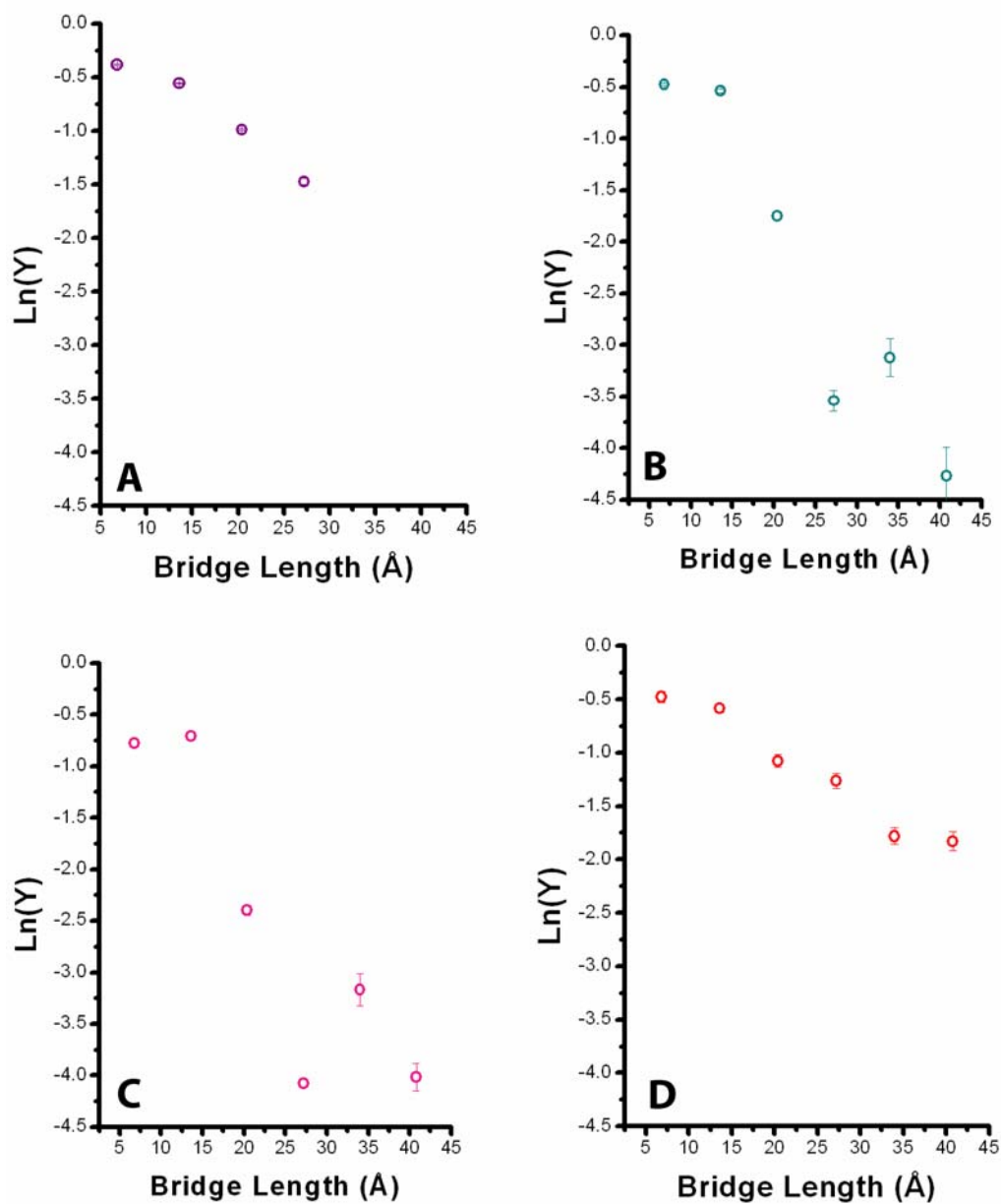


Figure 3.6. Semilog plots showing the distance dependence of CT yield (Y) through sequences containing various bridging bases. Experiments were repeated three times and the results averaged. Shown in (A) is the decomposition as a function of repeating bridge length for the $(AT)_n$ series, in (B), the $(ATIC)_n$ series, in (C), the $(AITC)_n$ series and in (D), the $(AI)_n$ series. Conditions are as in Figure 3.3.

3.3.5 Photooxidations with guanine as the hole trap

Earlier systematic studies of long-range oxidative damage to unmodified guanine in our laboratory, as well as by others, had not shown any indication of periodic behavior [10, 11, 25, 43]. To test this specifically using analogous sequences, we prepared AQ-A_n sequences with G rather than ^{CP}G as the hole trap, introduced a 5'-³²P end label, and carried out photooxidations. Following subsequent cleavage with hot piperidine to reveal oxidative base damage, the samples were eluted through a 20% denaturing polyacrylamide gel. Quantitation of the damage yield at the double guanine site is shown in Figure 3.7. Damage yields show a simple decrease in CT efficiency as a function of distance. The periodic behavior in AQ-A_n apparent with ^{CP}G is not evident with guanine, a much slower radical trap.

3.3.6 Fluorescence quenching of 2-aminopurine through AT-tracts

Charge injection into a DNA bridge can be studied by comparing the fluorescence quenching of AP by redox-active guanine and redox-inactive inosine [31, 42]. A series of 36 base pair duplexes were designed to contain both Ap and either guanine or inosine, separated by a bridge of varying length AT repeats. As shown in Table 3.2, Ap(AT)_nY (n=1-5) duplexes have either a guanine (Y=G) or inosine (Y=I) positioned n AT base pairs away from Ap. Ap(AT)_nY5 and Ap(AT)_nY3 duplexes contain the same sequence, but the polarity of the strands are reversed so as to note any effects of directionality on CT.

Steady-state fluorescence quenching of the Ap(AT)_nY series does not show a similar trend in CT yield as a function of distance as compared with the Ap(A)_nY series

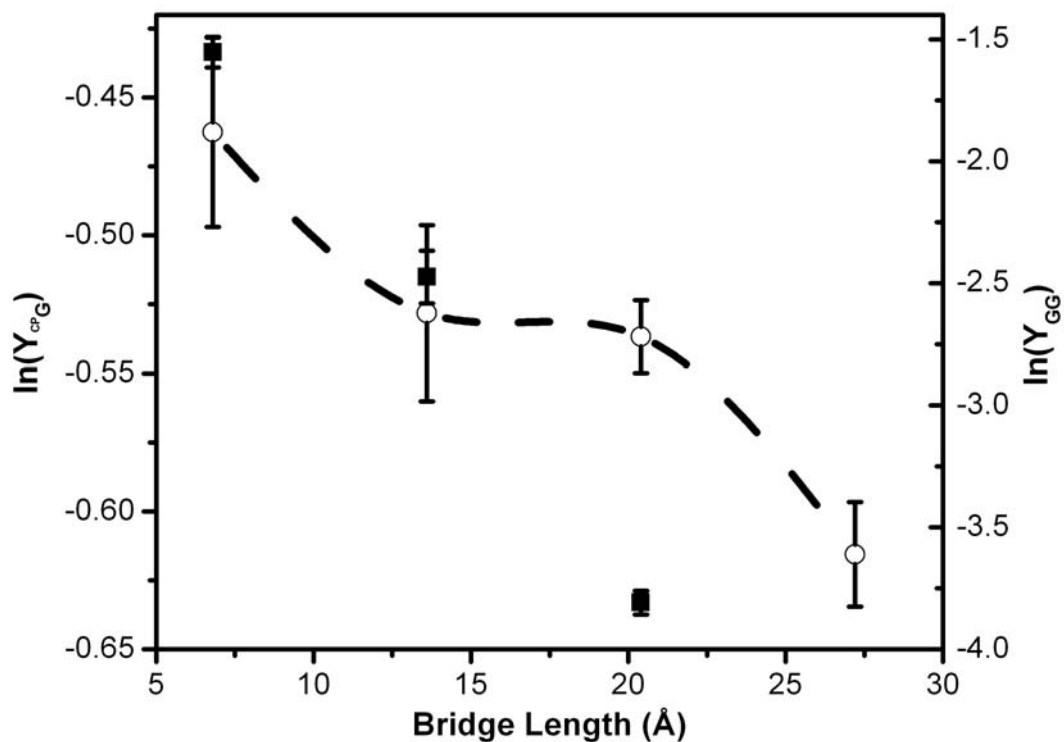


Figure 3.7. Semilog plot of the distance dependence of CT yield in the AQ-A_n series revealed with two oxidative traps, ^{CP}G (open circles) and guanine (closed squares). For the measurements of oxidative guanine damage, duplexes (4 μM) were irradiated at 350 nm in 20 mM sodium phosphate, 50 mM NaCl, pH 7 followed by piperidine treatment, gel electrophoresis and quantitation by phosphimager as detailed in Experimental.

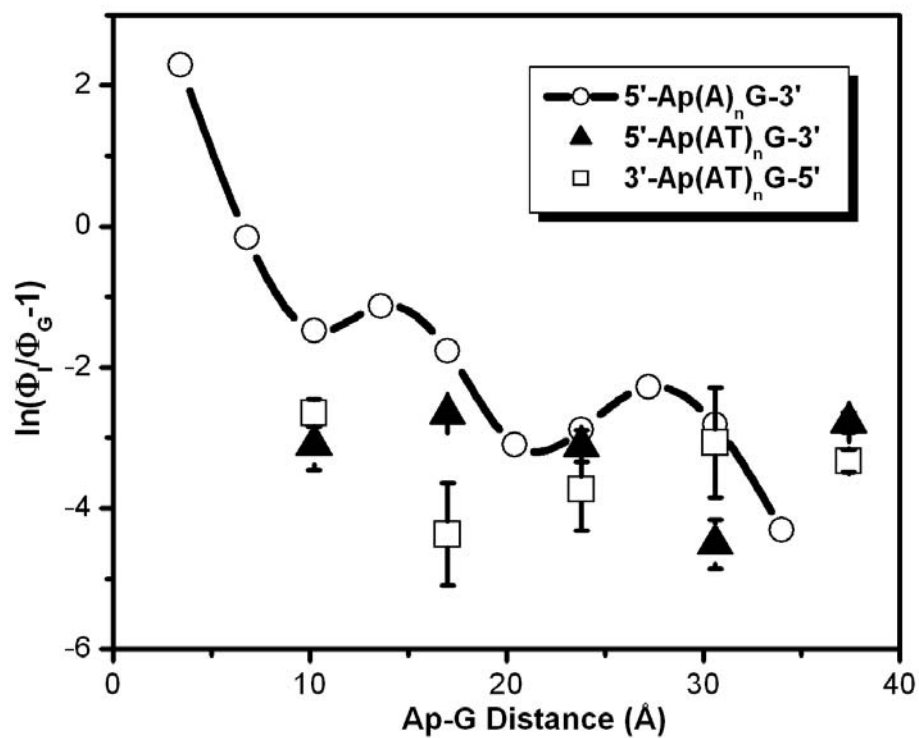


Figure 3.8. Comparison of distance dependence of charge injection into A and AT-tracts at 25 °C. Data (open circles) for the Ap(A)_nG set are adapted [31]. The distance dependence of charge injection into AT-tracts from both directions, 5' to 3' (closed triangles) and 3' to 5' (open squares), are shown with errors determined from at least three experiments with each series.

(Figure 3.8). Here the quenching yield is exceedingly low, although essentially constant with distance. Due to the low yield, periodicities that exceed the certainty in the measurement are difficult to establish. An equivalent low but consistent quenching is seen for duplexes with CT in the 5' - 3' direction and 3' - 5' direction.

3.4 Discussion

3.4.1 Distance dependence of DNA CT through A-tracts using ${}^{\text{CP}}\text{G}$

In this study, we examine the distance dependence of CT through increasing length A-tracts using the kinetically fast hole trap, ${}^{\text{CP}}\text{G}$. Using $[\text{Rh}(\text{phi})_2(\text{bpy}')]^{3+}$ and AQ as photooxidants, we observe shallow distance dependences over 50 Å. The decays observed with both the well-stacked rhodium and the end-capped anthraquinone show pronounced periodic variations in ring opening yield as a function of distance, which exceed the associated error, indicating that the non-monotonic decay is not specific to the photooxidant. With both photooxidants, similar periods and decays with distance are observed. The significant periodic nature of this data is best fit with either an exponential (superexchange) or geometric (hopping) decay containing a sinusoidal component. When these data are fit to an exponential or geometric decay without this component, the R values are considerably lower, even after adjusting for the number of parameters. This strongly implies that superexchange and hopping mechanisms on their own are insufficient to explain the CT yields observed in this system.

3.4.2 Conformational gating by base dynamics

These periodicities are also apparent at higher temperatures, where the overall yield of CT increases and the distance dependence becomes shallower (Figure 3.5). In a direct CT event, in which the donor and acceptor orbitals are already aligned, higher temperatures are likely to decrease the probability that the orbitals will remain aligned, and decreased CT results [31]. In contrast, when the donor and acceptor are separated by a bridge of dynamic base pairs, increasing the temperature allows a greater fraction of these duplexes to access a CT-active conformation resulting in enhanced CT. Indeed, in our system with the rhodium photooxidant intercalated at least 6 bases away from the trap, we observe increased CT for all bridge lengths as a function of temperature. Increased temperature has a more prominent effect on CT through longer adenine bridges because there is a lower initial probability of each base being aligned in a CT-active conformation. We have seen a similar periodic distance dependence of CT through A-tracts using a different system in which CT is monitored by fluorescence quenching of Ap by guanine [31]. The quenching event, which occurs on a subnanosecond time scale, provides information on base dynamics, which can significantly contribute to the CT process [42]. Here too, a periodic decay is seen as a function of distance but is an order of magnitude steeper. This is not surprising, given that our ^{CP}G trapping system does not monitor solely coherent CT events. Similarly to the present experiment, CT yield is also enhanced at higher temperatures as monitored by Ap quenching due to increased base dynamics which facilitate a duplex conformation suitable for undergoing a CT event. This conformational gating, influenced by DNA sequence, controls the CT process on extremely fast time scales governed by base motions.

3.4.3 Effects of base stacking on distance-dependent CT

We have established that base dynamics can dramatically influence the DNA CT process. Hole transport, which is exquisitely sensitive to the intervening bases, is also significantly influenced by the electronic coupling of the donor and acceptor to the intervening bridge. We have observed that increased stacking between the donor and acceptor enhances CT at longer distances such that shallower distance dependences are observed [42]. Hole injection into a duplex from a photooxidant that is not sufficiently electronically coupled to the orbitals of the DNA bases is strongly hindered and severely influenced by increasing distance. The steep distance dependences observed in systems associated with a superexchange mechanism result from poor coupling between the donor and the bridge. For example, when a distorted sugar radical, not electronically coupled with the DNA bases, is used as a photooxidant, a steep distance dependence is observed through the first three bases, as the injection is rate limiting when the hole effectively tunnels from the photooxidant to the base orbitals [43]. Conversely, in a system in which the photooxidant is extremely well electronically coupled to the DNA and the trap is isoenergetic to the bridge, distance-independent CT results [44]. The shallow distance dependence we observe through A-tracts is expected, given the efficient coupling of the rhodium complex with the DNA, and the inherent coupling of the ^{CP}G trap to the bridge.

While the coupling between the donor, bridge, and acceptor has a profound influence on the distance dependence of DNA CT, we find that the intervening bridge sequence can significantly alter the decay profile as a result of changes in stacking. We investigated the distance dependence of CT through various bridging bases using the rhodium photooxidant and the ^{CP}G trap. Interrupting the electronic coupling by using

non-homogeneous bridging bases decreases CT efficiency as a function of distance. Indeed, when alternating AT sequences are inserted into the bridge, as is the case in the Rh-(AT)_n series, a steeper distance dependence is observed, and periodicities are not apparent. Additionally, when we observe the distance dependence through AT-tracts using Ap fluorescence quenching, periodicities are not observed. Here, the purine-pyrimidine stacking results in diminished coupling between the orbitals and leads to decreased CT efficiency with distance [36]. Due to the flexible nature associated with AT-tracts, increased base pair motion might lead to dampened periodicities [45]. In contrast, a shallower, non-monotonic distance dependence results for a bridge consisting of alternating adenine and inosine base pairs, as seen for the Rh-(AI)_n series. The purine-purine stacking can lead to more efficient coupling between the bases and shallower CT as a function of distance. When mixed sequence bridges intervene between the rhodium photooxidant and the ^{CP}G trap, steeper, but still non-monotonic distance dependences are apparent. Interestingly, the Rh-(ATIC)_n and Rh-(AITC)_n series show similar decay profiles despite the fact that the base stacking between purines and pyrimidines is completely different in these duplexes. These results are consistent with studies in which A-tracts are interrupted by guanines and significant attenuation of CT yields are observed; homogeneous coupling and stacking of the intervening bridging bases are required for efficient CT over longer distances [25, 36, 46].

3.4.4 The importance of time scale in monitoring CT processes through DNA

It is interesting to compare the results for the A-tracts monitored with the slow guanine trap to our fast ^{CP}G trap and fluorescent Ap probe. Distance dependences

obtained from biochemical studies monitoring the guanine radical trapping here and in previous experiments show shallow decay profiles but lack the periodicities we find using our fast reporters [25, 43]. Owing to its millisecond lifetime, the guanine radical can undergo multiple reactions including BET prior to radical trapping inevitably convoluting the CT process [38, 39]. Indeed, when we compare CT yield for the AQ-A_n sequences as monitored by ^{CP}G ring opening to that monitored by guanine radical trapping, drastically different decay profiles are evident. It should be noted that previous studies using a rhodium photooxidant and guanine trap are mitigated by fast BET [35]. Just as information as to rapid BET is lost with double guanines, it also appears that the periodicities in long-range DNA CT as a function of distance may also be dampened with the slower guanine radical trap.

In the present study, ring opening, occurring on the picosecond time scale, is competitive with BET and our results are therefore not limited by hole recombination. Our ring opening reaction is also faster than the overall transport process, since we observe differing decomposition yields as a function of sequence. Thus the yield of ^{CP}G decomposition is an appropriate proxy for the CT rate. We have now seen in several experiments that DNA CT is gated by base pair motions on the picosecond time scale [28-30]. Both the Ap and ^{CP}G systems are sensitive to variations on this time scale and should not be affected by slow oxidative trapping at guanine. This underscores the lack or reliability in utilizing oxidative guanine damage in mechanistic studies of CT. Importantly, these differences highlight the sensitivity of DNA CT chemistry to DNA dynamics on a fast time scale.

3.4.5 Comparison with other DNA CT systems

It is now apparent that coupling between the photooxidant, acceptor, and bridge, bridge homogeneity, and time scale are critical in studying mechanistic DNA CT. Our current system utilizing a fast reporter which is well coupled to the bridge, a well-intercalated photooxidant, and a structurally homogeneous A-tract bridge result in efficient CT with a prominent periodic decay. There have been many reported studies investigating distance dependences through A-tracts, but with the exception of the Ap-quenching experiment, periodic distance dependence has not been observed. The lack of periodicities seen in these experiments can be reconciled by examining the time scale and stacking associated with the system. Majima and co-workers investigated yields of charge separation and rates of recombination as a function of bridge length using transient absorption spectroscopy with NDI as a hole donor and PTZ or 8-oxoguanine as the acceptor [46]. Here, no apparent periodicities were observed in transport yields and the distance dependences were steeper than what we find using the $^{\text{CP}}\text{G}$ trap. However, the lack of error bars associated with these data make it difficult to interpret. Moreover, the charge separation yields as measured by formation of the NDI radical are inevitably convoluted by BET processes which will dampen any periodic behavior. Indeed, NDI radical formation was not observable in the absence of PTZ, indicating that BET dominates hole migration along the bridge. Our Ap quenching experiment is similar but because BET events cannot contribute to the quenching measurement, a prominent periodic distance dependence is evident [31]. Similarly, the slower rate of BET to rhodium and AQ obviates this process as the dominant contributor to our measured yields in the present work, such that periodicity is not dampened. Interestingly, a picosecond

transient absorption study using stilbene-capped hairpins also found a similar dependence for longer distances, but steeper variations were apparent for shorter distances [47]. The data were interpreted as supporting three regimes of CT, such that the mechanism changes from superexchange to localized hopping to delocalized hopping with increasing distance. Given the distortion of these doubly capped hairpins, it is likely that hole injection is rate limiting near the stilbene. Further from the photooxidant, the DNA is less distorted, yielding the smooth transition to a weaker distance dependence. This process will obscure any periodicity from well coupled CT.

Significantly, the profile is similar to that found using the distorted sugar radical as the photooxidant and a double guanine site as the hole acceptor [43]. In this study, the sugar radical must migrate from the backbone to the π -stack, a rate-limiting process that leads to the initial superexchange regime. The subsequent shallow distance dependence is characteristic of faster transport once the charge occupies the bridge. A similar explanation can be used for the results from the stilbene transient absorption study.

3.4.6 Conformational gating through delocalized domains

We have suggested that conformational gating by delocalized base pair domains naturally induces a periodic distance dependence [31]. The motions of neighboring bases depend upon the sequence-dependent dynamics of DNA, and for some sequences, these motions can become correlated, or coherent. This coherent collection of bases, existing on the time scale of CT, represents a domain, the size of which is limited by the persistence length of the coherent motion. When the base motions are coherent, the probability of consecutive groups of bases being in CT-active conformations also become

correlated; charge is delocalized over the domain. Note that electronically coherent CT beyond the length of a single domain requires that a second domain be present, and in a conformation that is CT-active with respect to the first domain [48].

Ap quenching experiments, in which we first observed a periodic distance dependence, assay the coherent injection and transport processes in the DNA duplex but not the trapping event. In those experiments, the periodicities reflect the varying probabilities of coherent CT with distance, which we ascribe to the varying probabilities of finding a coherent domain on the time scale of CT.

Coherent motions of the bases may also generate periodic behavior with incoherent CT, as we measure here through the yield of acceptor ring opening. In this case, each CT event depends upon the probability of bases aligning in a coherent domain. Transport occurs between two domains that acquire a mutually CT-active conformation, forming a larger domain, but only on the time scale of CT. Thus the two domains need *not* be in mutually CT-active conformations *at the same time*. Hence, a similar periodic distance dependence should follow as with coherent CT, but be shallower and dampened by incoherent steps. Note that base pair motions have also been considered in the context of CT through polarons [11, 18, 19].

Base motions furthermore may be coherent on the time scale of CT but incoherent on the time scale of trapping. On this longer time scale, one or more bases in the domain may move out of the CT-active conformation, while other bases move in. The net result of such a process is a translation of the delocalized domain along the duplex. Such translations should also have a tendency to dephase the periodicities in the acceptor decomposition yield, lowering the amplitude of periodicities.

It is interesting to compare these results to those of a system in which the A-tract length is fixed. This was accomplished by monitoring decomposition of cyclopropyladenine (^{CP}A) serially substituted at each position within a 14 base pair adenine tract [44]. In contrast to the guanine trapping situation, there is no periodic variation of the yield with ^{CP}A position for a given A-tract length. This is consistent with our domain model, as a set length A-tract will accommodate a similar domain structure regardless of the placement of the trap.

3.4.7 Other theoretical predictions of periodic distance dependences

Periodic distance dependences have been predicted theoretically but not examined experimentally. In particular, on-resonant CT, occurring when the energies of the donor, bridge, and acceptor are similar, has been described in the context of a periodic distance dependence [49-51]. In theoretical studies of molecular wires, while an exponential distance dependence for off-resonance CT was described, for on-resonance coupling, smooth, bounded periodicities were predicted; energetic inhomogeneities along the bridge could attenuate the periodicities [50]. Although these studies modeled the wire between metals, it was theorized that the same analyses could apply to a sufficiently gated charge transfer system. It is possible that DNA fulfills that requirement based on the apparent conformational gating from temperature studies. Periodicities in on-resonant transfer have also been explored in a novel approach to determine the coupling across a molecular bridge by means of formulating the lengthening of the bridge as iterative perturbations. Here too, periodicities were predicted for on-resonant transfer, but the periods were unstable with respect to the coupling parameters [51].

Interestingly, Renger and Marcus have calculated a periodic distance dependence for CT across an A-tract DNA bridge when using a model that allowed delocalization of the electron hole over several bases [52]. These periodicities were eliminated by incorporation of a static disorder term. Though the result is intriguing, the physical basis for the periodicities is not clear.

3.4.8 Implications of the periodic distance dependence to mechanisms for DNA-mediated CT

The periodic distance dependence we observe using probes for CT on a fast time scale but not with slow guanine trapping is fully consistent with DNA CT being governed by coherent base motions. The periods are ~4-5 base pairs for A-tracts measured both by Ap quenching and ^{CP}G decomposition. The decay parameters are smaller for ^{CP}G decomposition, since multiple CT events should make the distance dependence shallower. Long-range DNA-mediated CT measured by ^{CP}G decomposition appears to be at least partially an incoherent process. The decrease in amplitude at longer distances is furthermore indicative of dephasing by base motions.

We cannot establish whether the periodicities depend solely upon coherent base motion or also reflect underlying quantum periodicities due to on-resonance transfer within a domain. The periodicities are essentially constant with respect to their periods for different photooxidants, Ap, Rh, AQ, and with different measurements; this similarity would argue that correlated base motions are most important. Some variations are also apparent with sequence, notably in the absence of periodicities for Rh-(AT)_n. For quantum periodicities, changing the sequence should generate different bridge energies

and different couplings, which should in turn affect the period. In the coherent motion model, however, the periodicities directly reveal the size of the domains over which base motion is correlated, and over which CT-active conformations are more readily achieved. Here we expect domain size to be roughly dictated by the local sequence-dependent DNA structure. Thus with both models, sequence variations are expected. Only the coherent motion model, however, predicts that serially inserting a ^{CP}A trap along a fixed length A-tract will eliminate the periodicity; a quantum or symmetry effect would be, if anything, more pronounced in such a system [44].

It is remarkable that we are able to observe these periodicities in DNA CT using disparate assays so long as the experiments monitor events on a fast time scale. The observations here underscore the utility of applying cyclopropylamine-modified bases as fast traps for CT. Perhaps more importantly these results highlight the criticality of sequence-dependent motions of the DNA bases in defining CT.

3.5 References

- [1] Hall, D.B.; Holmlin, R.E.; Barton, J.K. Oxidative DNA damage through long-range electron transfer. *Nature* **382**, 731-735 (1996).
- [2] Delaney, S.; Barton, J.K. Long-range DNA charge transport. *J. Org. Chem.* **68**, 6475-6483 (2003).
- [3] O'Neill, M.A.; Barton, J.K. Charge transfer in DNA: From mechanism to application. Wagenknecht, H.A., Ed.; Wiley: New York, pp 27-75 (2005).
- [4] Schuster, G.B. Long-range charge transfer in DNA: transient structural distortions control the distance dependence. *Acc. Chem. Res.* **33**, 253-260 (2000).
- [5] Schuster, G.B.; Landman, U. The mechanism of long-distance radical cation transport in duplex DNA: ion-gated hopping of polaron-like distortions. *Top. Curr. Chem.* **236**, 139-162 (2004).
- [6] Giese, B. Long-distance charge transport in DNA: the hopping mechanism. *Acc. Chem. Res.* **33**, 631-636 (2000).
- [7] Giese, B. Hole injection and hole transfer through DNA: the hopping mechanism. *Top. Curr. Chem.* **236**, 27-44 (2004).
- [8] Nakatani, K.; Saito, I. Charge transport in duplex DNA containing modified nucleotide bases. *Top. Curr. Chem.* **236**, 163-186 (2004).
- [9] Lewis, F.D.; Wasielewski, M.R. Dynamics and equilibrium for single step hole transport processes in duplex DNA. *Top. Curr. Chem.* **236**, 45-65 (2004).
- [10] Nuñez, M.E.; Hall, D.B.; Barton, J.K. Long-range oxidative damage to DNA: effects of distance and sequence. *Chem. Biol.* **6**, 85-97 (1999).

- [11] Henderson, P.T.; Jones, D.; Hampikian, G.; Kan, Y.Z.; Schuster, G.B. Long-distance charge transport in duplex DNA: the phonon-assisted polaron-like hopping mechanism. *Proc. Natl. Acad. Sci. USA*. **96**, 8353-8358 (1999).
- [12] (a) Drummond, T.G.; Hill, M.G.; Barton, J.K. Electrochemical DNA sensors. *Nat. Biotechnol.* **21**, 1192-1199 (2003). (b) Boon, E.M.; Ceres, D.M.; Drummond, T.G.; Hill, M.G.; Barton, J.K. Mutation detection by electrocatalysis at DNA-modified electrodes. *Nat. Biotechnol.* **18**, 1096-1100 (2000). (c) Boon, E.M.; Salas, J.E.; Barton, J.K. An electrical probe of protein-DNA interactions on DNA-modified surfaces. *Nat. Biotechnol.* **20**, 282-286 (2002).
- [13] Nuñez, M.E.; Noyes, K.T.; Barton, J. K. Oxidative charge transport through DNA in nucleosome core particles. *Chem. Biol.* **9**, 403-415 (2002).
- [14] (a) Boon, E.M.; Livingston, A.L.; Chmiel, N.H.; David, S.S.; Barton, J.K. DNA-mediated charge transport for DNA repair. *Proc. Natl. Acad. Sci. USA*. **100**, 12543-12547 (2003); **2004**, *101*, 4718; (b) Yavin, E.; Boal, A.K.; Stemp, E.D.A.; Boon, E.M.; Livingston, A.L.; O'Shea, V.L.; David, S.S.; Barton, J.K. Protein-DNA charge transport: redox activation of a DNA repair protein by guanine radical. *Proc. Natl. Acad. Sci. USA*. **102**, 3546-3551 (2005); (c) Boal, A.K.; Yavin, E.; Lukianova, O.A.; O'Shea, V.L.; David, S.S.; Barton, J.K. DNA-bound redox activity of DNA repair glycosylases containing [4Fe-4S] clusters. *Biochemistry* **44**, 8397-8407 (2005).
- [15] Jortner, J.; Bixon, M; Voityuk, A.A.; Rosch, N. Superexchange-mediated charge hopping in DNA. *J. Phys. Chem. A*. **106**, 7599-7606 (2002).

- [16] (a) Bixon, M.; Jortner, J. Long-range and very long-range charge transport in DNA. *Chem Phys.* **281**, 393-408 (2002). (b) Bixon, M.; Jortner, J. Hole trapping, detrapping, and hopping in DNA. *J. Phys. Chem. A.* **105**, 10322-10328 (2001). (c) Bixon, M.; Jortner, J. Charge transport in DNA via thermally induced hopping. *J. Am. Chem. Soc.* **123**, 12556-12567 (2001). (d) Bixon, M.; Jortner, J. Electronic coupling for charge transfer and transport in DNA. *J. Phys. Chem. B.* **104**, 3906-3913 (2000).
- [17] (a) Berlin, Y.A.; Burin, A.L.; Ratner, M.A. Elementary steps for charge transport in DNA: thermal activation vs. tunneling. *Chem. Phys.* **275**, 61-74 (2002). (b) Berlin, Y.A.; Burin, A.L.; Ratner, M.A. On the long-range charge transfer in DNA. *J. Phys. Chem. A.* **104**, 443-445 (2000).
- [18] Conwell, E.M.; Rakhmanova, S.V. Polarons in DNA. *Proc. Natl. Acad. Sci. USA.* **97**, 4556-4560 (2000).
- [19] Conwell, E.M. Charge transport in DNA in solution: the role of polarons. *Proc. Natl. Acad. Sci. USA.* **102**, 8795-8799 (2005).
- [20] Grozema, F.C.; Berlin, Y.A.; Siebbeles, L.D.A. Sequence-dependent charge transfer in donor-DNA-acceptor systems: A theoretical study. *Int. J. Quantum Chem.* **75**, 1009-1016 (1999).
- [21] Tong, G.S.M.; Kurnikov, I.V.; Beratan, D.N. Tunneling energy effects on GC oxidation in DNA. *J. Phys. Chem. B.* **106**, 2381-2392 (2002).
- [22] Li, X. Q.; Zhang, H. Y.; Yan, Y. J. A superexchange-mediated sequential hopping theory for charge transfer in DNA. *J. Phys. Chem. A.* **105**, 9563-9567 (2001).

- [23] Zhang, H.Y.; Li, X.Q.; Han, P.; Yu, X.Y.; Yan, Y.J. A partially incoherent rate theory of long-range charge transfer in deoxyribose nucleic acid. *J. Chem. Phys.* **117**, 4578-4584 (2002).
- [24] (a) Bixon, M.; Giese, B.; Wessely, S.; Langenbacher, T.; Michel-Beyerle, M.E.; Jortner, J. Long-range charge hopping in DNA. *Proc. Natl. Acad. Sci. USA.* **96**, 11713-11716 (1999). (b) Jortner, J.; Bixon, M.; Langenbacher, T.; Michel-Beyerle, M.E. Charge transfer and transport in DNA. *Proc. Natl. Acad. Sci. USA.* **95**, 12759-12765 (1998).
- [25] Williams, T.T.; Odom, D.T.; Barton, J.K. Variations in DNA charge transport with nucleotide composition and sequence. *J. Am. Chem. Soc.* **122**, 9048-9049 (2000).
- [26] Yoo, J.; Delaney, S.; Stemp, E.D.A.; Barton, J.K. Rapid radical formation by DNA charge transport through sequences lacking intervening guanines. *J. Am. Chem. Soc.* **125**, 6640-664 (2003).
- [27] Shao, F.; O'Neill, M.A.; Barton, J.K. Long-range oxidative damage to cytosines in duplex DNA. *Proc. Natl. Acad. Sci. USA.* **101**, 17914-17919 (2004).
- [28] Wan, C.Z.; Fiebig, T.; Kelley, S.O.; Treadway, C.R.; Barton, J.K.; Zewail, A.H. Femtosecond dynamics of DNA-mediated electron transfer. *Proc. Natl. Acad. Sci. USA.* **96**, 6014-6019 (1999).
- [29] O'Neill, M.A.; Becker, H.C.; Wan, C.; Barton, J.K.; Zewail, A.H. Ultrafast dynamics in DNA-mediated electron transfer: base gating and the role of temperature. *Angew. Chem. Int. Ed.* **42**, 5896-5900 (2003).

- [30] O'Neill, M.A.; Barton, J.K. DNA-mediated charge transport requires conformational motion of the DNA bases: elimination of charge transport in rigid glasses at 77 K. *J. Am. Chem. Soc.* **126**, 13234-13235 (2004).
- [31] O'Neill, M.A.; Barton, J.K. DNA charge transport: conformationally gated hopping through stacked domains. *J. Am. Chem. Soc.* **126**, 11471-11483 (2004).
- [32] Nakatani, K.; Dohno, C.; Saito, I. Design of a hole-trapping nucleobase: termination of DNA-mediated hole transport at N₂-cyclopropyldeoxyguanosine. *J. Am. Chem. Soc.* **123**, 9681-9682 (2001).
- [33] Dohno, C.; Ogawa, A.; Nakatani, K.; Saito, I. Hole trapping at N₆-cyclopropyldeoxyadenosine suggests a direct contribution of adenine bases to hole transport through DNA. *J. Am. Chem. Soc.* **125**, 10154-10155 (2003).
- [34] O'Neill, M.A.; Dohno, C.; Barton, J.K. Direct chemical evidence for charge transfer between photoexcited 2-aminopurine and guanine in duplex DNA. *J. Am. Chem. Soc.* **126**, 1316-1317 (2004).
- [35] Williams, T.T.; Dohno, C.; Stemp, E.D.A.; Barton, J.K. Effects of the photooxidant on DNA-mediated charge transport. *J. Am. Chem. Soc.* **126**, 8148-8158 (2004).
- [36] Shao, F.; Augustyn, K.E.; Barton, J.K. Sequence dependence of charge transport through DNA domains. *J. Am. Chem. Soc.* **127**, 17445-17452 (2005).
- [37] Musa, O.M.; Horner, J.H.; Shahin, H.; Newcomb, M. A kinetic scale for dialkylaminyl radical reactions. *J. Am. Chem. Soc.* **118**, 3862-3868 (1996).

- [38] Stemp, E.D.A.; Arkin, M.R.; Barton, J.K. Oxidation of guanine in DNA by $\text{Rh}(\text{phen})_2(\text{dppz})^{3+}$ using the flash-quench technique. *J. Am. Chem. Soc.* **119**, 2921-2925 (1997).
- [39] (a) Douki, T.; Ravanat, J.L.; Angelov, D.; Wagner, R.; Cadet, J. Effects of duplex stability on charge transfer efficiency within DNA. *Top. Curr. Chem.* **236**, 1-25 (2004). (b) Burrows, C.J.; Muller, J.G. Oxidative nucleobase modifications leading to strand scission. *Chem. Rev.* **98**, 1109-1152 (1998).
- [40] Holmlin, R.E.; Dandliker, P.J.; Barton, J.K. Synthesis of metallointercalator-DNA conjugates on solid support. *Bioconjug. Chem.* **10**, 1122-1130 (1999).
- [41] Gasper, S.M.; Schuster, G.B. Intramolecular photoinduced electron transfer to anthraquinones linked to duplex DNA: the effect of gaps and traps on long-range radical cation migration. *J. Am. Chem. Soc.* **119**, 12762-12771 (1997).
- [42] Kelley, S.O.; Barton, J.K. Electron transfer between bases in double helical DNA. *Science* **283**, 375-381 (1999).
- [43] Giese, B.; Amaudrut, J.; Kohler, A.K.; Spormann, M.; Wessely, S. Direct observation of hole transfer through DNA by hopping between adenine bases and by tunneling. *Nature* **412**, 318-320 (2001).
- [44] Augustyn, K.E.; Genereux, J.C.; Barton, J.K. Distance-independent DNA charge transport across an adenine tract. *Angew. Chem. Int. Ed.* In press (2007).
- [45] (a) Dickerson, R.E. *Structure, motion, interaction, and expression of biological macromolecules*. 17-36 (1998). (b) Dickerson, R.E. DNA bending: the prevalence of kinkiness and the virtues of normality. *Nucleic Acids Res.* **26**, 1906-1926 (1998). (c) Kim, J.L.; Nikolov, D.B.; Burley, S.K. Co-crystal structure of TBP

- recognizing the minor groove of a TATA element. *Nature* **365**, 520-527 (1993).
- (d) Kim, Y.C.; Geiger, J.H.; Hahn, S.; Sigler, P.B. Crystal structure of a yeast TBP/TATA-box complex. *Nature* **365**, 512-520 (1993).
- [46] (a) Takada, T.; Kawai, K.; Cai, X.; Sugimoto, A.; Fujitsuka, M.; Majima, T. Charge separation in DNA via consecutive adenine hopping. *J. Am. Chem. Soc.* **126**, 1125-1129 (2004). (b) Takada, T.; Kawai, K.; Fujitsuka, M.; Majima, T. Direct observation of hole transfer through double-helical DNA over 100 Å. *Proc. Natl. Acad. Sci. USA.* **101**, 14002-14006 (2004). (c) Takada, T.; Kawai, K.; Fujitsuka, M.; Majima, T. Rapid long-distance hole transfer through consecutive adenine sequence. *J. Am. Chem. Soc.* **128**, 11012-11013 (2006).
- [47] (a) Lewis, F.D.; Zhu, H.; Daublain, P.; Fiebig, T.; Raytchev, M.; Wang, Q.; Shafirovich, V. Crossover from superexchange to hopping as the mechanism for photoinduced charge transfer in DNA hairpin conjugates. *J. Am. Chem. Soc.* **128**, 791-800 (2006). (b) Lewis, F.D.; Zhu, H.; Daublain, P.; Cohen, B.; Wasielewski, M.R. Hole mobility in DNA A-tracts. *Angew. Chem. Int. Ed.* **45**, 7982-7985 (2006).
- [48] Note the distinction between coherent motion, where coherence refers to spatial correlation of consecutive bases, and coherent CT, where coherence refers to CT occurring as a single process.
- [49] Reimers, J.R.; Hush, N.S. Electron transfer and energy transfer through bridged systems II. Tight binding linkages with zero asymptotic band gap. *Chem. Phys.* **146**, 89-103 (1990).

- [50] (a) Mujica, V.; Kemp, M.; Ratner, M.A. Electron conduction in molecular wires I: a scattering formalism. *J. Chem. Phys.* **101**, 6856-6864 (1994). (b) Kemp, M.; Mujica, V.; Ratner, M.A. Molecular electronics: disordered molecular wires. *J. Chem. Phys.* **101**, 5172-5178 (1994).
- [51] Hsu, C.P.; Marcus, R.A. A sequential formula for electronic coupling in long-range bridge-assisted electron transfer. Formulation of theory and application to alkanethiol monolayers. *J. Chem. Phys.* **106**, 584-598 (1997).
- [52] Renger, T.; Marcus, R.A. Variable-range hopping electron transfer through disordered bridge states: application to DNA. *J. Phys. Chem. A.* **107**, 8404-8419 (2003).

Chapter 4

A Role for DNA-Mediated Charge Transport in Regulating p53: Oxidation of the DNA- Bound Protein from a Distance

Adapted from Augustyn, K.E.; Barton, J.K. Submitted for publication in 2007.

4.1 Introduction

The protein p53 is a 393 amino acid tumor suppressor protein involved in controlling cellular pathways that include apoptosis, cell cycle arrest, and DNA repair [1, 2]. Functioning as a transcription factor controlling the expression of myriad downstream genes, p53 must distinguish between promoters in order to regulate pathways under different cellular pressures, such as hypoxia and oxidative stress [3]. It is no surprise that a protein this crucial to cellular integrity is tightly regulated; a critical negative regulator of p53 function is Mdm2, an E3 ubiquitin ligase that, when bound to p53, facilitates its degradation [4]. Here we show how the affinity of p53 for specific promoter sequences, including that encoding the *Mdm2* gene, can be altered from a distance through DNA-mediated oxidation of p53. A consensus p53 binding site as well as DNA promoters regulated by p53, (i) *Gadd45*, a gene encoding a DNA repair protein, (ii) *p21*, encoding a cyclin dependent kinase inhibitor, and (iii) *Mdm2*, encoding the negative regulator of p53, were synthesized containing a tethered DNA photooxidant, anthraquinone [4-6]. With photoactivation to initiate oxidation at long range mediated by the DNA π -stack, we observe dissociation of p53 from its consensus site, *Gadd45* and *Mdm2* promoters but not from the *p21* promoter. Introduction of an intervening CA mismatch, which inhibits DNA-mediated charge transport (CT), prevents this dissociation of p53; photoactivation occurs from a distance. Furthermore, MALDI-TOF mass spectrometry supports the chemical oxidation of the protein. Oxidation of p53 bound to DNA can thus be accomplished from a distance through DNA-mediated CT and yields promoter-specific changes in p53 binding. These results suggest a novel

mechanism utilizing DNA-mediated CT by which p53 activity on different promoters may be controlled under conditions of oxidative stress.

The sequence-specific activation of transcription by p53 depends upon its ability to bind to a consensus sequence within the promoter region. The consensus sequences for p53 consist of two symmetric response elements PuPuPuC(A/T)(T/A)GPyrPyrPyr spaced 0-13 base pairs apart [7]. Many of the natural promoter sequences that bind p53 do not have a 100% consensus match. Conversely, some sequences that share 100% homology with the consensus sequence do not bind p53 [8]. Most p53 mutations found in human tumors are located in the DNA-binding domain and involve amino acid residues that contact DNA or are required for proper folding [9, 10]. The strength of p53 binding to a specific DNA sequence is also influenced by post translational modification and the redox state of the protein [8, 11-13]. In particular, oxidative conditions decrease the specific affinity of p53 for certain promoters. In the DNA binding domain are ten conserved cysteines, of which three are involved in zinc coordination [9]. Interestingly, cysteine 277, seen hydrogen bonded to the consensus sequence in the crystal structure of p53 bound to DNA, has been proposed to undergo disulfide bond formation with cysteine 275, which would alter p53 binding to DNA in a redox-sensitive manner [14]. Cysteines 141 and 135, only 3.8 Å apart, are also in close proximity to the DNA bases and represent additional targets for disulfide bond formation that could alter DNA binding.

Oxidative damage to DNA arising at long range through DNA-mediated CT has now been demonstrated using a variety of pendant, distally bound photooxidants [15-19]. We have shown that oxidative damage to DNA can occur at least 200 Å away from the tethered oxidant [16]. Although this reaction displays a shallow distance dependence, it

is exquisitely sensitive to perturbations in the intervening base pair stack; DNA binding-proteins, intervening mismatches, and base lesions can serve to attenuate charge migration [20]. This sensitivity of DNA CT to stacking perturbations has led to its application in developing novel electrochemical sensors [21, 22]. DNA CT has also been proposed to play a biological role in the detection of base lesions by DNA repair proteins [23]. Moreover, long-range oxidative DNA damage through CT has been demonstrated to occur within nucleosomes and within the cell nucleus [24, 25]. DNA CT can furthermore be harnessed to promote a variety of redox reactions on DNA triggered from a distance. We have shown that thymine dimers in DNA can be repaired at long range through DNA-mediated CT [26]. Most recently, we have determined that DNA CT can be utilized to promote the formation of disulfide bonds from thiols incorporated into the DNA backbone [27]. It is this chemistry, triggered from a distance, that we considered might also be useful in promoting reactions of proteins bound to DNA. Since p53 contains cysteine residues in close proximity within the DNA binding domain, we wondered if we could selectively oxidize the DNA-bound protein and in so doing, alter DNA binding through long-range CT. This chemistry from a distance, mediated by DNA, would then provide a completely new mechanism to globally regulate p53 binding. Figure 4.1 schematically illustrates this general chemistry.

4.2 Experimental

4.2.1 DNA synthesis

The consensus sequence with and without a mismatch, oligonucleotides containing the *p21* and *Gadd45* promoter region as well as the primers for the *Mdm2*

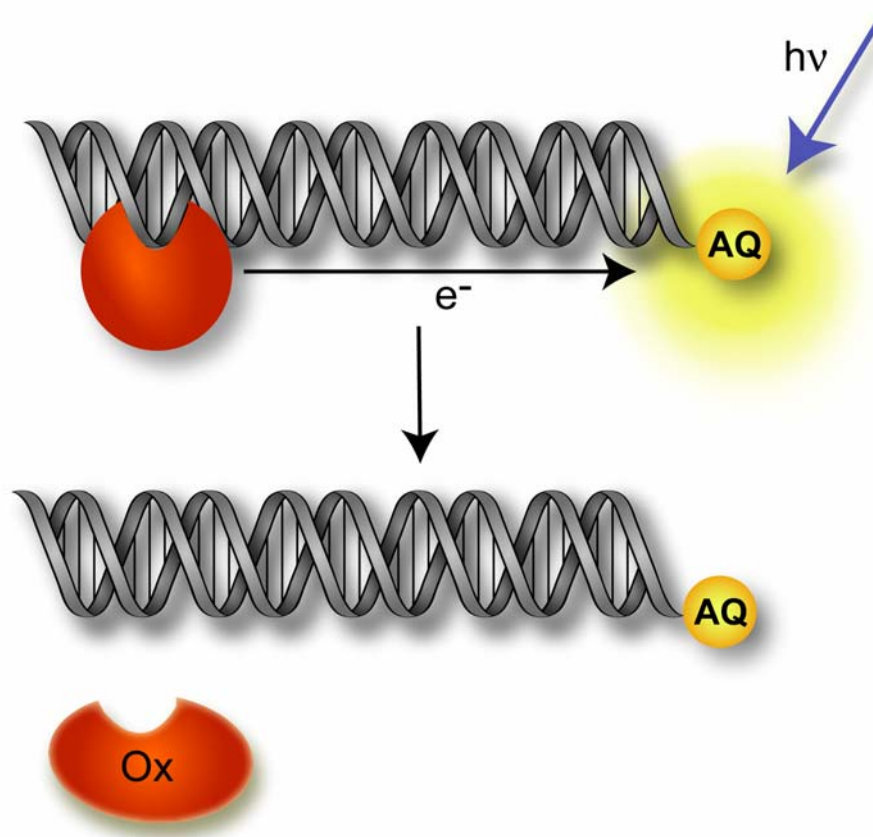


Figure 4.1. Schematic illustration of DNA-mediated charge transport to promote oxidation and dissociation of p53 (red), where anthraquinone (AQ) serves as the tethered, distally located photooxidant. Upon photoexcitation, the anthraquinone injects an electron hole into the DNA duplex that can migrate through the DNA to p53, resulting in protein oxidation. Oxidation can induce a conformational change in the DNA-binding domain of p53, promoting its dissociation from the DNA.

sequence were synthesized on an ABI 394 DNA synthesizer using standard phosphoramidite chemistry. Sequences not containing anthraquinone were synthesized with the trityl group intact and were deprotected and cleaved from the resin in NH_4OH overnight at 60 °C. The oligonucleotides were subsequently purified by reverse-phase HPLC before and after trityl group removal in 80% acetic acid and characterized by MALDI-TOF mass spectrometry. In synthesizing strands containing the anthraquinone photooxidant, including the primer for Mdm2, an anthraquinone derivative [anthraquinone-2-carboxylic acid (2-hydroxyethyl) amide], AQ-1 was used which was converted into its respective phosphoramidite and incorporated onto the 5' end of the sequence with a 15 minute coupling time [31]. Strands were cleaved from the resin and deprotected in NH_4OH at 60 °C overnight. AQ-DNA was purified once by reverse-phase HPLC and characterized by MALDI-TOF mass spectrometry. The oligonucleotides were quantified using UV-visible spectroscopy and annealed to their respective duplexes by heating equal moles of complementary strands to 90 °C for 5 minutes and slow cooling to ambient temperature in a buffer containing 5 mM sodium phosphate, 50 mM NaCl, pH 7. The resulting duplexes were purified on a 10% native acrylamide gel at 4° C to remove excess single strand. The desired duplex band was excised from the gel by UV shadowing and eluted into 1 mM Tris pH 8.5 buffer over night at 4 °C. The DNA was then ethanol precipitated and resuspended in a buffer containing 5 mM sodium phosphate, 50 mM NaCl, pH 7. DNA duplexes were labeled at the 5' end with [^{32}P] γ -ATP using polynucleotide kinase, and excess ATP was removed using a Micro Bio-Spin 6 chromatography column (Biorad). A small amount of the labeled duplex was mixed with a known concentration of cold duplex.

The 150 base pair duplex containing the human *Mdm2* promoter was constructed from a HeLa DNA template and primers synthesized as described above for standard PCR amplification. The primers used were 5'-GCTTTTCCTCTTGAGCTGGTC-3' (forward) or the anthraquinone-tethered analogue and 5'-CGTGCCCCACAGGTCTACC-3' (reverse). After incubation at 95 °C for 4.5 minutes, 40 cycles were performed as follows: 94 °C for 30 seconds; 55 °C for 1 minute; 72 °C for 30 seconds. The PCR product was purified using a QIAquick PCR purification kit (Qiagen), desalted using a Micro Bio-Spin 6 chromatography column (Biorad), and quantified by agarose gel electrophoresis running a 1 kb ladder standard for comparison. DNA strands were labeled at the 5' end with [³²P] γ -ATP using polynucleotide kinase, and excess ATP was removed using a Micro Bio-Spin 6 chromatography column (Biorad). A small amount of the labeled duplex was mixed with a known concentration of cold duplex.

4.2.2 Gel mobility shift assay

Human p53 used in binding experiments was purchased from Protein One. Protein was allowed to bind to the DNA by incubating 0.5 μ M p53 with 0.125 μ M labeled duplex in the presence of 5 μ M poly d(AT) (Amersham pharmaceuticals), 0.1% np-40, 0.1 mg/mL BSA (New England Biolabs) in 20 mM Tris-Cl pH 8, 20% glycerol, 100 mM KCl, and 0.2 mM EDTA for 1 hour at ambient temperature. The samples were subsequently either irradiated at 350 nm for 30 or 45 minutes using a 1000 W Hg/Xe lamp with a 320 nm long-pass filter and monochromator or stored in the dark prior to gel loading. Samples containing the *Mdm2* promoter complexed with p53 were loaded onto a 4-20% gradient acrylamide gel (Biorad) in 0.3% TBE with 0.1% Triton-X while those

containing the consensus sequence, *p21*, or *Gadd45* promoters were run on an 8% acrylamide gel. The gradient gels were electrophoresed for 3 hours at 50 V at 4° C, vacuum dried, and imaged using a Storm 820 phosphorimager (Molecular Dynamics/GE Healthcare) while the 8% gels were electrophoresed for 1.5 hours at 50 V at 4° C, and directly imaged as described above. The fraction of bound DNA was quantified using Image Quant 5.2. Each experiment was performed at least 2 times and the resulting quantifications averaged.

4.2.3 Mass spectrometry of oxidized p53

Samples containing p53 (1.2 μ M) were incubated with 0.3 μ M AQ-Con-1 for 1 hour in 20 mM Tris-Cl, pH 8, 20% glycerol, 100 mM KCl, and 0.2 mM EDTA. The samples were then either irradiated at 350 nm on the 1000 W Hg/Xe lamp for 3 hours or stored in the dark. The samples were digested with 0.4 μ g of trypsin (Promega) at 37 °C overnight. Digestion was quenched with 4 μ L acetic acid. The resulting peptides were concentrated and desalted using a C18 zip tip (Millipore) and mixed with an α -Cyano matrix. Samples were analyzed using a Voyager De-Pro MALDI (PerSeptive Biosystems) mass spectrometer and calibrated against Sequazyme standards.

4.3 Results and Discussion

4.3.1 DNA-mediated oxidation of p53 bound to a consensus sequence

In order to test whether DNA-bound p53 could be oxidized from a distance, a 100% consensus match sequence (LC-Con-1) and the analogous sequence (AQ-Con-1) containing the potent photooxidant anthraquinone (AQ) were synthesized and binding by

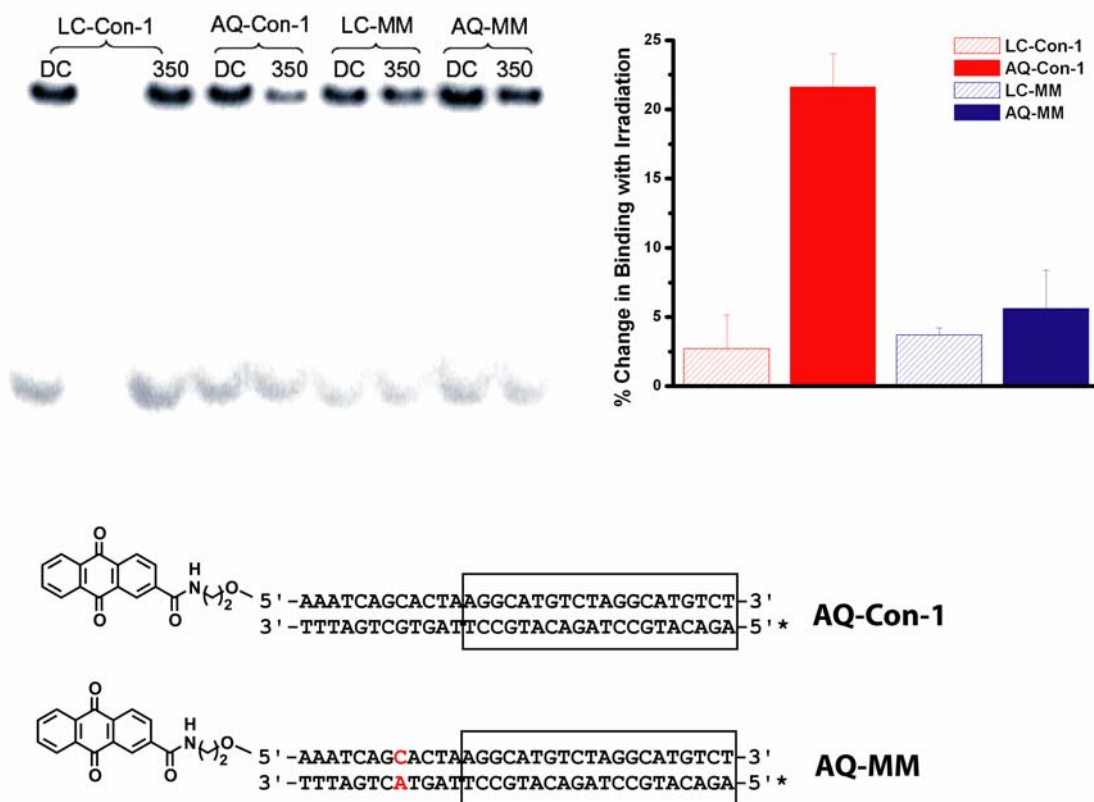


Figure 4.2. Oxidation of p53 bound to the consensus sequence with and without a base pair mismatch. The electrophoretic mobility shift assay (top left) is shown as an autoradiogram after electrophoresis under non-denaturing conditions of LC-Con-1, the consensus sequence without appended oxidant, LC-MM, the consensus sequence containing a CA mismatch, AQ-Con-1, the consensus sequence with tethered anthraquinone and AQ-MM, the mismatch containing consensus sequence with tethered anthraquinone both in the absence of irradiation (**DC**) and with irradiation for 30 min at 350 nm (**350**) in the presence of p53. The sequences for AQ-Con-1 and AQ-MM are shown below with the p53 binding site boxed and the site of ^{32}P -end labeling indicated by an asterisk; the CA mismatch is highlighted in red. A bar graph (top right) quantifying the percent change in binding with irradiation for the different sequences with and without the AQ photooxidant is also shown. The percent change in binding was determined as a ratio of the percentage of bound DNA in the dark control to that in the irradiated sample. Error bars reflect the standard deviations obtained from multiple trials. Samples contained 0.125 μM duplex, 0.5 μM p53, 5 mM poly d(AT), 0.1% np-40, 0.1 mg/mL BSA in 20 mM Tris-Cl, pH 8, 20% glycerol, 100 mM KCl, and 0.2 mM EDTA. See Experimental.

p53 determined by electrophoretic mobility shift assay (Figure 4.2). After incubating p53 with LC-Con-1 or AQ-Con-1, the sample was either irradiated at 350 nm for 30 minutes to activate AQ or left in the dark as a control. Following native gel electrophoresis, the amounts of p53 bound to AQ-Con-1 and LC-Con-1 with and without irradiation were compared. As can be seen in Figure 4.2, the amount of p53 bound to LC-Con-1 does not change with irradiation, nor does functionalization of the consensus DNA with AQ (AQ-Con-1) in the absence of light affect p53 binding. However, when AQ-Con-1 is irradiated, promoting DNA-mediated oxidation, the amount of bound DNA decreases; DNA-mediated CT appears to promote the dissociation of p53. To investigate further that the decrease in binding with photoactivation of AQ is the result of a DNA-mediated process, we examined binding to an AQ-functionalized consensus DNA containing a single CA mismatch intervening between the photooxidant and the p53 binding site (AQ-MM). It has been demonstrated extensively that single base mismatches perturb DNA-mediated CT [20, 21]. As can be seen also in Figure 4.2, little change is observed as a function of irradiation with the mismatch intervening; the introduction of a mismatch attenuates p53 dissociation. These results are consistent with p53 dissociation being the consequence of DNA-mediated CT.

4.3.2 DNA-mediated oxidation of p53 bound to promoter sequences

To test natural promoter sequences, promoter regions for the *p21* (LC-p21 and AQ-p21) and *Gadd45* (LC-G45 and AQ-G45) genes were synthesized with and without an anthraquinone photooxidant. The *p21* gene encodes a cyclin dependent kinase inhibitor, WAF1, involved in G₁ arrest while *Gadd45* encodes a protein active in G₂

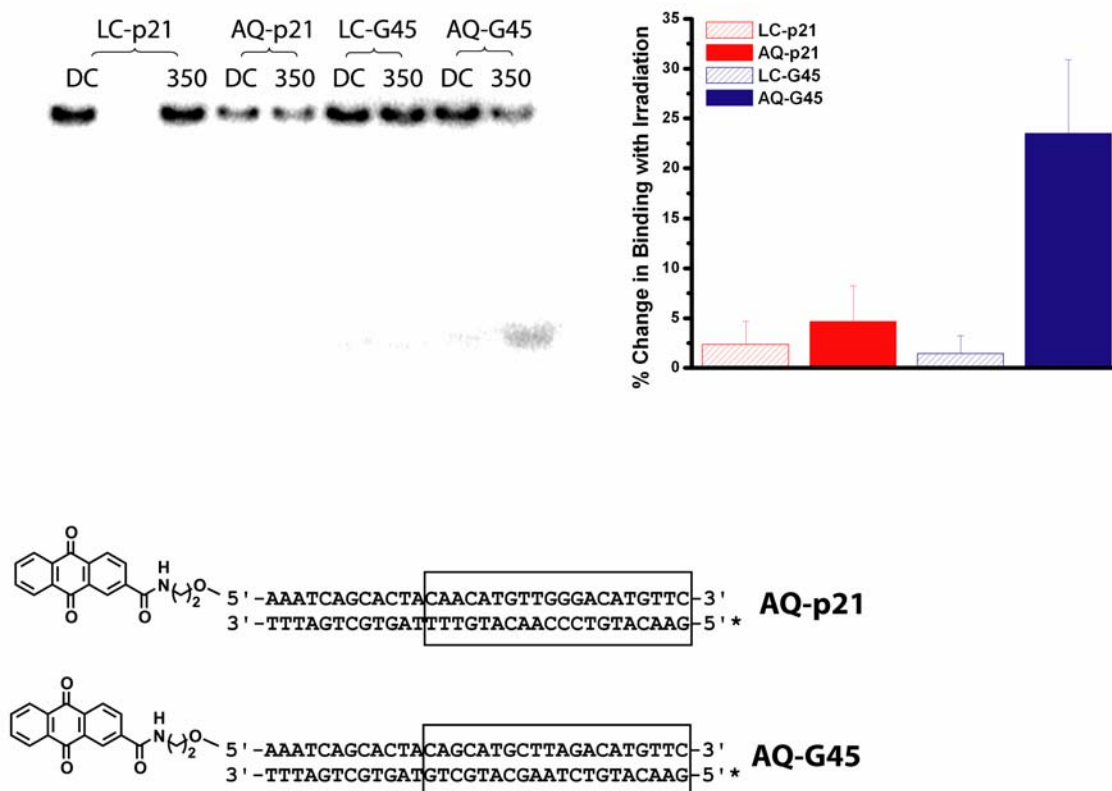


Figure 4.3. Sequence-selectivity in photooxidation of p53. Shown (top left) is an autoradiogram for the gel shift assay after electrophoresis under non-denaturing conditions of LC-p21, AQ-p21, LC-G45, and AQ-G45 both without irradiation (DC) and with irradiation for 30 min at 350 nm (350) in the presence of p53. The sequences of AQ-p21 and AQ-G45 with the p53 binding sites boxed are indicated below, where the asterisk indicates the site of ³²P-end labeling. A bar graph quantifying the percent change in binding with irradiation for the different sequences with and without the AQ photooxidant is also shown (top right). The percent change in binding was determined as a ratio of the percentage of bound DNA in the dark control to that in the irradiated sample. Error bars reflect the standard deviations obtained from multiple trials. Samples contained 0.125 μ M duplex, 0.5 μ M p53, 5 mM poly d(AT), 0.1% np-40, 0.1 mg/mL BSA in 20 mM Tris-Cl, pH 8, 20% glycerol, 100 mM KCl, and 0.2 mM EDTA. See Experimental.

arrest as well as in DNA repair [5, 6]. The two promoter sequences differ in four positions within the recognition element but have similar binding affinities [28]. Following incubation with p53, samples were irradiated or left in the dark, and binding of p53 to the two promoters was examined. Figure 4.3 shows that while p53 dissociates from the *Gadd45* sequence as a function of irradiation, the binding of p53 remains relatively unaltered on the *p21* promoter under analogous conditions. Therefore this oxidative dissociation, despite being triggered from distance, is sequence selective.

The fact that only certain sequences are affected by long-range oxidation provides a mechanism through which oxidized p53 can discriminate among promoters depending upon cellular conditions. Oxidative stress can lead to the generation of guanine radicals throughout the genome through DNA-mediated CT. The observation that binding to the *p21* promoter is not strongly affected by DNA-mediated CT suggests that, with oxidative stress, this cell cycle arrest protein is still transcribed. In contrast, based upon these results, the transcription of *Gadd45* would be expected to be down regulated; with substantial generation of guanine radicals, the DNA would be damaged beyond the capabilities of repair.

The E3 ubiquitin ligase, Mdm2, is a crucial protein involved in the regulation of p53 activity [4]. Binding of Mdm2 to p53 promotes its ubiquitination and signals for its transport to the cytoplasm where it is degraded. In turn, p53 transcribes the *Mdm2* gene resulting in a negative feedback loop for p53 transcriptional activity. We therefore considered whether conditions of severe oxidative stress would lead to decreased transcription of *Mdm2*, ensuring higher levels of p53 and therefore increased transcription of proapoptotic genes.

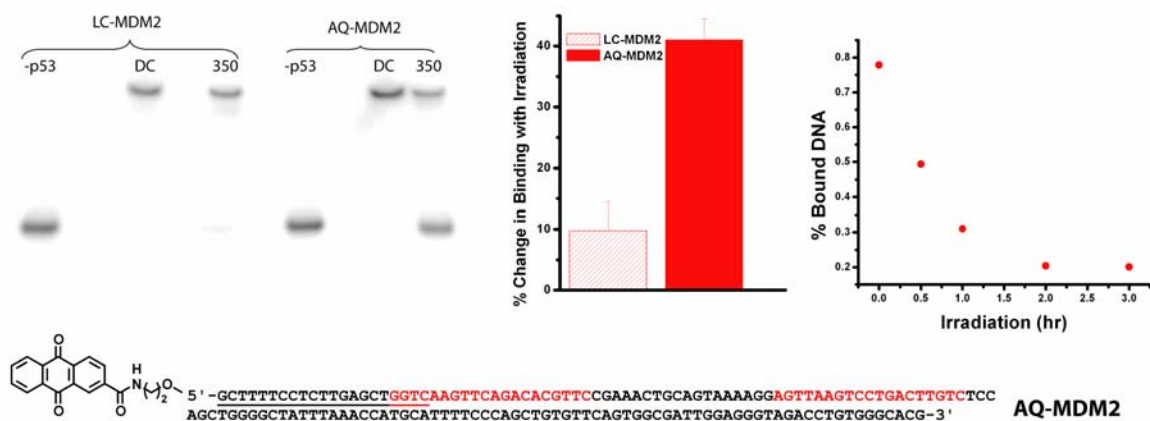


Figure 4.4. Oxidation of p53 bound to the *Mdm2* promoter. The gel shift assay shows an autoradiogram after electrophoresis under non-denaturing conditions of LC-MDM2, the sequence without appended oxidant and AQ-MDM2, the sequence containing a tethered anthraquinone both in the absence of irradiation (**DC**) and with irradiation for 45 min at 350 nm (**350**) in the presence of p53. Lanes marked -p53 contain only DNA. Quantification of the percent change in binding is also shown in a bar graph (top center), where the error bars reflect standard deviations from multiple trials. A time course for p53 dissociation from AQ-MDM2 is also shown (top right) as a function of irradiation. The *Mdm2* sequence tethered with anthraquinone is indicated below (the complementary ³²P-labeled strand is not shown), where the p53 binding sites are highlighted in red and the primers used are underlined. Samples contained 0.125 μ M duplex, 0.5 μ M p53, 5 mM poly d(AT), 0.1% np-40, 0.1 mg/mL BSA in 20 mM Tris-Cl, pH 8, 20% glycerol, 100 mM KCl, and 0.2 mM EDTA. See Experimental.

A 150 base pair fragment containing the human *Mdm2* promoter (LC-MDM2) was constructed as was an analogous fragment with tethered anthraquinone (AQ-MDM2). LC-MDM2 and AQ-MDM2 sequences were incubated with p53 and either irradiated at 350 nm for 45 minutes or left in the dark. The fraction of bound DNA is found to decrease as a function of irradiation for AQ-MDM2, where long-range CT occurs, but remains relatively unaltered for LC-MDM2, the fragment lacking the photooxidant (Figure 4.4). Increasing the extent of irradiation results in increased dissociation of p53 from the *Mdm2* promoter, as can be seen in an irradiation time course monitored by gel shift assay. Thus it appears that the dissociation of p53 can be triggered by photoinduced DNA CT with the photooxidant bound ~ 60 Å away. Importantly, this result supports the idea that, under conditions of oxidative stress, where p53 is essential, its level may be regulated through DNA-mediated oxidation, which, in turn, leads to the inhibition of the transcription of its negative regulator.

4.3.3 p53 oxidation by MALDI-TOF mass spectrometry

In order to confirm that the dissociation of p53 from certain DNA sequences is due to chemical oxidation of the protein, we analyzed peptides resulting from a tryptic digest of p53 after irradiation in the presence of AQ-Con-1. Digestion with trypsin results in multiple peptide fragments, one of which contains cysteine 141, a residue located near the DNA-binding region of the protein. This fragment, with a mass of 1854 is detected in the absence of irradiation and corresponds to a fragment with cysteine 141 in the reduced state (Figure 4.5). Following 3 hours of irradiation at 350 nm of AQ-Con-1 in the presence of p53, however, this peak is lost. A likely explanation is that

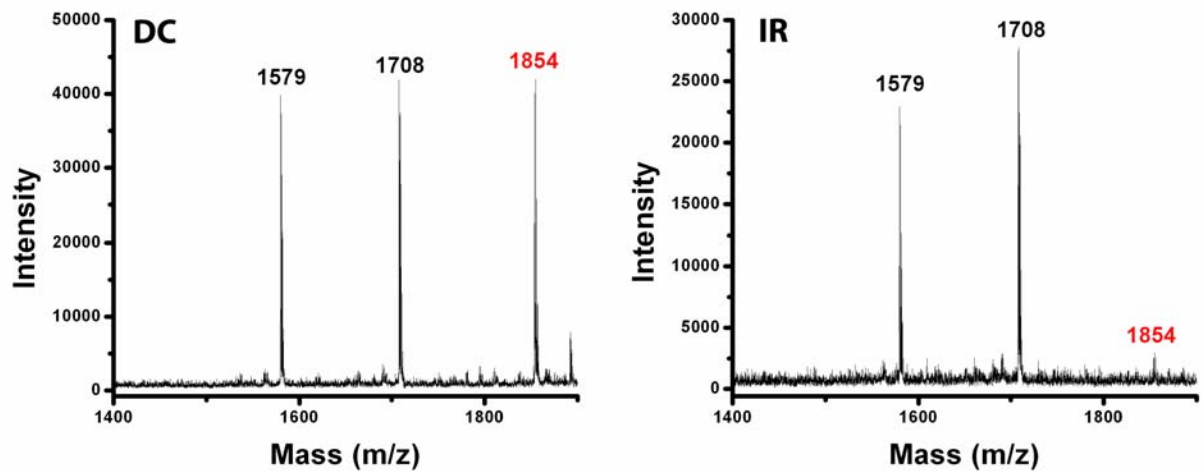


Figure 4.5. MALDI-TOF mass spectrometry of a p53 tryptic digest following incubation with AQ-Con-1 without (**DC**) or with (**IR**) 3 hours of irradiation at 350 nm. Samples contained 0.3 μM duplex and 1.2 μM p53 in 20 mM Tris-Cl, pH 8, 20% glycerol, 100 mM KCl, and 0.2 mM EDTA. See Experimental. The fragment with a mass of 1854 corresponds to the peptide TCPVQWVDSTPPPGTR containing cysteine 141.

DNA-mediated oxidation promotes formation of a disulfide bond between cysteine 141 and the nearby cysteine 135 (associated with another tryptic fragment) that yields a much larger molecular weight fragment after trypsin digestion; cysteine, in fact, has the lowest oxidation potential of all the residues, and significantly lower than guanine. It is noteworthy, however, that the 1854 molecular weight fragment additionally contains a tryptophan, a residue that also may be easily oxidized in an electron transfer reaction [29]. However tryptophan oxidation would be expected to yield a fragment of ~1870 which we do not observe. Oxidation of cysteines 275 and 277 had earlier been proposed as a possible redox regulatory switch associated with p53 binding [14]. Trypsin digestion of p53 leads to two fragments with molecular weights of 1708 and 1709, one of which contains both cysteine 275 and 277. We could not reliably resolve these peaks from one another and from the cysteine 275-277 disulfide product. It is therefore difficult to determine whether cysteines 275 and 277 also undergo oxidation. Nonetheless, the specific changes in fragmentation pattern we observe with irradiation, particularly the loss of the 1854 molecular weight fragment, establish clearly that DNA-bound p53 is chemically changed. Photoactivation of the tethered AQ leads to oxidation of the DNA-bound protein from a distance.

The activation and functions of p53 are exquisitely sensitive to the cellular environment. Indeed, increasing levels of oxidative stress can cause p53 to transcribe either proapoptotic or antiapoptotic genes, depending upon cellular pressures, thus allowing the cell either to survive and undergo repair under conditions of low stress, or undergo apoptosis under conditions of high stress [30]. Our results provide a chemical basis to understand these opposing biological responses. The oxidation of DNA-bound

p53 from a distance, generated by photooxidation in our experiments and presumably through charge migration among guanine radicals within the cell, is sequence selective, requiring the intimate association of p53 with DNA to promote charge transfer from the DNA and protein oxidation. Without this protein-DNA interaction, p53 oxidation and subsequent dissociation from the DNA does not occur. Hence DNA-mediated CT, reflecting the extent of oxidative stress in the cell, can provide a general route at long range to regulate p53 binding to different promoters.

4.4 References

- [1] Vogelstein, B.; Lane, D.; Levine, A.J. Surfing the p53 network. *Nature* **408**, 307-10 (2000).
- [2] Vousden, K.H.; Lu, X. Live or let die: the cell's response to p53. *Nat. Rev. Cancer* **2**, 594-604 (2002).
- [3] Prives, C.; Hall, P.A. The p53 pathway. *J. Pathol.* **187**, 112-126 (1999).
- [4] Brooks, C.L.; Gu, W. p53 ubiquitination:mdm2 and beyond. *Mol. Cell* **21**, 307-315 (2006).
- [5] El-Deiry, W.S.; Tokino, T.; Velculescu, V.E.; Levy, D.B.; Parsons, R.; Trent, J.M.; Lin, D.; Mercer, W.E.; Kinzler, K.W.; Vogelstein, B. WAF1, a potential mediator of p53 tumor suppression. *Cell* **75**, 817-825 (1993).
- [6] Kastan, M.B.; Zhan, Q.; el-Deiry, W.S.; Carrier, F.; Jacks, T.; Walsh, W.V.; Plunkett, B.S.; Vogelstein, B.; Fornace, A. A mammalian cell cycle checkpoint pathway utilizing p53 and GADD45 is defective in ataxia-telangiectasia. *Cell* **71**, 587-597 (1992).
- [7] El-Deiry, W.S.; Kern, S.E.; Pietenpol, J.A.; Kinzler, K.W.; Vogelstein, B. Definition of a consensus binding site for p53. *Nat. Genet.* **1**, 45-49 (1992).
- [8] Kim, E.; Albrechtsen, N.; Deppert, W. DNA-conformation is an important determinant of sequence-specific DNA binding by tumor suppressor p53. *Oncogene* **15**, 857-869 (1997).
- [9] Cho, Y.; Gorina, S.; Jeffrey, P.D.; Pavletich, N.P. Crystal structure of a p53 tumor suppressor-DNA complex: understanding tumorigenic mutations. *Science* **265**, 346-354 (1994).

- [10] Ho, W.C.; Fitzgerald, M.X.; Marmorstein, R. Structure of the p53 core domain dimer bound to DNA. *J. Biol. Chem.* **281**, 20494-20502 (2006).
- [11] Meplan, C.; Richard, M.J.; Hainaut, P. Redox signalling and transition metals in the control of the p53 pathway. *Biochem. Pharm.* **59**, 25-33 (2000).
- [12] Hainaut, P.; Milner, J. Redox modulation of p53 conformation and sequence-specific DNA binding in vitro. *Cancer Res.* **53**, 4469-4473 (1993).
- [13] Rainwater, R.; Parks, D.; Anderson, M.E.; Tegmeyer, P.; Mann, K. Role of cysteine residues in regulation of p53 function. *Mol. Cell. Biol.* **15**, 3892-903 (1995).
- [14] Buzek, J.; Latonen, L.; Kurki, S.; Peltonen, K.; Laiho, M. Redox state of tumor suppressor p53 regulates its sequence-specific DNA binding in DNA-damaged cells by cysteine 277. *Nucleic Acids Res.* **30**, 2340-2348 (2002).
- [15] Hall, D.B.; Holmlin, E.R.; Barton, J.K. Oxidative DNA damage through long-range electron transfer. *Nature* **382**, 731-735 (1996).
- [16] Nuñez, M.E.; Hall, D.B.; Barton, J.K. Long-range oxidative damage to DNA: effects of distance and sequence. *Chem. Biol.* **6**, 85-97 (1999).
- [17] Henderson, P.T.; Jones, D.; Hampikian, G.; Kan, Y.Z.; Schuster, G.B. Long-distance charge transport in duplex DNA: the phonon-assisted polaron-like hopping mechanism. *Proc. Natl. Acad. Sci. USA.* **96**, 8353-8358 (1999).
- [18] Bixon, M.; Giese, B.; Wessely, S.; Langenbacher, T.; Michel-Beyerle, M.E.; Jortner, J. Long-range charge hopping in DNA. *Proc. Natl. Acad. Sci. USA.* **96**, 11713-11716 (1999).

- [19] Dohno, C.; Ogawa, A.; Nakatani, K.; Saito, I. Hole trapping at N₆-cyclopropyldeoxyadenosine suggests a direct contribution of adenine bases to hole transport through DNA. *J. Am. Chem. Soc.* **125**, 10154-10155 (2003).
- [20] Delaney, S.; Barton, J.K. Long-range DNA charge transport. *J. Org. Chem.* **68**, 6475-6483 (2003).
- [21] Boon, E.M.; Ceres, D.M.; Drummond, T.G.; Hill, M.G.; Barton, J.K. Mutation detection by electrocatalysis at DNA-modified electrodes. *Nat. Biotechnol.* **18**, 1096-1100 (2000).
- [22] Boon, E.M.; Salas, J.E.; Barton, J.K. An electrical probe of protein-DNA interactions on DNA-modified surfaces. *Nat. Biotechnol.* **20**, 282-286 (2002).
- [23] Boal, A.K.; Yavin, E.; Lukianova, O.A.; O'Shea, V.L.; David, S.S.; Barton, J.K. DNA-bound redox activity of DNA repair glycosylases containing [4Fe-4S] clusters. *Biochemistry* **44**, 8397-8407 (2005).
- [24] Nuñez, M.E.; Noyes, K.T.; Barton, J.K. Oxidative charge transport through DNA in nucleosome core particles. *Chem. Biol.* **9**, 403-415 (2002).
- [25] Nuñez, M.E.; Holmquist, G.P.; Barton, J. K. Evidence for charge transport in the nucleus. *Biochemistry* **23**, 12465-12471 (2001).
- [26] Dandliker, P.J.; Holmlin, E.R.; Barton, J.K. Oxidative thymine dimer repair in the DNA helix. *Science* **275**, 1465-1468 (1997).
- [27] Takada, T.; Barton, J.K. DNA charge transport leading to disulfide bond formation. *J. Am. Chem. Soc.* **127**, 12204-12205 (2005).

- [28] Weinberg, R.L.; Veprintsev, D.B.; Bycroft, M.; Fersht, A.R. Comparative binding of p53 to its promoter and DNA recognition elements. *J. Mol. Biol.* **348**, 589-596 (2005).
- [29] Wagenknecht, H.A.; Stemp, E.D.A.; Barton, J.K. Evidence of electron transfer from peptides to DNA: Oxidation of DNA-bound tryptophan using the flash-quench technique. *J. Am. Chem. Soc.* **122**, 1-7 (2000).
- [30] Sablina, A.A.; Budanov, A.V.; Ilyinkaya, G.V.; Agapova, L.S.; Kravchenko, J.E.; Chumakov, P.M. The antioxidant function of the p53 tumor suppressor. *Nat. Med.* **11**, 1306-1313 (2005).
- [31] Gasper, S.M.; Schuster, G.B. Intramolecular photoinduced electron transfer to anthraquinones linked to duplex DNA: The effect of gaps and traps on long-range radical cation migration. *J. Am. Chem. Soc.* **119**, 12762-12771 (1997).

Chapter 5

Charge Separation in Ruthenium-Quencher Conjugates Bound to DNA

*Adapted from Augustyn, K.E.; Barton, J.K. Submitted for publication in 2007.

5.1 Introduction

It is well established that the π -stack of the DNA double helix can serve as an efficient medium for charge transport [1-5]. With reactions spanning distances over 200 Å, this process is acutely sensitive to the intervening bridging bases [6, 7]. Oxidative base damage resulting from DNA-mediated charge transport reaction has particular relevance in the field of aging and in many diseases including cancer and neurodegenerative disorders [8-10]. Guanine, having the lowest oxidation potential of the naturally occurring bases can effectively serve as a hole trap [11]. Upon oxidation, the neutral guanine radical, with a millisecond lifetime, can react irreversibly with water or oxygen to form permanent damage products such as 8-oxo-G, oxazolone, and imidazolone [12]. While biochemical techniques to probe guanine damage yields at long range have been auspicious in underscoring the exquisite sensitivity of charge transport to base stacking and sequence, due to the slow trapping rate of the guanine radical, these studies are inevitably convoluted by processes such as back electron transfer and hence provide information several steps removed from the initial transport event [13].

Elucidating the kinetics of charge transport through DNA is a fundamental aspect of mechanistically understanding this process. Previous studies have measured charge transport rates through relatively short DNA assemblies using techniques such as pulse radiolysis [14] and transient absorption spectroscopy [15, 16]. However, these studies probe transport using external reporters, and do not directly detect base radicals. Although guanine oxidation can be detected spectroscopically owing to the characteristic absorption of its radical centered at 390 nm, the small extinction coefficient of the

guanine radical can pose a significant challenge in delineating charge transport rates particularly if it overlaps with absorbances from the photooxidant.

Our lab has extensively studied DNA charge transport reactions using rhodium and ruthenium metallointercalators as photooxidants [17]. These complexes are ideal probes for charge transport reactions due to the strong electronic coupling between the intercalating ligand and the DNA π -stack. Both the phi complexes of rhodium (III) and the dppz complexes of ruthenium (II) can be utilized to probe biochemically charge transport through techniques such as gel electrophoresis. More recently these complexes have served as potent photooxidants in charge transport studies utilizing cyclopropylamine-substituted bases as hole traps. With irreversible oxidative ring opening occurring on the picosecond time scale, cyclopropylamine-substituted nucleosides provide a means to delineate hole transport on time scales competitive with back electron transfer [18-21]. The dppz complexes of ruthenium (II) have an added advantage in that they can be used to probe spectroscopically charge transport kinetics using a modified flash-quench technique [22].

Pioneered by Gray and co-workers to study high driving force reactions in cytochrome c [23], flash-quench methodologies have been modified to successfully monitor rates of guanine radical formation in DNA [24, 25]. Adapting the flash-quench technique to systems involving DNA requires assemblies in which a polypyridyl ruthenium (II) metallointercalator, upon excitation into its MLCT, donates an electron to an external quencher such as $[\text{Ru}(\text{NH}_3)_6]^{3+}$, methyl viologen, or $[\text{Co}(\text{NH}_3)_5\text{Cl}]^{2+}$. The powerful ground state oxidant Ru(III) thus generated *in situ*, and with a 1.5 V electrochemical potential, is capable of oxidizing guanine. Rates of hole injection into the

duplex and rates of transport between Ru(III) and guanine can thus be determined from the formation of the transiently generated Ru(III) and the guanine radical.

Previously our lab utilized the flash-quench technique to measure rates of DNA-mediated charge transport between the artificial base 4-methylindole and the tris heteroleptic ruthenium complex, $[\text{Ru}(\text{phen})(\text{dppz})(\text{bpy}')]^{2+}$ [26, 27]. 4-methylindole was used in place of a selected guanine residue in this study due the favorable spectroscopic properties of its radical, low oxidation potential (~ 1.0 V vs. NHE) and the ability to fix effectively the distance between the donor and acceptor without interference from additional guanines. Interestingly, regardless of the sequence or the distance between the donor and acceptor, all rates of methylindole radical formation were found to be on the order of 10^7 s^{-1} , coincident with the rate of hole injection. As hole injection rates are measured by the decay of the Ru(II) oxidant, they are dependent on diffusional quenching, which in this particular system is rate-limiting.

Thus, in order to measure rates occurring on a faster time scale than that of diffusional quenching, we have developed a system in which the quencher is covalently tethered to the ruthenium complex, effectively eliminating the rate-limiting quenching step. Several groups have covalently tethered quencher moieties to ruthenium complexes. One study showed that a viologen tethered ruthenium complex exhibits a long-lived charge separated state and is able to photocleave DNA under inert atmosphere [28]. In another study, intramolecular electron transfer was observed between ruthenium complexes covalently tethered to quenchers through Schiff base bridges [29]. Intermolecular quenching has also been observed in ruthenium complexes in which a bipyridine ligand is covalently tethered to a quinone functionality [30].

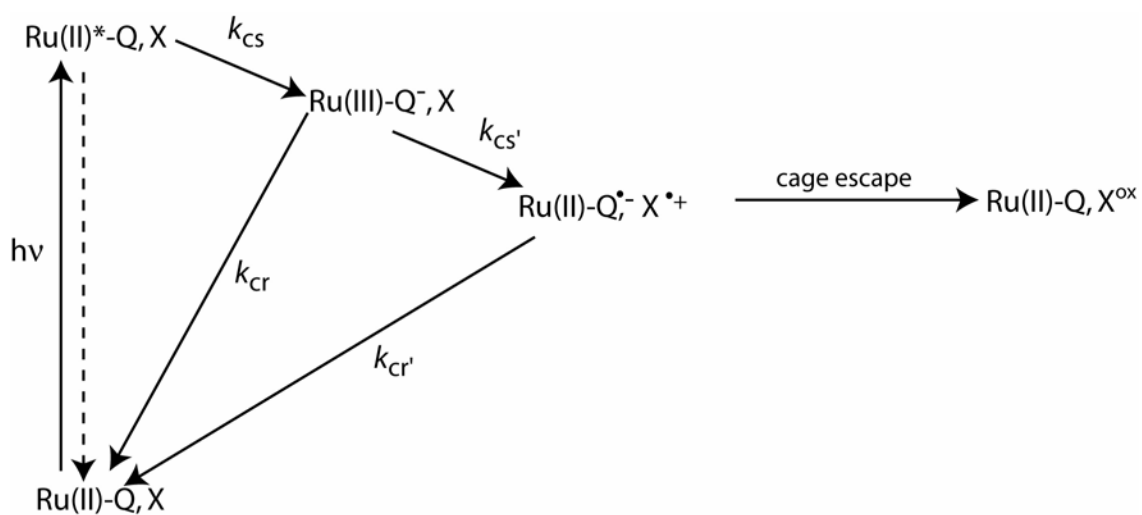


Figure 5.1. Modified flash-quench scheme for a covalently tethered Ru(II) quencher complex. Upon excitation with 450 nm light, the ruthenium (II) is raised to its excited state and is subsequently oxidized by the tethered quencher to form the powerful ground state oxidant, Ru(III). Ru(III) is capable of oxidizing DNA but can also recombine with the reduced quencher to form the ground state starting materials. X denotes a nucleotide base such as guanine which may be oxidized by Ru(III).

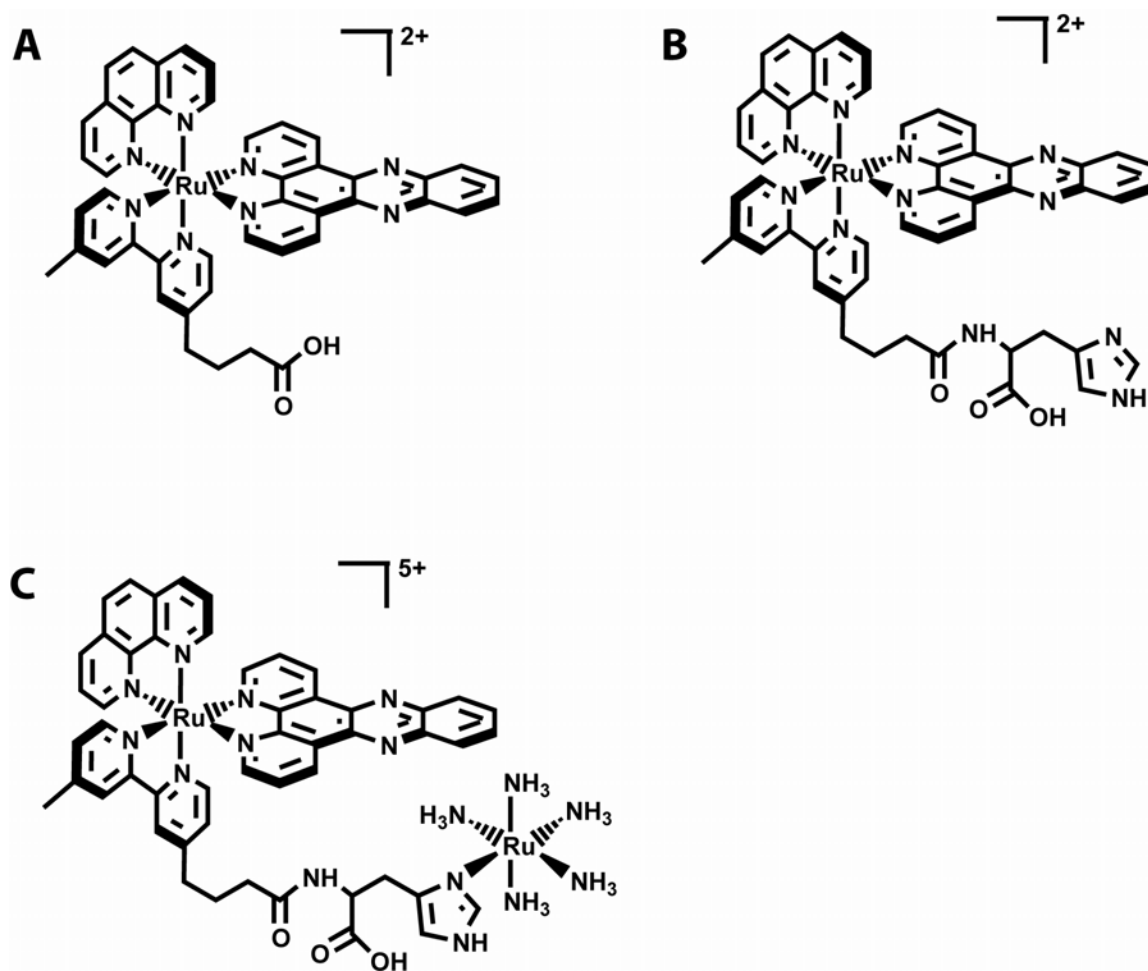


Figure 5.2. Tris heteroleptic dipyrrophenazine complexes of ruthenium (II) used in the study. The parent complex, $[\text{Ru}(\text{phen})(\text{dppz})(\text{bpy}')]^{2+}$ is shown in **A**, the histidine modified complex $[\text{Ru}(\text{phen})(\text{dppz})(\text{bpy}'\text{-his})]^{2+}$ is shown in **B**, and the ruthenium pentammine coordinated complex $[\{\text{Ru}(\text{phen})(\text{dppz})(\text{bpy}'\text{-his})\} \{\text{Ru}(\text{NH}_3)_5\}]^{5+}$ is shown in **C**.

In the current study we describe the synthesis and characterization of a ruthenium quencher conjugate in which a ruthenium pentaammine quencher is covalently tethered to a tris heteroleptic ruthenium complex via coordination to the imidazole of a bridging histidine. This system allows us to observe flash-quench generated guanine damage in addition to novel charge separation pathways reflecting the rich redox chemistry of ruthenium complexes interacting with DNA. Figure 5.1 illustrates this intramolecular flash-quench scheme.

5.2 Experimental

5.2.1 DNA synthesis

DNA polymers were purchased from Amersham and dialyzed against a buffer of 10 mM sodium phosphate, 50 mM NaCl, pH 7 prior to use. Reagents for solid-phase DNA syntheses were purchased from Glen Research. Oligonucleotides with without cyclopropylamine-modified bases were prepared on an Applied Biosystems 394 DNA synthesizer using standard phosphoramidite chemistry leaving the 5' dimethoxytrityl group intact. Cyclopropylamine-containing strands were synthesized using the precursor bases 2-fluoroinosine and 4-thiouracil for ^{CP}G and ^{CP}C respectively. Cyclopropyl substitution was accomplished by incubating the resin in 1 M diaza(1,3)bicyclo[5.4.0]undecane (DBU) in acetonitrile for 2 hours prior to overnight incubation in 6 M aqueous cyclopropylamine at 60 °C resulting in simultaneous cleavage, deprotection, and substitution. Oligonucleotides without cyclopropyl substitutions were cleaved from the resin and deprotected by incubation in NH₄OH overnight at 60 °C. Strands were purified by reverse-phase HPLC using a C18 column (Varian). The trityl

group was removed by treatment with 80% acetic acid for 15 minutes, and the resulting strands were purified again by reverse-phase HPLC. All strands were characterized by MALDI-TOF mass spectrometry. Duplexes were annealed by heating equimolar amounts of complementary strands determined by absorbance at 260 nm to 90 °C and slow cooling to ambient temperature.

5.2.2 Synthesis and characterization of $[Ru(phen)(dppz)(bpy'-his)]Cl_2$

All solid-phase reactions used dry solvents purchased from Fluka stored over molecular sieves. $[Ru(phen)(dppz)(bpy'-his)]^{2+}$ ($bpy'-his$ = 4' methyl-2,2'-bipyridine-4-butanoic acid (histidinyl)-amide, $dppz$ = dipyrido[3,2-a:2',3'-c]phenazine) (Figure 5.2) was prepared starting with $[Ru(phen)(dppz)(bpy')]^{2+}$, the synthesis of which has been described [31, 32]. Resin-bound Fmoc-His(Fmoc) was purchased from Bachem and the Fmoc group removed with 20% piperidine in DMF prior to synthesis. The resin-bound histidine was combined with racemic $[Ru(phen)(dppz)(bpy')]^{2+}$ (1 equiv), PyBOP (3 equiv), and diisopropylethylamine (6 equiv) in DMF and stirred at ambient temperature overnight in the dark. The complex was cleaved from the resin by stirring with 95% aqueous TFA for 1 hr, precipitated by filtration into ice-cold tert-butyl methyl ether, washed with cold ether and dried *in vacuo*. $[Ru(phen)(dppz)(bpy'-his)]^{2+}$ was purified by reverse-phase HPLC on a semipreparative Microsorb (Varian) C18 column using a water-acetonitrile (0.1% TFA) gradient and a flow rate of 4 mL/min. The percentage of acetonitrile was held constant at 15% for 15 minutes and then increased to 40% over 75 minutes. Chromatograms were monitored at 260, 370, and 450 nm with the desired isomer peaks eluting at 41 and 46 minutes.

ESI and MALDI-TOF mass spectrometries were used to successfully characterize $[\text{Ru}(\text{phen})(\text{dppz})(\text{bpy}'\text{-his})]^{2+}$ (calculated: 478.1 (+2), found: 478.5). ^1H NMR (600 MHz, CD_3CN) δ (aromatic Hs: 9.56(m), 8.69(d), 8.56(m), 8.45(m), 8.29(m), 8.12(m), 7.98(d), 7.84(m), 7.74(m), 7.68(m), 7.60(m), 7.50(m), 7.18(m) δ (aliphatic Hs): 4.64(d), 3.28(d), 3.17(m), 3.07(d), 2.73(s), 2.52(s), 2.22(s), 1.23(m). The aromatic to aliphatic proton ratio was 23:12. As the absorbance of histidine does not effect the 440 nm MLCT transition of ruthenium complexes, $[\text{Ru}(\text{phen})(\text{dppz})(\text{bpy}'\text{-his})]^{2+}$ was confirmed to have a similar extinction coefficient to $[\text{Ru}(\text{phen})(\text{dppz})(\text{bpy}')]^{2+}$ of $19,500 \text{ M}^{-1}\text{cm}^{-1}$ as shown by ICP-MS.

5.2.3 Synthesis and characterization of $[\{\text{Ru}(\text{phen})(\text{dppz})(\text{bpy}'\text{-his})\}\{\text{Ru}(\text{NH}_3)_5\}]\text{Cl}_5$

$[\{\text{Ru}(\text{phen})(\text{dppz})(\text{bpy}'\text{-his})\}\{\text{Ru}(\text{NH}_3)_5\}]^{5+}$ (Figure 5.2) was synthesized in a similar manner to $[\text{Ru}(\text{phen})(\text{dppz})(\text{bpy}'\text{-his})]^{2+}$ as described above with one additional step. Following coupling with $[\text{Ru}(\text{phen})(\text{dppz})(\text{bpy}')]^{2+}$, the reddish orange resin was reacted with chloropentaammineruthenium (III) chloride by procedures set forth by Gray et al. for preparing ruthenium-modified proteins [23]. The $[\text{Ru}(\text{phen})(\text{dppz})(\text{bpy}')]^{2+}$ tethered histidine-bound resin was stirred for 1.5 days under argon in aqueous 50 mM $[\text{Ru}(\text{NH}_3)_5(\text{H}_2\text{O})]^{2+}$ prepared from reduction of $[\text{Ru}(\text{NH}_3)_5\text{Cl}]^{2+}$ (Strem) with zinc amalgam [33, 34]. The complex was cleaved from the resin following the same procedure as described above for $[\text{Ru}(\text{phen})(\text{dppz})(\text{bpy}'\text{-his})]^{2+}$. HPLC analysis following precipitation and lyophilization showed the presence of two isomers. These eluted at 39 and 43 minutes respectively using the same gradient as described above for $[\text{Ru}(\text{phen})(\text{dppz})(\text{bpy}'\text{-his})]^{2+}$ purification.

ESI and MALDI-TOF mass spectrometric analysis of $[\{\text{Ru}(\text{phen})(\text{dppz})(\text{bpy}'\text{-his})\}\{\text{Ru}(\text{NH}_3)_5\}]^{5+}$ showed mainly a decomposition product with the same mass and isotopic distribution as $[\text{Ru}(\text{phen})(\text{dppz})(\text{bpy}'\text{-his})]^{2+}$. HPLC analysis post irradiation with a 442 nm laser indicated decomposition to the $[\text{Ru}(\text{phen})(\text{dppz})(\text{bpy}'\text{-his})]^{2+}$ complex (vide infra). The ruthenium content of equimolar solutions of $[\text{Ru}(\text{phen})(\text{dppz})(\text{bpy}'\text{-his})]^{2+}$ and $[\{\text{Ru}(\text{phen})(\text{dppz})(\text{bpy}'\text{-his})\}\{\text{Ru}(\text{NH}_3)_5\}]^{5+}$ was measured by ICP-MS and $[\{\text{Ru}(\text{phen})(\text{dppz})(\text{bpy}'\text{-his})\}\{\text{Ru}(\text{NH}_3)_5\}]^{5+}$ was found to contain twice the ruthenium content as $[\text{Ru}(\text{phen})(\text{dppz})(\text{bpy}'\text{-his})]^{2+}$. Predicted ruthenium ratio for $[\text{Ru}(\text{phen})(\text{dppz})(\text{bpy}'\text{-his})]^{2+}$: $[\{\text{Ru}(\text{phen})(\text{dppz})(\text{bpy}'\text{-his})\}\{\text{Ru}(\text{NH}_3)_5\}]^{5+} = 2:1$, found 1.95:1.

5.2.4 Steady- state fluorescence

Steady-state emission spectra of the ruthenium complexes were recorded at ambient temperature using an ISS K2 spectrofluorimeter with a 5 mm pathlength. Ruthenium-containing samples (prepared to have an absorbance of 0.15 at 440 nm in either acetonitrile or buffer of 10 mM sodium phosphate, 50 mM NaCl, pH 7 with 1 mM poly d(AT) or poly d(GC)) were excited at 440 nm and emission recorded over a wavelength range of 500- 800 nm.

5.2.5 Electrochemistry

Ground state oxidation and reduction potentials for $[\{\text{Ru}(\text{phen})(\text{dppz})(\text{bpy}'\text{-his})\}\{\text{Ru}(\text{NH}_3)_5\}]^{5+}$, $[\text{Ru}(\text{phen})(\text{dppz})(\text{bpy}'\text{-his})]^{2+}$, and $[\text{Ru}(\text{phen})(\text{dppz})(\text{bpy})]^{2+}$ were obtained under an argon atmosphere using a CH Instruments Electrochemical

Workstation analyzer. A glassy carbon working electrode, Ag/AgCl reference electrode, and Pt auxiliary electrode were used in a single cell sample apparatus. Ferrocence carboxylic acid was used as an external reference. Samples were prepared for oxidation measurements in dry acetonitrile while those for reduction measurements were prepared in dry DMF. All solutions contained 100 mM tetrabutylammonium hexafluorophosphate as the supporting electrolyte and were degassed by bubbling argon through the sample prior to the reading. Metal concentrations for electrochemical analysis ranged from 0.1-0.5 mM.

5.2.6 Irradiation experiments and gel electrophoresis

DNA strands were labeled at the 5' end with [^{32}P] γ -ATP using polynucleotide kinase [35] and purified on a 20% denaturing polyacrylamide gel (Sequagel). The desired band was identified by autoradiography, excised from the gel and eluted into 500 mM NH_4OAc . Labeled DNA was isolated using Micro Bio-Spin 6 columns (BioRad) and hybridized to the complimentary strand in a 10 mM sodium phosphate, 50 mM sodium chloride pH 7 buffer. 30 μl aliquots of 4 μM duplex were incubated with equimolar ruthenium complex and 80 μM $[\text{Ru}(\text{NH}_3)_6]^{3+}$ quencher (if added externally) and irradiated under 442 nm light for 30 minutes using a Liconix He:Cd laser (~12 mW at 442 nm). Following irradiation, samples were treated with 10% piperidine, heated to 90 $^\circ\text{C}$ for 30 minutes, and dried *in vacuo*. Samples were run on 20% denaturing polyacrylimide gels for 1.5 hours at 90 W and imaged on a Storm 820 phosphoimager (Molecular Dynamics/ GE Healthcare). Oxidative damage products were quantified by phosphoimagery using Image Quant 5.2 (Molecular Dynamics).

5.2.7 Irradiation experiments and analysis of ^{CP}G/^{CP}C ring opening

Ruthenium-containing samples (5 μ M metal, 5 μ M duplex, and 50 μ M [Ru(NH₃)₆]³⁺ quencher (if used) in 30 μ L of 10 mM sodium phosphate, 50 mM NaCl, pH 7) were prepared by utilizing the freeze-pump-thaw method and stored under argon in air tight cuvettes (NMR tubes welded onto a Teflon gastight top (J. Young)). Samples were irradiated on a Liconix 442 nm He:Cd laser (~12 mW) for various time increments between 5 and 60 minutes [36]. For rhodium oxidations, aliquots contained 5 μ M duplex and 5 μ M [Rh(phi)₂(bpy)]³⁺. Rhodium samples were irradiated for 0-10 minutes at 365 nm, using a 1000 W Hg/Xe lamp equipped with a 320 nm long-pass filter and a monochromator. Light controls (DNA, no metal) at 30 and 60 minutes were obtained. Following irradiation, the duplexes were digested into deoxynucleosides by overnight incubation at 37 °C with alkaline phosphatase (Roche), phosphodiesterase I (USB), and SI nuclease (Amersham Biosciences). Once the digestion was complete samples were diluted with water and analyzed by reverse-phase HPLC using a Chemcobond 5-ODS C18 column. Deoxynucleosides eluted between 7 and 18 minutes using a gradient of 2-14% MeCN against 50 mM NH₄OAc over 30 minutes. The cyclopropylguanine deoxynucleoside eluted at 25 minutes and the ring-opened product, hydroxypropylguanine, eluted at 19 minutes. The cyclopropylcytosine deoxynucleoside eluted at 19 minutes.

5.2.8 EPR spectroscopy

EPR spectra were recorded at 20 K using an X-band Bruker EMX spectrometer equipped with a standard rectangular TE₁₀₂ cavity. Experiments were conducted with an

Oxford (ES9000) continuous-flow helium cryostat (temperature range 3.6-300 K). Frequency values were accurately measured using a frequency counter built into the microwave bridge. Samples were irradiated in standard EPR quartz tubes while simultaneously freezing in an unsilvered Dewar filled with liquid nitrogen. The light source was a 300 W Xe-arc lamp (Varian, Eimac division, Light R300-3) powered by an illuminator power supply (Varian, Eimac division, model PS 300-1). UV filters were employed to eliminate light < 320 nm. Samples contained 0.1 mM [$\{\text{Ru}(\text{phen})(\text{dppz})(\text{bpy}'\text{-his})\}\{\text{Ru}(\text{NH}_3)_5\}^{5+}$] and 1.5 mM base pairs of DNA polymer in 10 mM sodium phosphate, 50 mM NaCl, pH 7. EPR parameters were as follows: receiver gain, 5.64×10^3 ; modulation amplitude, 4 G; and microwave power, 1.27 mW.

5.2.9 Laser spectroscopy

Time-resolved emission and transient absorption measurements were recorded using a frequency doubled Nd:YAG pumped OPO laser for excitation of the ruthenium lumiphore ($\lambda_{\text{ex}} = 480$ nm) [22]. A pulsed 75 W Xe-arc lamp (Photon Technology International) was used as the probe source for the transient absorption measurements. Individual data sets were the average of 1000 shots. Data were collected using an oscilloscope (LeCroy) and transferred to a computer using Scope Explorer 2.19 (LeCroy). Data fitting was accomplished using a nonlinear least-squares analysis in Origin 6.1 (Microcal). Difference spectra were generated by subtracting the average of pretrigger absorbances from an average of posttrigger absorbances at a particular time point. Unless otherwise specified difference spectra were measured using 30 μM metal

complex in 1 mM base pairs of polymer in 10 mM sodium phosphate, 50 mM NaCl, pH 7.

Experiments at low pH were done in 10 mM sodium acetate, 50 mM NaCl, pH 5 and experiments investigating the effect of Zn^{2+} were done in 2.5 mM ZnCl_2 , 10 mM sodium phosphate, 50 mM NaCl, pH 7. Samples were measured in a stirring cuvette (Starna) and were continuously stirred during the acquisition. Experiments utilizing $[\text{Ru}(\text{NH}_3)_5(\text{H}_2\text{O})]^{2+}$ were carried out in an air tight stirring cuvette (Starna) with a fused top connecting to an additional freeze-pump-thaw chamber. $[\text{Ru}(\text{NH}_3)_5(\text{H}_2\text{O})]^{2+}$ was generated by mixing $[\text{Ru}(\text{NH}_3)_5\text{Cl}]\text{Cl}_2$ with zinc amalgam until it reduced and solubilized. The reduced $[\text{Ru}(\text{NH}_3)_5(\text{H}_2\text{O})]^{2+}$ was then combined with a $[\text{Ru}(\text{phen})(\text{dppz})(\text{bpy}'\text{-his})]^{2+}$, poly d(AT) solution in 10 mM sodium phosphate, 50 mM NaCl, pH 7 that had been degassed using the freeze-pump-thaw technique. The final sample concentration was 0.3 mM $[\text{Ru}(\text{NH}_3)_5(\text{H}_2\text{O})]^{2+}$, 30 μM $[\text{Ru}(\text{phen})(\text{dppz})(\text{bpy}'\text{-his})]^{2+}$ in 1 mM poly d(AT). Single wavelength measurements were obtained using 30 μM complex in 1 mM base pairs of polymer in the same buffer.

5.3 Results

5.3.1 Experimental design

These studies characterize the properties and DNA interactions of a novel tris heteroleptic ruthenium complex with a tethered ruthenium pentaammine quencher moiety. As shown in Figure 5.1, direct attachment of the quencher to the bipyridine ligand via a bridging histidine circumvents the rate-limiting step of diffusional quenching in traditional flash-quench methodologies. Here we compare the properties of the tethered quencher complex, $[\{\text{Ru}(\text{phen})(\text{dppz})(\text{bpy}'\text{-his})\}\{\text{Ru}(\text{NH}_3)_5\}]^{5+}$ with the parent complex

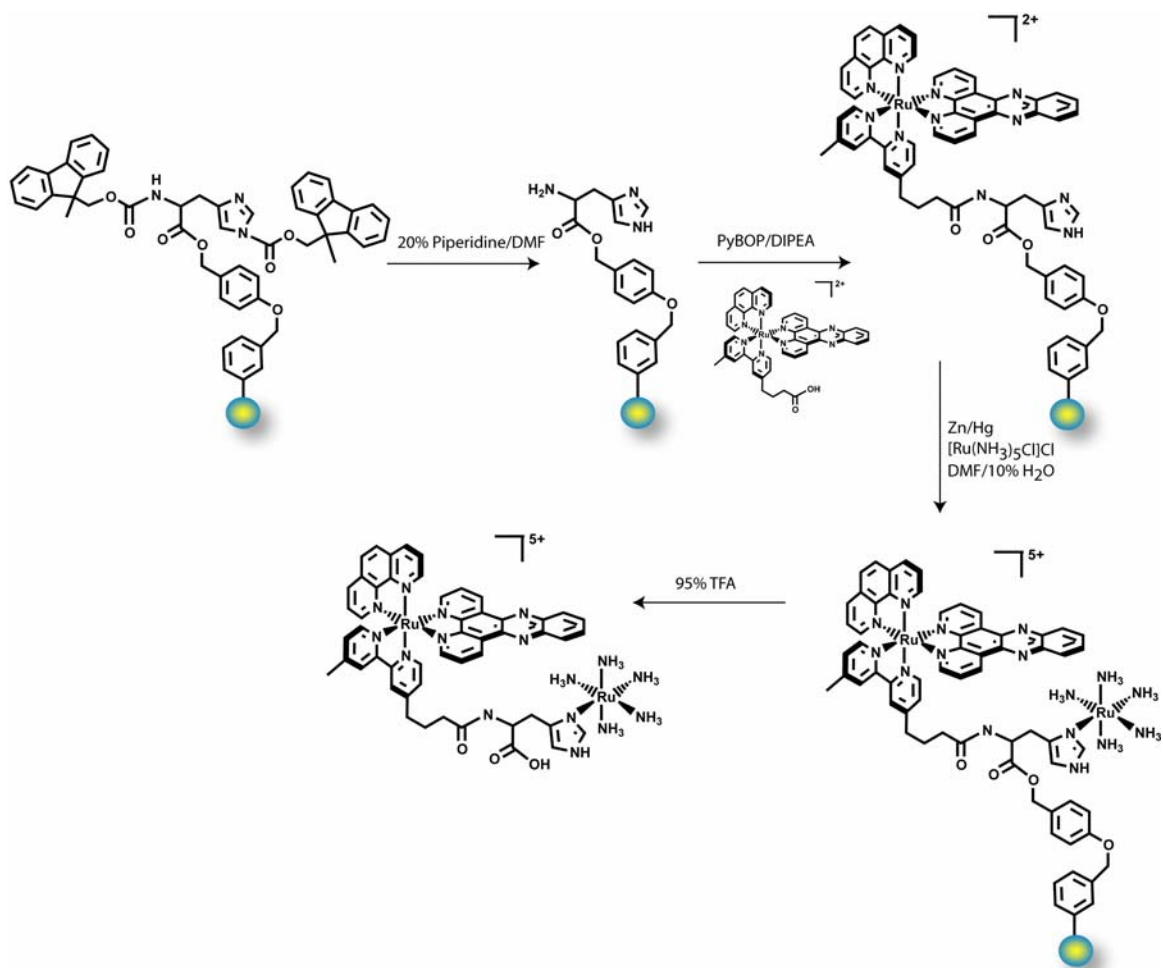


Figure 5.3. Scheme for generating $[\text{Ru}(\text{phen})(\text{dppz})(\text{bpy}'\text{-his})]^{2+}$ and $[\{\text{Ru}(\text{phen})(\text{dppz})(\text{bpy}'\text{-his})\}\{\text{Ru}(\text{NH}_3)_5\}]^{5+}$ using solid-phase peptide chemistry. Fmoc-His(Fmoc) is deprotected with piperidine and reacted with $[\text{Ru}(\text{phen})(\text{dppz})(\text{bpy}')]^{2+}$. This can be cleaved from the resin with TFA to yield $[\text{Ru}(\text{phen})(\text{dppz})(\text{bpy}'\text{-his})]^{2+}$ or further reacted with $[\text{Ru}(\text{NH}_3)_5\text{Cl}]\text{Cl}_2$ to form $[\{\text{Ru}(\text{phen})(\text{dppz})(\text{bpy}'\text{-his})\}\{\text{Ru}(\text{NH}_3)_5\}]^{5+}$.

$[\text{Ru}(\text{phen})(\text{dppz})(\text{bpy}')]^{2+}$ and the histidine-modified complex $[\text{Ru}(\text{phen})(\text{dppz})(\text{bpy}'\text{-his})]^{2+}$ (Figure 5.2).

5.3.2 Synthesis and characterization of $[\{\text{Ru}(\text{phen})(\text{dppz})(\text{bpy}'\text{-his})\}\{\text{Ru}(\text{NH}_3)_5\}]^{5+}$ and $[\text{Ru}(\text{phen})(\text{dppz})(\text{bpy}'\text{-his})]^{2+}$

Solid-phase peptide chemistry was used to couple histidine to the carboxylic acid functionalized $[\text{Ru}(\text{phen})(\text{dppz})(\text{bpy}')]^{2+}$ resulting in the formation of $[\text{Ru}(\text{phen})(\text{dppz})(\text{bpy}'\text{-his})]^{2+}$ (Figure 5.3). Further reaction with reduced ruthenium pentaammine afforded $[\{\text{Ru}(\text{phen})(\text{dppz})(\text{bpy}'\text{-his})\}\{\text{Ru}(\text{NH}_3)_5\}]^{5+}$. The complexes were successfully synthesized with yields ranging from 1-5% $[\{\text{Ru}(\text{phen})(\text{dppz})(\text{bpy}'\text{-his})\}\{\text{Ru}(\text{NH}_3)_5\}]^{5+}$ and 15-30% $[\text{Ru}(\text{phen})(\text{dppz})(\text{bpy}'\text{-his})]^{2+}$. The identity of $[\text{Ru}(\text{phen})(\text{dppz})(\text{bpy}'\text{-his})]^{2+}$ was confirmed by ESI and MALDI-TOF mass spectrometries while that of $[\{\text{Ru}(\text{phen})(\text{dppz})(\text{bpy}'\text{-his})\}\{\text{Ru}(\text{NH}_3)_5\}]^{5+}$ was confirmed by ICP-MS.

As there are four isomers of the starting material $[\text{Ru}(\text{phen})(\text{dppz})(\text{bpy}')]^{2+}$, $[\text{Ru}(\text{phen})(\text{dppz})(\text{bpy}'\text{-his})]^{2+}$ and $[\{\text{Ru}(\text{phen})(\text{dppz})(\text{bpy}'\text{-his})\}\{\text{Ru}(\text{NH}_3)_5\}]^{5+}$ also consist of four isomers; Λ , Δ , axial, and equatorial [37]. Of these four isomers, only the axial and equatorial forms were resolvable by HPLC analysis as two distinct peaks. Both peaks were collected and combined for subsequent experiments. The two isomer peaks of $[\{\text{Ru}(\text{phen})(\text{dppz})(\text{bpy}'\text{-his})\}\{\text{Ru}(\text{NH}_3)_5\}]^{5+}$ are shifted by ~ 1 minute from those of $[\text{Ru}(\text{phen})(\text{dppz})(\text{bpy}'\text{-his})]^{2+}$ which are in turn shifted by ~ 1 minute from those of the starting complex, $[\text{Ru}(\text{phen})(\text{dppz})(\text{bpy}')]^{2+}$ (Figure 5.4A).

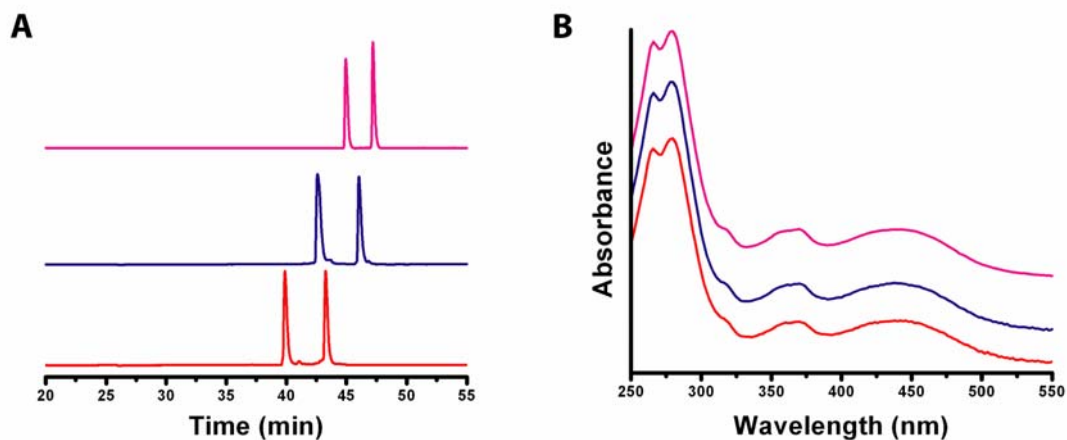


Figure 5.4. Reverse-phase HPLC chromatograms monitoring at 450 nm for the three complexes used in this study are depicted in **A**. The two isomers of $[\{\text{Ru}(\text{phen})(\text{dppz})(\text{bpy}'\text{-his})\}\{\text{Ru}(\text{NH}_3)_5\}]^{5+}$ elute first (red trace, bottom), followed by the two isomers of $[\text{Ru}(\text{phen})(\text{dppz})(\text{bpy}'\text{-his})]^{2+}$ (blue trace, middle) while the two isomers of $[\text{Ru}(\text{phen})(\text{dppz})(\text{bpy}')]^{2+}$ elute last (pink trace, top). The absorbance spectra of these complexes are shown in **B** with analogous color coding as in **A**.

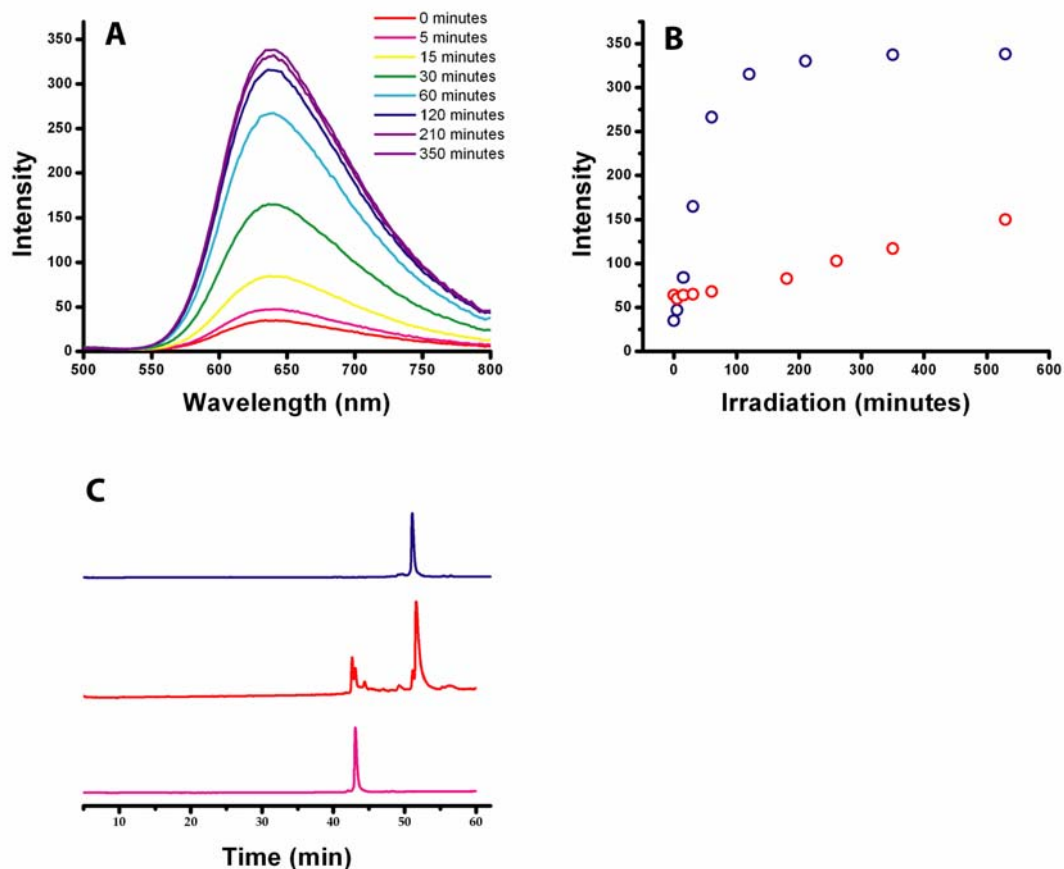


Figure 5.5. Effect of 442 nm irradiation on $[\{\text{Ru}(\text{phen})(\text{dppz})(\text{bpy}'\text{-his})\}\{\text{Ru}(\text{NH}_3)_5\}]^{5+}$. Emission spectra ($\lambda_{\text{ex}}=440$ nm) of the complex in acetonitrile as a function of irradiation time is shown in **A**. A plot of the intensity at 650 nm as a function of irradiation at 442 nm is shown in **B** for the complex in acetonitrile (blue circles) and in 1 mM poly d(AT) in 10 mM sodium phosphate, 50 mM NaCl, pH 7. HPLC chromatogram of the complex in acetonitrile following 530 minutes of irradiation at 442 nm is shown as the middle red trace in **C**. $[\{\text{Ru}(\text{phen})(\text{dppz})(\text{bpy}'\text{-his})\}\{\text{Ru}(\text{NH}_3)_5\}]^{5+}$ (pink trace, bottom) and $[\text{Ru}(\text{phen})(\text{dppz})(\text{bpy}'\text{-his})]^{2+}$ (blue trace, top) are shown for comparison.

The $[\{\text{Ru}(\text{phen})(\text{dppz})(\text{bpy}'\text{-his})\}\{\text{Ru}(\text{NH}_3)_5\}]^{5+}$ complex is unstable under conditions of constant irradiation at 442 nm as evidenced by a loss of emission quenching and a shift in HPLC retention time (Figure 5.5). The emission intensity of $[\{\text{Ru}(\text{phen})(\text{dppz})(\text{bpy}'\text{-his})\}\{\text{Ru}(\text{NH}_3)_5\}]^{5+}$ in poly d(AT) and in acetonitrile was measured prior to irradiation at 442 nm. After 60 minutes of irradiation, the intensity of $[\{\text{Ru}(\text{phen})(\text{dppz})(\text{bpy}'\text{-his})\}\{\text{Ru}(\text{NH}_3)_5\}]^{5+}$ in both samples increases dramatically but is more pronounced in acetonitrile. The irradiated samples were then subjected to HPLC analysis which revealed decomposition of the complex to $[\text{Ru}(\text{phen})(\text{dppz})(\text{bpy}'\text{-his})]^{2+}$. All experiments in this study were performed under conditions in which the complex was stable and not subject to constant irradiation.

5.3.3 Steady-state luminescence

Owing to their rich photophysical and photochemical properties, the dipyrrophenazine complexes of ruthenium (II) have been extensively exploited in our laboratory for use as photooxidants. Upon excitation into a metal to ligand charge transfer band, these complexes are highly emissive when intercalated into DNA, but show significant quenching when measured in aqueous buffer due to hydrogen bonding to the phenazine nitrogens. Thus, these complexes exhibit a “light-switch” effect in DNA, as intercalation of the dppz ligand into the DNA π -stack protects the phenazine nitrogens from quenching by aqueous solvent restoring luminescence [38]. To determine if the novel complexes exhibit light-switch behavior, we measured their luminescence properties in organic solvent and DNA. The steady-state quantum yields of $[\text{Ru}(\text{phen})(\text{dppz})(\text{bpy}'\text{-his})]^{2+}$ and $[\{\text{Ru}(\text{phen})(\text{dppz})(\text{bpy}'\text{-his})\}\{\text{Ru}(\text{NH}_3)_5\}]^{5+}$ relative to

Table 5.1 Steady-state luminescence quantum yields^a

Complex^b	MeCN	Poly d(GC)^c	Poly d(AT)^c
[{Ru(phen)(dppz)(bpy ³ -his)} {Ru(NH ₃) ₅ }] ⁵⁺	0.10	0.15	0.12
[Ru(phen)(dppz)(bpy ³ -his)] ²⁺	0.84	0.43	0.32
[Ru(phen)(dppz)(bpy ³)] ²⁺	0.99	0.44	0.34

a. Relative to [Ru(bpy)₃]²⁺ in MeCN with excitation at 440 nm. Errors are less than 6%.

b. Complexes were measured to have an absorbance of 0.15 at 440 nm.

c. Measured at 20 °C in 1 mM nucleotides in 10 mM sodium phosphate, 50 mM NaCl, pH 7.

$[\text{Ru}(\text{bpy})_3]^{2+}$ measured in acetonitrile and the DNA polymers poly d(AT) and poly d(GC) are shown in Table 5.1. Similar to $[\text{Ru}(\text{phen})(\text{dppz})(\text{bpy}')^{2+}]^{2+}$ and related dipyrrophenazine complexes of ruthenium (II), $[\text{Ru}(\text{phen})(\text{dppz})(\text{bpy}'\text{-his})]^{2+}$ and $[\{\text{Ru}(\text{phen})(\text{dppz})(\text{bpy}'\text{-his})\}\{\text{Ru}(\text{NH}_3)_5\}]^{5+}$ are non-emissive in water as hydrogen bonding to the phenazine nitrogens severely quenches the luminescence. These complexes also luminesce in acetonitrile, providing a comparison for DNA-specific characteristics. $[\text{Ru}(\text{phen})(\text{dppz})(\text{bpy}'\text{-his})]^{2+}$ and $[\text{Ru}(\text{phen})(\text{dppz})(\text{bpy}')^{2+}]^{2+}$ show substantial emission in acetonitrile, poly d(GC), and poly d(AT). $[\{\text{Ru}(\text{phen})(\text{dppz})(\text{bpy}'\text{-his})\}\{\text{Ru}(\text{NH}_3)_5\}]^{5+}$, however, is quenched in all three conditions and its emission is comparable to that of $[\text{Ru}(\text{phen})(\text{dppz})(\text{bpy}'\text{-his})]^{2+}$ and $[\text{Ru}(\text{phen})(\text{dppz})(\text{bpy}')^{2+}]^{2+}$ with added $[\text{Ru}(\text{NH}_3)_6]^{3+}$ quencher (data not shown). All three complexes show emission when intercalated into the DNA polymers with intensities being slightly higher in d(AT) than in d(GC). It should be noted that the maximum wavelength for emission is blue shifted upon binding to the GC polymer (620 nm) relative to the AT polymer or in acetonitrile (630 nm) consistent with previously published results for $[\text{Ru}(\text{phen})_2(\text{dppz})]^{2+}$ and $[\text{Ru}(\text{bpy})_2(\text{dppz})]^{2+}$ [39].

5.3.4 Time-resolved emission

Steady-state luminescence measurements indicate that the $[\{\text{Ru}(\text{phen})(\text{dppz})(\text{bpy}'\text{-his})\}\{\text{Ru}(\text{NH}_3)_5\}]^{5+}$ complex is substantially quenched in organic solvent and when intercalated in DNA relative to the parent complexes. To further probe this chemistry, we compared the excited state lifetimes of the $[\{\text{Ru}(\text{phen})(\text{dppz})(\text{bpy}'\text{-his})\}\{\text{Ru}(\text{NH}_3)_5\}]^{5+}$ complex to those of the parent complexes in the two DNA polymers,

poly d(AT) and poly d(GC). The excited state of intercalated ruthenium complexes decays with two lifetimes in the presence of DNA corresponding to different binding modes. As previous studies have shown, these binding modes arise from the position of the phenazine-metal axis with respect to that of the DNA base pair; the longer lifetime component corresponds to a binding mode in which the intercalated dppz ligand stacks between the bases from the major groove with the metal-phenazine axis perpendicular to the base pair long axis protecting both phenazine nitrogens, while the shorter lifetime corresponds to the “side-on” binding mode where one of the phenazine nitrogens is not protected from the solvent [40].

Monitoring at 610 nm, the maximum for complex emission, we observe the decay of the excited state following the laser pulse. In the presence of DNA, time-resolved measurements show a biexponential decay of emission for $[\text{Ru}(\text{phen})(\text{dppz})(\text{bpy}'\text{-his})]^{2+}$ and $[\{\text{Ru}(\text{phen})(\text{dppz})(\text{bpy}'\text{-his})\}\{\text{Ru}(\text{NH}_3)_5\}]^{5+}$ indicating that two DNA binding modes exist for the complexes (Table 5.2). Consistent with the steady-state emission intensities, both lifetimes in $[\{\text{Ru}(\text{phen})(\text{dppz})(\text{bpy}'\text{-his})\}\{\text{Ru}(\text{NH}_3)_5\}]^{5+}$ are reduced when compared with those of $[\text{Ru}(\text{phen})(\text{dppz})(\text{bpy}'\text{-his})]^{2+}$. In poly d(AT) similar amounts of each lifetime exist for $[\text{Ru}(\text{phen})(\text{dppz})(\text{bpy}'\text{-his})]^{2+}$ and $[\{\text{Ru}(\text{phen})(\text{dppz})(\text{bpy}'\text{-his})\}\{\text{Ru}(\text{NH}_3)_5\}]^{5+}$. However, in poly d(GC), the majority of $[\{\text{Ru}(\text{phen})(\text{dppz})(\text{bpy}'\text{-his})\}\{\text{Ru}(\text{NH}_3)_5\}]^{5+}$ decays with the shorter lifetime. Addition of the external quencher, $[\text{Ru}(\text{NH}_3)_6]^{3+}$ results in a shortening of both lifetimes in $[\text{Ru}(\text{phen})(\text{dppz})(\text{bpy}'\text{-his})]^{2+}$. This effect was not seen in $[\{\text{Ru}(\text{phen})(\text{dppz})(\text{bpy}'\text{-his})\}\{\text{Ru}(\text{NH}_3)_5\}]^{5+}$, where the addition of external quencher has negligible effects on emission lifetimes.

Table 5.2 Ru(II)* emission lifetimes

Complex ^b	Poly d(GC) ^c		Poly d(AT) ^c	
	τ_1 ns (%)	τ_2 ns (%)	τ_3 ns (%)	τ_4 ns (%)
[{Ru(phen)(dppz)(bpy ['] -his)} {Ru(NH ₃) ₅ }] ⁵⁺	55.6 (40)	17.2 (60)	154 (11)	32.8 (89)
[{Ru(phen)(dppz)(bpy ['] -his)} {Ru(NH ₃) ₅ }] ⁵⁺ + Q ^d	60.9 (10)	18.9 (90)		19.7 (100)
[Ru(phen)(dppz)(bpy ['] -his)] ²⁺	203 (38)	53.1 (62)	192 (42)	54.2 (58)
[Ru(phen)(dppz)(bpy ['] -his)] ²⁺ + Q	49.3 (9)	16.5 (91)	167 (3)	21.2 (97)

a. Measured at 610 nm, excitation $\lambda = 480$ nm. Data were fit to $y(t) = 100[C_1 \exp(-t/\tau_1) + (1-C_1) \exp(-t/\tau_2)]$ by a nonlinear least-squares method with convolution of the instrument response function using Origin 6.1 as described previously [54].

b. Measured in 1 mM nucleotides, 10 mM sodium phosphate, 50 mM NaCl, pH 7.

c. Complex concentrations were 30 μ M.

d. Q = [Ru(NH₃)₆]³⁺.

5.3.5 Electrochemistry of ruthenium complexes

As shown in Table 5.3 and Figure 5.6, the three complexes $[\text{Ru}(\text{phen})(\text{dppz})(\text{bpy})]^{2+}$, $[\text{Ru}(\text{phen})(\text{dppz})(\text{bpy}'\text{-his})]^{2+}$, and $[\{\text{Ru}(\text{phen})(\text{dppz})(\text{bpy}'\text{-his})\}\{\text{Ru}(\text{NH}_3)_5\}]^{5+}$ show electrochemical profiles with similar oxidation and reduction potentials. The oxidation profiles for $[\text{Ru}(\text{phen})(\text{dppz})(\text{bpy})]^{2+}$ and $[\text{Ru}(\text{phen})(\text{dppz})(\text{bpy}'\text{-his})]^{2+}$ reveal a single peak at ~ 1.5 V vs. NHE (data not shown). As can be seen in the reduction profile, three waves occur between -0.68 and -1.55 V vs. NHE consistent with reduction of each ligand. $[\text{Ru}(\text{phen})(\text{dppz})(\text{bpy})]^{2+}$ shows large reversible reduction waves, while $[\text{Ru}(\text{phen})(\text{dppz})(\text{bpy}'\text{-his})]^{2+}$ has weaker reduction waves which do not have as pronounced reversibility. Addition of the quencher moiety to $[\text{Ru}(\text{phen})(\text{dppz})(\text{bpy}'\text{-his})]^{2+}$ restores the large reversible reduction waves. Note that the relative intensities of the reduction peaks are different for $[\text{Ru}(\text{phen})(\text{dppz})(\text{bpy})]^{2+}$ and $[\text{Ru}(\text{phen})(\text{dppz})(\text{bpy}'\text{-his})]^{2+}$ as compared to $[\{\text{Ru}(\text{phen})(\text{dppz})(\text{bpy}'\text{-his})\}\{\text{Ru}(\text{NH}_3)_5\}]^{5+}$. For $[\text{Ru}(\text{phen})(\text{dppz})(\text{bpy}')]^{2+}$ and $[\text{Ru}(\text{phen})(\text{dppz})(\text{bpy}'\text{-his})]^{2+}$ the reductions at ~ -1.5 and -1.05 V vs. NHE are larger than the reduction at -0.7 V vs. NHE. However the first reduction peak at -0.7 V vs. NHE is larger than the other reductions in $[\{\text{Ru}(\text{phen})(\text{dppz})(\text{bpy}'\text{-his})\}\{\text{Ru}(\text{NH}_3)_5\}]^{5+}$.

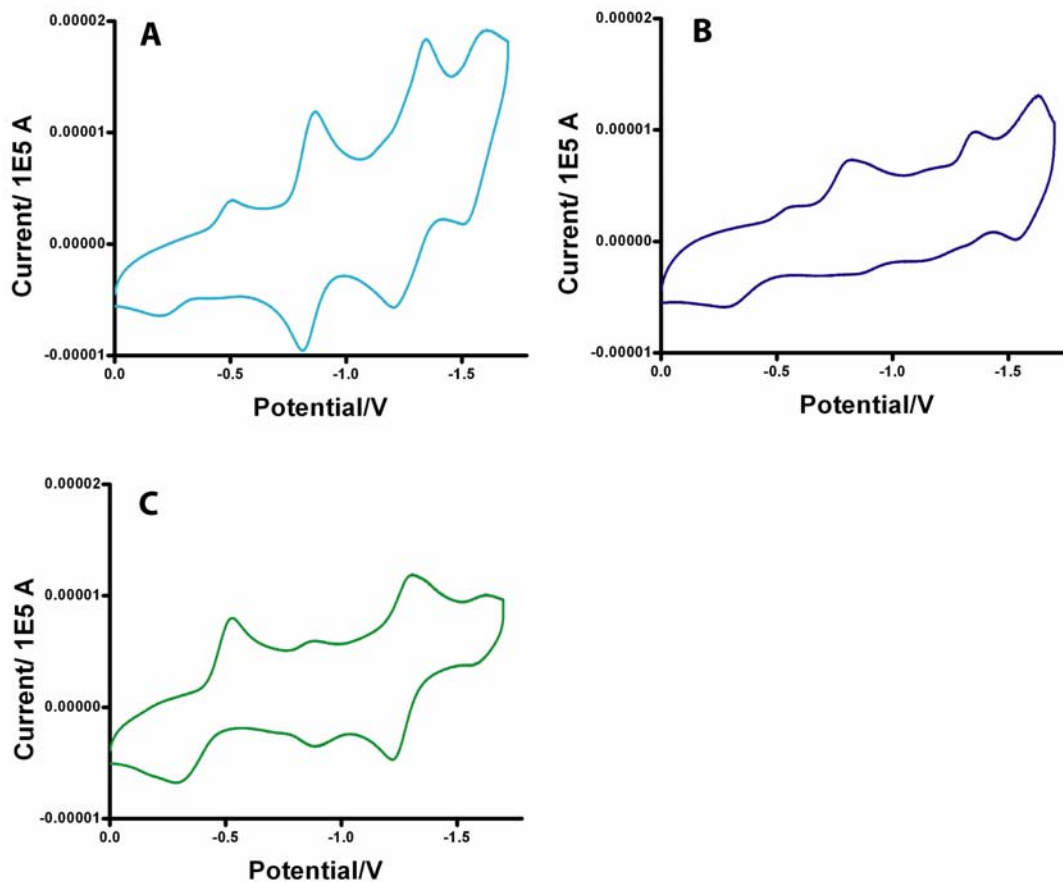


Figure 5.6. Electrochemistry of ruthenium complexes. Shown are cyclic voltammograms for reduction of [$\{\text{Ru}(\text{phen})(\text{dppz})(\text{bpy}'\text{-his})\}\{\text{Ru}(\text{NH}_3)_5\}^{\text{5+}}$] (A), [$\text{Ru}(\text{phen})(\text{dppz})(\text{bpy}'\text{-his})^{\text{2+}}$] (B), and [$\text{Ru}(\text{phen})(\text{dppz})(\text{bpy})^{\text{2+}}$] (C) measured in dry DMF with 0.1 M tetrabutylammonium hexafluorophosphate. See Experimental.

Table 5.3 Electrochemical potentials for ruthenium complexes^a

Complex	E ^o (3+/2+) ^b	Reductions ^c		
		1	2	3
[Ru(phen)(dppz)(bpy)] ²⁺	1.54	-0.68	-1.05	-1.53
[Ru(phen)(dppz)(bpy'-his)] ²⁺	1.55	-0.75	-1.01	-1.55
[{Ru(phen)(dppz)(bpy'-his)} {Ru(NH ₃) ₅ }] ⁵⁺		-0.71	-1.06	-1.49

a. Values reported in V vs. NHE.

b. Measured in dry MeCN with 0.1 M tetrabutylammonium hexafluorophosphate.

c. Measured in dry DMF with 0.1 M tetrabutylammonium hexafluorophosphate.

5.3.6 Analysis of oxidative products

Permanently damaged oxidative products resulting from the flash-quench technique are often detectable by gel electrophoresis. Guanine, having the lowest oxidation potential of the naturally occurring bases, is most the most readily oxidized [11]. As oxidized guanine residues are labile under treatment with piperidine, it is possible to determine the location and yield of guanine oxidation within a labeled duplex by strand scission in an electrophoresis experiment [41]. Using a ^{32}P 5'-end labeled sequence containing two sets of double guanine sites, flash-quench generated oxidative damage was determined for the three complexes with and without external $[\text{Ru}(\text{NH}_3)_6]^{3+}$ quencher (Figure 5.7). Considerable 5' specific guanine damage is observed for all three complexes in the presence of quencher. This 5' specific damage pattern is not observed for any of the complexes alone, consistent with previous reports in which permanent flash-quench generated oxidative damage requires both light and quencher [42].

It is initially surprising that $[\{\text{Ru}(\text{phen})(\text{dppz})(\text{bpy}'\text{-his})\}\{\text{Ru}(\text{NH}_3)_5\}]^{5+}$, being significantly quenched spectroscopically, does not generate permanently oxidized guanine products. As the guanine radical reacts on the millisecond time scale with water to form permanently damaged products, it is likely that fast back electron transfer between Ru(III) and reduced quencher competes with this process thus obscuring the detection of base oxidation. Thus we sought to find a method in which guanine oxidation could be observed on a faster time scale. Using the cyclopropylamine-modified nucleoside system originally developed by Saito [43], oxidative ring opening can be monitored on a nanosecond to picosecond time scale [21]. A similar sequence to that

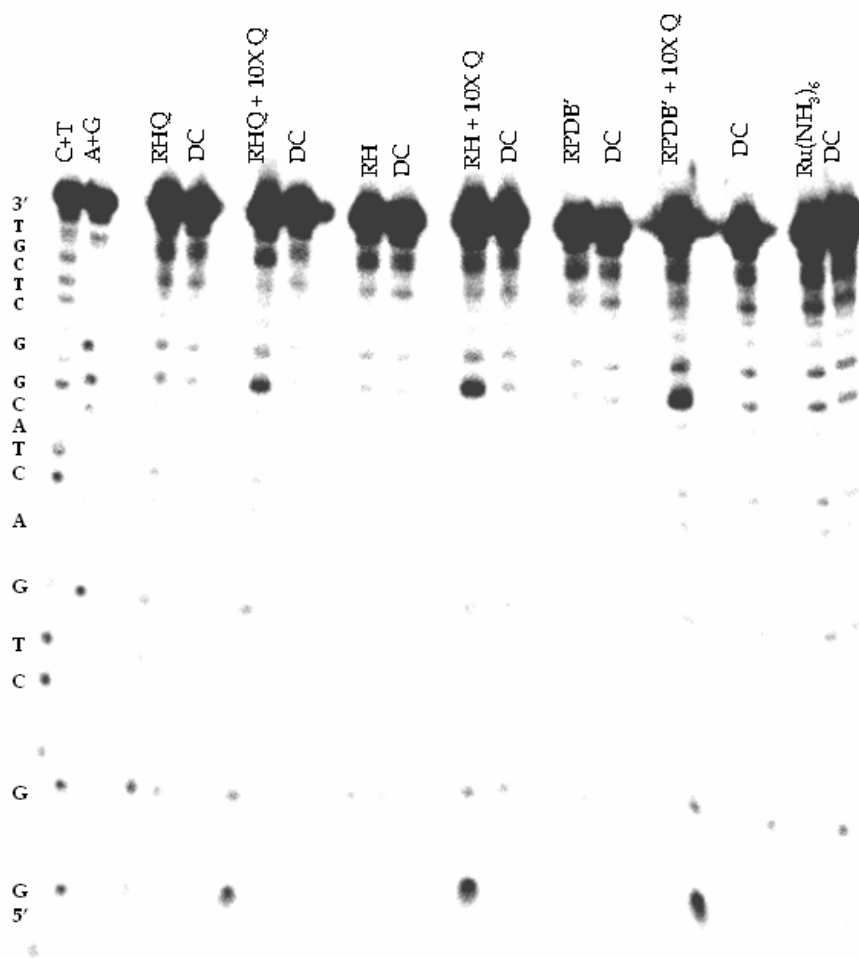


Figure 5.7. Phosphorimager following gel electrophoretic analysis of the sequence 3' TGCTCGGCATCAGTCGGCATA 5' after irradiation and piperidine treatment in the presence of the ruthenium complexes $[\text{Ru}(\text{phen})(\text{dppz})(\text{bpy}')]^{2+}$ (**RPDB'**), $[\text{Ru}(\text{phen})(\text{dppz})(\text{bpy}'\text{-his})]^{2+}$ (**RH**), and $[\{\text{Ru}(\text{phen})(\text{dppz})(\text{bpy}'\text{-his})\}\{\text{Ru}(\text{NH}_3)_5\}]^{5+}$ (**RHQ**). Also shown are the same complexes with added $[\text{Ru}(\text{NH}_3)_6]^{3+}$ quencher (**Q**). Dark control (**DC**) samples containing DNA and metal were not irradiated. All other samples were irradiated for 30 minutes using an excitation wavelength of 442 nm. Samples contained 4 μM duplex DNA, 4 μM ruthenium complex, and 40 μM $[\text{Ru}(\text{NH}_3)_6]^{3+}$ if added.

used in the gel electrophoresis experiments was altered such as to contain a cyclopropyl-modified guanine at the 5' of the second double guanine set (Table 5.4). We first characterized ${}^{\text{CP}}\text{G}$ and ${}^{\text{CP}}\text{C}$ ring opening using two standard complexes of known potential, $[\text{Ru}(\text{phen})(\text{dppz})(\text{bpy}')]^{2+}$ and $[\text{Rh}(\text{phi})_2(\text{bpy})]^{3+}$ and two duplexes, **G-2** and **C-1** containing ${}^{\text{CP}}\text{G}$ and ${}^{\text{CP}}\text{C}$ respectively. Since singlet oxygen is generated upon photolysis of the ruthenium complex in the absence of quencher [44, 45], and singlet oxygen can potentially contribute to ring opening, all ruthenium samples were irradiated under anaerobic conditions. When oxygen is eliminated from the system, damage patterns solely resulting from charge transfer events are revealed. It should be noted that in the presence of oxygen, ${}^{\text{CP}}\text{C}$ and ${}^{\text{CP}}\text{G}$ ring opening is observed with and without $[\text{Ru}(\text{NH}_3)_6]^{3+}$ quencher, although the effect is more pronounced in the case of ${}^{\text{CP}}\text{G}$. As ruthenium is a known sensitizer for singlet oxygen, this effect can be eliminated if the samples are irradiated under argon. Table 5.4 shows that considerable ring opening occurs only with quencher in **G-2**, which contains ${}^{\text{CP}}\text{G}$, while the ${}^{\text{CP}}\text{C}$ in **C-1** remains essentially intact. When no quencher is added to the irradiated samples, a small amount of ring opening occurs in **G-2**, but not **C-1**. ${}^{\text{CP}}\text{C}$, incorporated in DNA shows little reaction with $[\text{Ru}(\text{phen})(\text{dppz})(\text{bpy}')]^{2+}$ in the presence or absence of quencher. In contrast, ${}^{\text{CP}}\text{G}$ decomposes completely within 30 minutes of irradiation in the presence of $[\text{Ru}(\text{phen})(\text{dppz})(\text{bpy}')]^{2+}$ and quencher and to a small extent if the quencher is excluded. For comparison, we examined base decomposition using $[\text{Rh}(\text{phi})_2(\text{bpy})]^{3+}$ as the photooxidant, since the rhodium complex is a far more potent photooxidant. As shown in Table 5.4, ${}^{\text{CP}}\text{G}$ in **G-2** decomposes completely after 10 minutes of irradiation.

Table 5.4* % of ^{CP}C and ^{CP}G decomposition with noncovalently bound ruthenium and rhodium complexes

DNA	Sequence ^a	Photooxidant	% Decomposition of ^{CP} C or ^{CP} G ^b	
		[Rh(phi) ₂ (bpy)] ³⁺		57.6 ^c
C-1	3' -TGCTCGGCATCAGT ^{CP} CGGCATA-5' 5' -ACGAGCCGTAGTCA GCCGTAT-3'	[Ru(phen)(dppz)(bpy')] ²⁺	-Q ^d	2.5 ^e
			+Q	4.8
		[{Ru(phen)(dppz)(bpy'-his)} {Ru(NH ₃) ₅ }] ⁵⁺	-Q	1.0
G-2	3' -TGCTCGGCATCAGTCG ^{CP} GCATA-5' 5' -ACGAGCCGTAGTCAGC CGTAT-3'	[Rh(phi) ₂ (bpy)] ³⁺		100
			-Q	2.0
		[Ru(phen)(dppz)(bpy')] ²⁺	+Q	100
		[Ru(phen)(dppz)(bpy'-his)] ²⁺	-Q	3.0
			+Q	100
		[{Ru(phen)(dppz)(bpy'-his)} {Ru(NH ₃) ₅ }] ⁵⁺	-Q	60.0
			+Q	100

a. DNA strands were synthesized as described in Experimental.

b. Ruthenium photooxidations are averaged over at least 3 data sets. Uncertainties are less than 10%.

c. Amount of ^{CP}C remaining after 5 minutes of irradiation. Duplexes (5 μM) were irradiated with 5 μM [Rh(phi)₂(bpy)]³⁺ in 10 mM sodium phosphate, 50 mM NaCl, pH 7. Details are in Experimental.

d. Q refers to quencher, [Ru(NH₃)₆]³⁺. Details are in Experimental.

e. Amount of cyclopropyl nucleoside remaining after 30 minutes of irradiation. Duplexes (5 μM) were irradiated in 10 mM sodium phosphate, 50 mM NaCl, pH 7. Concentration of [Ru(phen)(dppz)(bpy')]²⁺ is 5 μM and that of [Ru(NH₃)₆]³⁺ is 50 μM if added. Details are in Experimental.

*Adapted from reference 36.

Decomposition of ${}^{\text{CP}}\text{C}$ in **C-1** is also significant, 58%, as compared to the case of ruthenium. Although the decomposition of ${}^{\text{CP}}\text{C}$ is less pronounced than that of ${}^{\text{CP}}\text{G}$, both of the cyclopropylamine bases are oxidized by $[\text{Rh}(\text{phen})_2(\text{bpy})]^{3+}$. Next, we examined the ring opening capabilities of the novel ruthenium complexes, $[\text{Ru}(\text{phen})(\text{dppz})(\text{bpy}'\text{-his})]^{2+}$ and $[\{\text{Ru}(\text{phen})(\text{dppz})(\text{bpy}'\text{-his})\}\{\text{Ru}(\text{NH}_3)_5\}]^{5+}$ with and without added quencher. Under anaerobic conditions ensuring ring opening is not the result of singlet oxygen sensitization, ${}^{\text{CP}}\text{G}$ decomposition was measured as a function of irradiation time (Figure 5.8). Light controls composed of DNA without any metal complex do not show cyclopropyl nucleoside decomposition (data not shown). Additionally, $[\text{Ru}(\text{phen})(\text{dppz})(\text{bpy}'\text{-his})]^{2+}$ and $[\text{Ru}(\text{phen})(\text{dppz})(\text{bpy}')]^{2+}$ do not facilitate cyclopropyl ring opening without added quencher. When quencher is added to these complexes, rapid decomposition of the ${}^{\text{CP}}\text{G}$ nucleoside is observed. Importantly, $[\{\text{Ru}(\text{phen})(\text{dppz})(\text{bpy}'\text{-his})\}\{\text{Ru}(\text{NH}_3)_5\}]^{5+}$ is able to generate complete decomposition of ${}^{\text{CP}}\text{G}$ after 60 minutes of irradiation without added quencher consistent with fast back electron transfer contributing to the lack of guanine damage detected by gel electrophoresis.

Recently our lab has observed hole occupation on pyrimidines using a cyclopropylcytosine trap [19]. Reductive ring opening was also observed using this system using a platinum complex [46]. As can be seen in Figure 5.8, neither $[\{\text{Ru}(\text{phen})(\text{dppz})(\text{bpy}'\text{-his})\}\{\text{Ru}(\text{NH}_3)_5\}]^{5+}$ nor $[\text{Ru}(\text{phen})(\text{dppz})(\text{bpy}'\text{-his})]^{2+}$ and $[\text{Ru}(\text{phen})(\text{dppz})(\text{bpy}')]^{2+}$ are capable of opening the ${}^{\text{CP}}\text{C}$ ring by oxidation or reduction, as would be predicted based on their electrochemical potentials (Table 5.3).

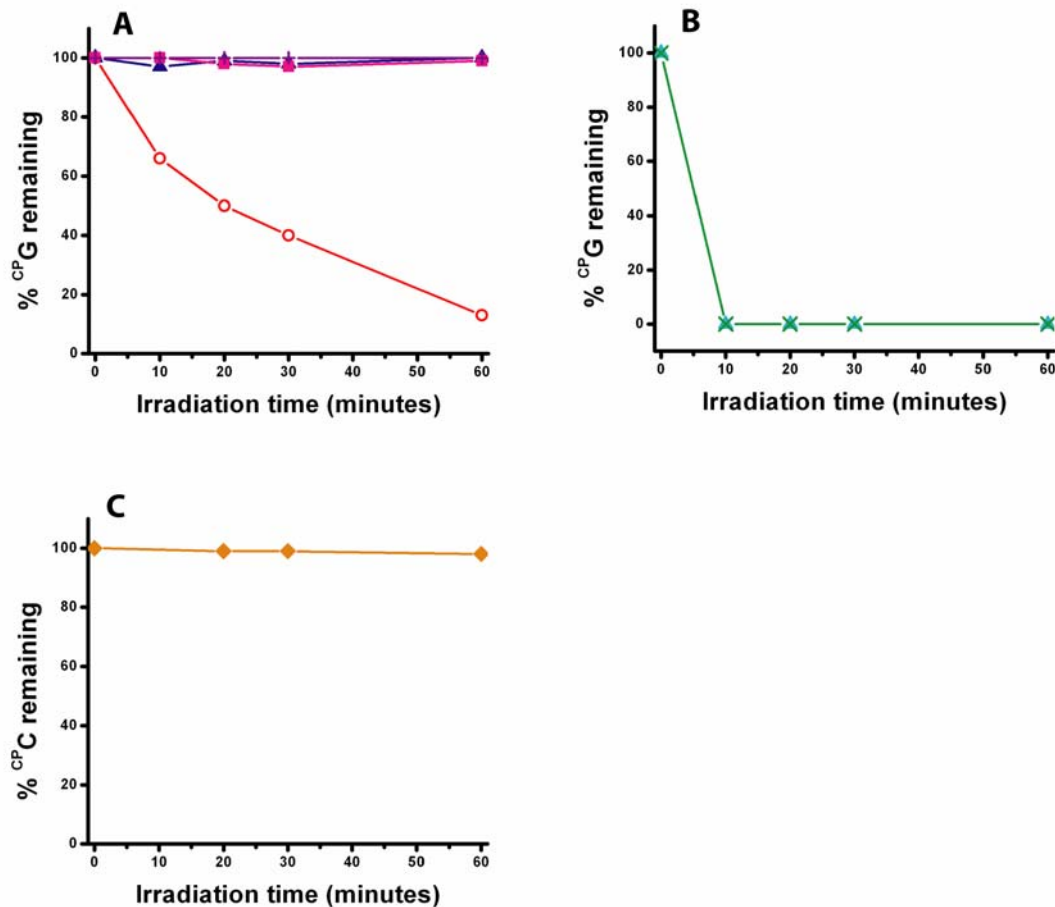


Figure 5.8 **A:** Decomposition of ^{CP}G in the **G-2** duplex as a function of irradiation time for ruthenium complexes without added $[Ru(NH_3)_6]^{3+}$ quencher. Red circles correspond to $[\{Ru(phen)(dppz)(bpy'-his)\} \{Ru(NH_3)_5\}]^{5+}$, blue triangles correspond to $[Ru(phen)(dppz)(bpy')]^{2+}$, pink squares correspond to $[Ru(phen)(dppz)(bpy'-his)]^{2+}$, and purple crosses correspond to $[Ru(phen)(dppz)(bpy'-his)]^{2+}$ at pH 5. **B:** Decomposition of ^{CP}G in the **G-2** duplex as a function of irradiation for ruthenium complexes in the presence of $[Ru(NH_3)_6]^{3+}$ quencher. The turquoise triangles correspond to $[Ru(phen)(dppz)(bpy')]^{2+}$ while the green Xs correspond to $[Ru(phen)(dppz)(bpy'-his)]^{2+}$. **C:** The effect of irradiation on ^{CP}C in the **C-1** duplex in the presence of $[\{Ru(phen)(dppz)(bpy'-his)\} \{Ru(NH_3)_5\}]^{5+}$ (orange diamonds). All experiments were done under anaerobic conditions using an excitation wavelength of 442 nm. Experiments were done in 10 mM sodium phosphate, 50 mM NaCl, pH 7 in the presence of 5 μ M duplex, 5 μ M ruthenium complex and 100 μ M $[Ru(NH_3)_6]^{3+}$. The experiment at low pH was done in 10 mM NaOAc, 50 mM NaCl, pH 5. See Experimental.

5.3.7 EPR spectroscopy

We have established that $[\{\text{Ru}(\text{phen})(\text{dppz})(\text{bpy}'\text{-his})\}\{\text{Ru}(\text{NH}_3)_5\}]^{5+}$ can facilitate $^{\text{CP}}\text{G}$ ring opening when non-covalently bound to duplex DNA. In order to further probe this reaction, we used EPR to spectroscopically detect the guanine radical. Previous reports have demonstrated that flash-quench generated guanine radicals can be observed using EPR spectroscopy [47]. Organic radicals have G values around 2 and as shown in Figure 5.9, $[\{\text{Ru}(\text{phen})(\text{dppz})(\text{bpy}'\text{-his})\}\{\text{Ru}(\text{NH}_3)_5\}]^{5+}$ in the presence of poly d(GC) shows a small signal comparable to that of guanine [48, 49] with a G value of 2.004. This signal is not evident for $[\{\text{Ru}(\text{phen})(\text{dppz})(\text{bpy}'\text{-his})\}\{\text{Ru}(\text{NH}_3)_5\}]^{5+}$ in the presence of poly d(AT), further assigning the signal to that of the guanine radical. It should also be noted that this result is consistent with previous findings that flash-quench methodologies using $[\text{Ru}(\text{phen})_2(\text{dppz})]^{3+}$ do not generate adenine radical cations.

5.3.8 Nanosecond transient absorption

In addition to EPR, transient absorption spectroscopy can be used to detect guanine radical formation using the flash-quench technique. We examined the spectroscopic characteristics of $[\{\text{Ru}(\text{phen})(\text{dppz})(\text{bpy}'\text{-his})\}\{\text{Ru}(\text{NH}_3)_5\}]^{5+}$ and $[\text{Ru}(\text{phen})(\text{dppz})(\text{bpy}'\text{-his})]^{2+}$ in the presence and absence of DNA. Inspection of the data in Figure 5.10A which compares the behavior of the two complexes in poly d(AT), shows an initial bleach at 440 nm corresponding to the Ru(II) excited state. For $[\text{Ru}(\text{phen})(\text{dppz})(\text{bpy}'\text{-his})]^{2+}$, in the absence of $[\text{Ru}(\text{NH}_3)_6]^{3+}$ quencher, this bleach decays back to baseline. In the presence of quencher, a longer-lived negative absorbance following the initial bleach is consistent with formation of Ru(III), which like Ru(II)*,

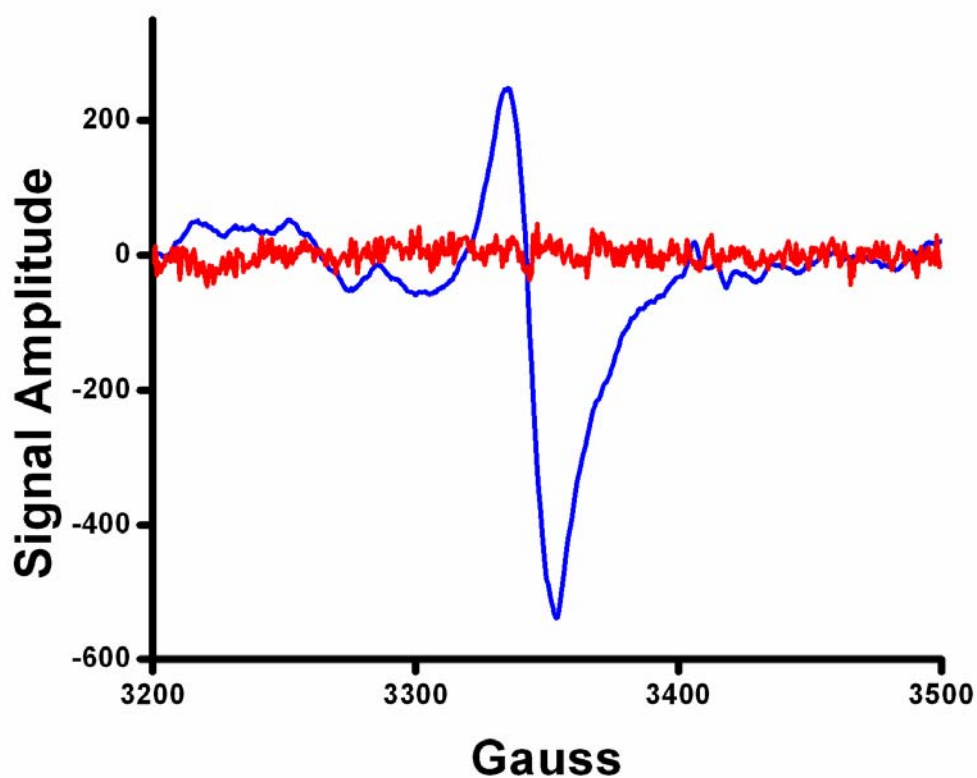


Figure 5.9. Guanine radical formation by $[\{\text{Ru}(\text{phen})(\text{dppz})(\text{bpy}'\text{-his})\}\{\text{Ru}(\text{NH}_3)_5\}]^{5+}$. EPR spectra measured at 20 K of 0.1 mM $[\{\text{Ru}(\text{phen})(\text{dppz})(\text{bpy}'\text{-his})\}\{\text{Ru}(\text{NH}_3)_5\}]^{5+}$ in 1.5 mM poly d(AT) (red trace) or poly d(GC) (blue trace). Buffer was composed of 10 mM sodium phosphate, 50 mM NaCl, pH 7. See Experimental.

absorbs less at 440 nm than does ground state Ru(II). In contrast, [$\{\text{Ru}(\text{phen})(\text{dppz})(\text{bpy}'\text{-his})\}\{\text{Ru}(\text{NH}_3)_5\}]^{5+}$, in the absence of quencher, yields a long-lived positive signal following the excited state bleach at 440 nm. The signal forms faster than the detection limit of the instrument giving it a formation rate with a lower limit of $1 \times 10^8 \text{ s}^{-1}$. As can be seen in Figure 5.10B, the magnitude of this signal is larger in poly d(AT) than in poly d(GC), and is not evident in the absence of DNA, such as when the complex is in acetonitrile. Similarly to $[\text{Ru}(\text{phen})(\text{dppz})(\text{bpy}'\text{-his})]^{2+}$, when quencher is added to $\text{Ru}(\text{phen})(\text{dppz})(\text{bpy}'\text{-his})\{\text{Ru}(\text{NH}_3)_5\}^{5+}$, a long-lived negative absorbance follows the initial excited state bleach, indicative of Ru(III) formation (Figure 5.10B).

Figure 5.11A shows a difference spectrum obtained for [$\{\text{Ru}(\text{phen})(\text{dppz})(\text{bpy}'\text{-his})\}\{\text{Ru}(\text{NH}_3)_5\}]^{5+}$ in both DNA polymers. This spectrum markedly contrasts with the difference spectrum obtained for $[\text{Ru}(\text{phen})(\text{dppz})(\text{bpy}'\text{-his})]^{2+}$ in poly d(AT) in the presence and absence of quencher (Figure 5.11A inset). The long-lived transient formed in [$\{\text{Ru}(\text{phen})(\text{dppz})(\text{bpy}'\text{-his})\}\{\text{Ru}(\text{NH}_3)_5\}]^{5+}$ in both poly d(AT) and poly d(GC) contains two positive extrema, centered at 410 and 560 nm. The magnitude of the transient is larger in poly d(AT) than in poly d(GC) as would be expected based on the single wavelength measurements at 440 nm. In contrast, the difference spectra for the Ru(II)* \rightarrow Ru(II) and Ru(III) \rightarrow Ru(II) transitions generated from excitation of $[\text{Ru}(\text{phen})(\text{dppz})(\text{bpy}'\text{-his})]^{2+}$ in poly d(AT) in the presence and absence of quencher are notably negative at 440 nm.

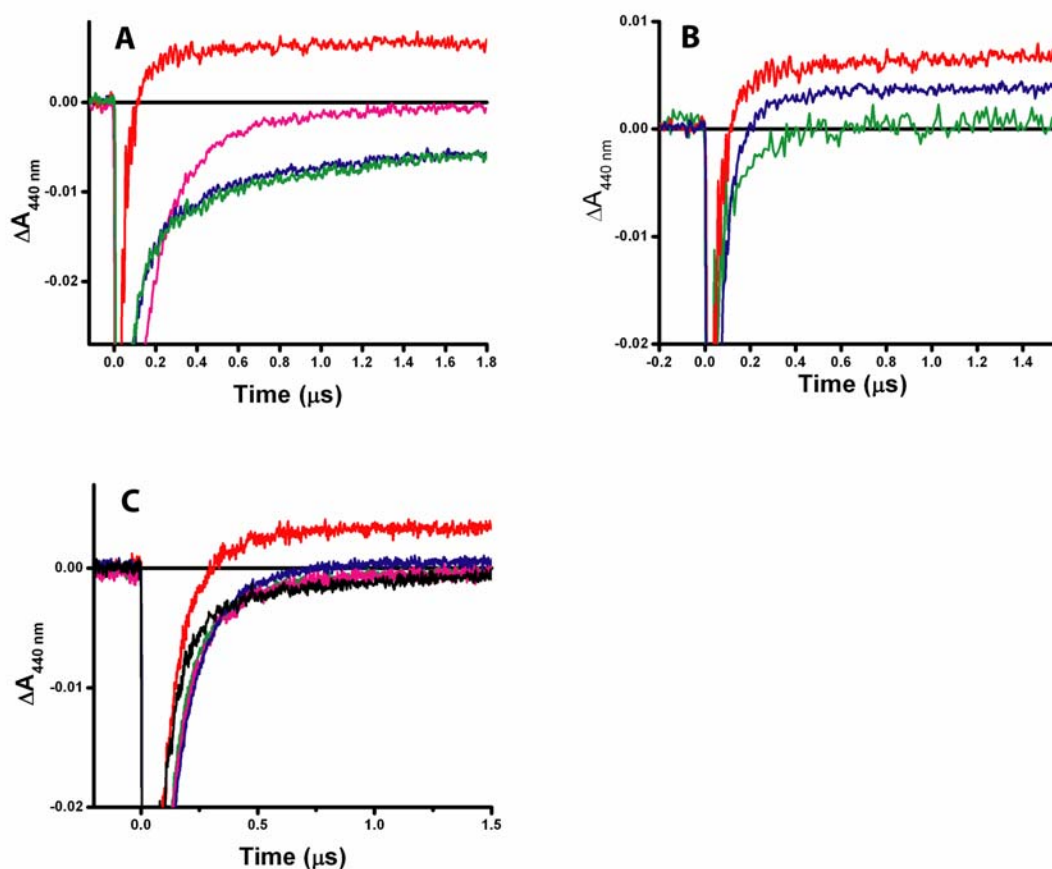


Figure 5.10. Transient absorption at 440 nm of the ruthenium complexes. **A** shows $[\{\text{Ru}(\text{phen})(\text{dppz})(\text{bpy}'\text{-his})\}\{\text{Ru}(\text{NH}_3)_5\}]^{5+}$ and $[\text{Ru}(\text{phen})(\text{dppz})(\text{bpy}'\text{-his})]^{2+}$ in the presence (blue and green traces respectively) and absence (red and pink traces respectively) of $[\text{Ru}(\text{NH}_3)_6]^{3+}$ measured in 1 mM poly d(AT) in 10 mM NaPO_4 , 50 mM NaCl , pH 7.0. A comparison of the $[\{\text{Ru}(\text{phen})(\text{dppz})(\text{bpy}'\text{-his})\}\{\text{Ru}(\text{NH}_3)_5\}]^{5+}$ signal in 1 mM poly d(AT) (red trace) or poly d(GC) (blue trace), and acetonitrile (green trace) is shown in **B**. The effect of pH, zinc, and $[\text{Ru}(\text{NH}_3)_5(\text{H}_2\text{O})]^{2+}$ on the $[\text{Ru}(\text{phen})(\text{dppz})(\text{bpy}'\text{-his})]^{2+}$ 440 nm signal is examined in **C**. The red and blue traces correspond to $[\text{Ru}(\text{phen})(\text{dppz})(\text{bpy}'\text{-his})]^{2+}$ in the presence of 1 mM poly d(AT) and poly d(GC) respectively in 10 mM NaOAc , 50 mM NaCl , pH 5. The green and pink traces correspond to $[\text{Ru}(\text{phen})(\text{dppz})(\text{bpy}'\text{-his})]^{2+}$ in the presence of 2.5 mM ZnCl_2 and 1 mM poly d(AT) or poly d(GC) respectively in 10 mM sodium phosphate, 50 mM NaCl , pH 7. The black trace corresponds to $[\text{Ru}(\text{phen})(\text{dppz})(\text{bpy}'\text{-his})]^{2+}$ in the presence of 0.3 mM $[\text{Ru}(\text{NH}_3)_5(\text{H}_2\text{O})]^{2+}$ in 1 mM poly d(AT). Experiments were done using 30 μM ruthenium complex and 300 μM $[\text{Ru}(\text{NH}_3)_6]^{3+}$ as the quencher. See Experimental.

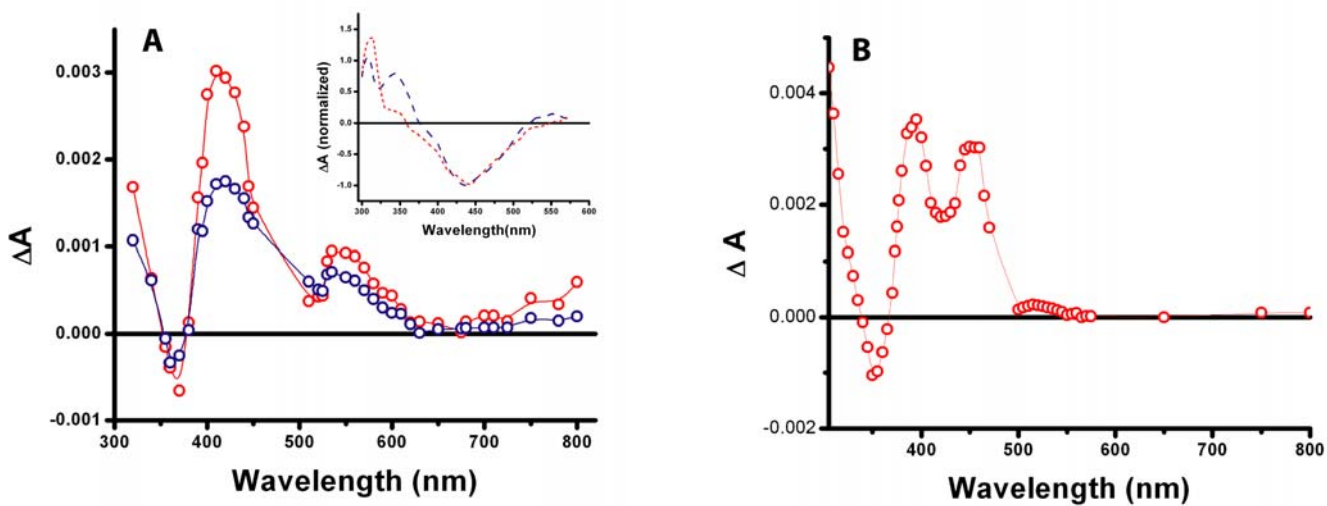


Figure 5.11. **A:** Transient absorption difference spectrum for 30 μM $[\{\text{Ru}(\text{phen})(\text{dppz})(\text{bpy}'\text{-his})\}\{\text{Ru}(\text{NH}_3)_5\}]^{5+}$ in 1 mM poly d(GC) (blue circles) and poly d(AT) (red circles). The inset shows difference spectra for 30 μM $[\text{Ru}(\text{phen})(\text{dppz})(\text{bpy}'\text{-his})]^{2+}$ in poly d(AT) with (red line) and without (blue line) 300 μM $[\text{Ru}(\text{NH}_3)_6]^{3+}$. Samples were measured in 10 mM sodium phosphate, 50 mM NaCl, pH 7. **B:** Transient absorption difference spectrum for 30 μM $[\text{Ru}(\text{phen})(\text{dppz})(\text{bpy}'\text{-his})]^{2+}$ in the presence of 25 mM ascorbate measured in acetonitrile.

5.3.9 Charge effect on the transient absorption profile of $[\text{Ru}(\text{phen})(\text{dppz})(\text{bpy}'\text{-his})]^{2+}$

To further probe the long-lived transient species formed upon excitation of $[\{\text{Ru}(\text{phen})(\text{dppz})(\text{bpy}'\text{-his})\}\{\text{Ru}(\text{NH}_3)_5\}]^{5+}$ in the presence of both DNA polymers, we investigated the effect of a positive charge on the imidazole ring of $[\text{Ru}(\text{phen})(\text{dppz})(\text{bpy}'\text{-his})]^{2+}$. We examined the transient absorption profiles of $[\text{Ru}(\text{phen})(\text{dppz})(\text{bpy}'\text{-his})]^{2+}$ in the presence of positively charged coordinating species such as Zn^{2+} and $[\text{Ru}(\text{NH}_3)_5(\text{H}_2\text{O})]^{2+}$ as well as at a pH lower than the pKa of histidine to determine if we could mimic the environment of the charged imidazole in $[\{\text{Ru}(\text{phen})(\text{dppz})(\text{bpy}'\text{-his})\}\{\text{Ru}(\text{NH}_3)_5\}]^{5+}$. At pH 5, the transient absorption spectrum of $[\text{Ru}(\text{phen})(\text{dppz})(\text{bpy}'\text{-his})]^{2+}$ in the presence of the two DNA polymers shows a positive signal at 440 nm as depicted in Figure 5.10C. This signal is more pronounced in poly d(AT) than in poly d(GC). Note that at pH 7, this positive signal is not apparent. The emission of $[\text{Ru}(\text{phen})(\text{dppz})(\text{bpy}'\text{-his})]^{2+}$ as monitored at 620 nm is not quenched in intensity or lifetime as a result of lowered pH (data not shown). In contrast, when measurements were taken in the presence of 2.5 mM Zn^{2+} , or 0.3 mM $[\text{Ru}(\text{NH}_3)_5(\text{H}_2\text{O})]^{2+}$, no change in the $[\text{Ru}(\text{phen})(\text{dppz})(\text{bpy}'\text{-his})]^{2+}$ transient absorption spectrum is observed. Interestingly, $[\text{Ru}(\text{NH}_3)_5(\text{H}_2\text{O})]^{2+}$ has a small quenching effect on the lifetime of $[\text{Ru}(\text{phen})(\text{dppz})(\text{bpy}'\text{-his})]^{2+}$ in 1 mM poly d(AT). This effect is not seen in the presence of Zn^{2+} (data not shown).

As can be seen in Figure 5.8, $^{\text{CP}}\text{G}$ ring opening is not observed when $[\text{Ru}(\text{phen})(\text{dppz})(\text{bpy}'\text{-his})]^{2+}$ at pH 5 is used as the photooxidant suggesting that the transient formed spectroscopically, is not responsible for the oxidation process. This is

consistent with the time-resolved and steady-state emission data at pH 5, which show no increase in quenching at lower pHs.

5.4 Discussion

5.4.1 $[\{\text{Ru}(\text{phen})(\text{dppz})(\text{bpy}'\text{-his})\}\{\text{Ru}(\text{NH}_3)_5\}]^{5+}$ is quenched relative to $[\text{Ru}(\text{phen})(\text{dppz})(\text{bpy}'\text{-his})]^{2+}$ and $[\text{Ru}(\text{phen})(\text{dppz})(\text{bpy}')]^{2+}$

$[\{\text{Ru}(\text{phen})(\text{dppz})(\text{bpy}'\text{-his})\}\{\text{Ru}(\text{NH}_3)_5\}]^{5+}$, a ruthenium complex with a tethered quencher, is capable of oxidizing guanine bases in DNA without an added quencher. Based on steady-state and time-resolved emission, $[\{\text{Ru}(\text{phen})(\text{dppz})(\text{bpy}'\text{-his})\}\{\text{Ru}(\text{NH}_3)_5\}]^{5+}$ is significantly quenched relative to $[\text{Ru}(\text{phen})(\text{dppz})(\text{bpy}'\text{-his})]^{2+}$ and $[\text{Ru}(\text{phen})(\text{dppz})(\text{bpy}')]^{2+}$ in DNA and organic solvents as would be expected if an external quencher, such as $[\text{Ru}(\text{NH}_3)_6]^{3+}$ is present.

Transient absorption and time-resolved emission measurements indicate that although the excited state lifetime of the $[\{\text{Ru}(\text{phen})(\text{dppz})(\text{bpy}'\text{-his})\}\{\text{Ru}(\text{NH}_3)_5\}]^{5+}$ complex is drastically reduced relative to the parent complexes, formation of Ru(III) is not observable on the time scale of our measurement, suggesting that back electron transfer with the reduced quencher is a dominant pathway for this complex. Charge recombination is not surprising in this system, given that the quencher is in close proximity to the ruthenium center. Indeed, an initial benefit of the original flash-quench technique was spatial separation of charge between the quencher and ruthenium complex, thus reducing the probability of back electron transfer. As there is efficient coupling between the two metal centers in the $[\{\text{Ru}(\text{phen})(\text{dppz})(\text{bpy}'\text{-his})\}\{\text{Ru}(\text{NH}_3)_5\}]^{5+}$ complex, back electron transfer is enhanced.

5.4.2 [$\{Ru(phen)(dppz)(bpy'-his)\}\{Ru(NH_3)_5\}^{5+}$] can oxidize guanine

A long-lived charge separated state is requisite for the formation of permanently damaged DNA oxidation products, as the oxidized ruthenium must persist long enough for charge injection to occur within the duplex. These long-lived charge separated states are most often attained by ensuring that the driving force for charge recombination lies in the Marcus inverted region or by spatially separating the donor and acceptor [50]. Indeed, we cannot measure guanine damage by gel electrophoresis using the [$\{Ru(phen)(dppz)(bpy'-his)\}\{Ru(NH_3)_5\}^{5+}$] complex as the millisecond trapping rate of guanine radical is much slower than the rate of back electron transfer between the oxidized ruthenium and the reduced quencher. Contributions from back electron transfer to guanine oxidation can be eliminated by using a kinetically fast hole trap, which opens irreversibly upon oxidation on a picosecond time scale. By using such a system, we can probe charge transfer events between [$\{Ru(phen)(dppz)(bpy'-his)\}\{Ru(NH_3)_5\}^{5+}$] and DNA which are not apparent on the slow time scale of guanine radical trapping. Indeed, when [$\{Ru(phen)(dppz)(bpy'-his)\}\{Ru(NH_3)_5\}^{5+}$] is irradiated in the presence of duplex DNA containing a ^{CP}G hole trap, ring opening is observed consistent with charge injection into the DNA.

Interestingly, the efficiency of ^{CP}G ring opening is less for [$\{Ru(phen)(dppz)(bpy'-his)\}\{Ru(NH_3)_5\}^{5+}$] than for a complex with added quencher, suggesting that back electron transfer is still competitive with charge injection. Traditional flash-quench methodologies utilize a diffusible quencher, which, despite causing rate-limiting quenching, can freely diffuse from the ruthenium excited state, creating a spatial separation of charge and decreased back electron transfer. In contrast, in

the case of $[\{\text{Ru}(\text{phen})(\text{dppz})(\text{bpy}'\text{-his})\}\{\text{Ru}(\text{NH}_3)_5\}]^{5+}$, the reduced quencher moiety cannot freely diffuse, so back electron transfer remains a competing pathway.

We can spectroscopically detect guanine radical formation generated by excitation of $[\{\text{Ru}(\text{phen})(\text{dppz})(\text{bpy}'\text{-his})\}\{\text{Ru}(\text{NH}_3)_5\}]^{5+}$ using EPR. Consistent with guanine oxidation by $^{\text{CP}}\text{G}$ ring opening, we find that when a sample containing $[\{\text{Ru}(\text{phen})(\text{dppz})(\text{bpy}'\text{-his})\}\{\text{Ru}(\text{NH}_3)_5\}]^{5+}$ in poly d(GC) is irradiated while simultaneously freezing in liquid nitrogen, an organic radical around 2 G is detectable by EPR. This radical closely resembles that of the neutral guanine radical seen in previous experiments [48]. This radical does not form in sequences lacking guanines, or when $[\text{Ru}(\text{phen})(\text{dppz})(\text{bpy}'\text{-his})]^{2+}$ is irradiated in the absence of quencher in guanine containing duplexes consistent with intramolecular flash-quench generated oxidation by $[\{\text{Ru}(\text{phen})(\text{dppz})(\text{bpy}'\text{-his})\}\{\text{Ru}(\text{NH}_3)_5\}]^{5+}$.

5.4.3 Transient species formed in the presence of DNA

Although $[\{\text{Ru}(\text{phen})(\text{dppz})(\text{bpy}'\text{-his})\}\{\text{Ru}(\text{NH}_3)_5\}]^{5+}$ is capable of oxidizing guanine in DNA, it is apparent that competing processes exist which contribute to diminished $^{\text{CP}}\text{G}$ decomposition efficiency and lack of a prominent guanine radical as detected by transient absorption. As can be seen in Figure 5.11A, a new species is formed when $[\{\text{Ru}(\text{phen})(\text{dppz})(\text{bpy}'\text{-his})\}\{\text{Ru}(\text{NH}_3)_5\}]^{5+}$ is irradiated in the presence of both DNA polymers. This long-lived species persists on the millisecond time scale, and requires DNA, as the species is not detectable in acetonitrile. Although this transient is formed immediately following the initial excited state bleach at 440 nm, it is not necessary for the oxidation of DNA. Indeed, $[\text{Ru}(\text{phen})(\text{dppz})(\text{bpy}'\text{-his})]^{2+}$, at pH values

lower than the pK_a of histidine, generates an analogous transient, albeit on a slower time scale, but does not oxidize guanine as measured by ^{CP}G ring opening. Moreover, the excited state lifetime of $[Ru(phen)(dppz)(bpy'-his)]^{2+}$ is unaltered by this pH change, and steady-state emission shows no quenching. Thus, an extremely short-lived Ru(III) species must exist in $[\{Ru(phen)(dppz)(bpy'-his)\} \{Ru(NH_3)_5\}]^{5+}$ which is not detectable on the time scale of the measurement and is not required for the formation of the positive transient.

A positive charge on the histidine imidazole is required for formation of the long-lived transient formed in $[\{Ru(phen)(dppz)(bpy'-his)\} \{Ru(NH_3)_5\}]^{5+}$ and $[Ru(phen)(dppz)(bpy'-his)]^{2+}$ at low pH. Indeed, this species is not present in $[Ru(phen)(dppz)(bpy')]^{2+}$ at low pH, since this complex does not contain a histidine moiety. As a protonated histidine on $[Ru(phen)(dppz)(bpy'-his)]^{2+}$ results in the formation of the long-lived transient, we wondered if a positively charged coordinating metal would exhibit similar behavior. However, neither Zn^{2+} nor $[Ru(NH_3)_5(H_2O)]^{2+}$ facilitates formation of the long-lived transient. As $[Ru(NH_3)_5(H_2O)]^{2+}$ is the species used to synthesize $[\{Ru(phen)(dppz)(bpy'-his)\} \{Ru(NH_3)_5\}]^{5+}$, it is surprising that it does not have a similar effect. However, the experiment in which $[Ru(NH_3)_5(H_2O)]^{2+}$ was added to $[Ru(phen)(dppz)(bpy'-his)]^{2+}$ was done under anaerobic conditions, thus prohibiting the oxidation of $[Ru(NH_3)_5]^{2+}$ to $[Ru(NH_3)_5]^{3+}$ which is apparently requisite for the formation of the transient.

5.4.4 [$\text{Ru}(\text{phen})(\text{dppz})(\text{bpy}'\text{-his})\{\text{Ru}(\text{NH}_3)_5\}^{5+}$] forms a Ru(I)-like species in a DNA environment

The long-lived transient species detected when [$\text{Ru}(\text{phen})(\text{dppz})(\text{bpy}'\text{-his})\{\text{Ru}(\text{NH}_3)_5\}^{5+}$] is irradiated in the presence of DNA bears striking resemblance to that of a reduced ruthenium species [51]. To compare the chemical formation of Ru(I) with the transient observed in our system, we examined the spectrum of [$\text{Ru}(\text{phen})(\text{dppz})(\text{bpy}'\text{-his})\}^{2+}$] in the presence of the reductive quencher, ascorbate. When ruthenium (II) polypyridyl complexes are irradiated in the presence of ascorbate, a long-lived transiently generated Ru(I) species is generated (Figure 5.11B). Interestingly, Ru(I) as monitored by transient absorption has similar features to the transient generated by irradiating [$\text{Ru}(\text{phen})(\text{dppz})(\text{bpy}'\text{-his})\{\text{Ru}(\text{NH}_3)_5\}^{5+}$] or [$\text{Ru}(\text{phen})(\text{dppz})(\text{bpy}'\text{-his})\}^{2+}$] at pH 5 in the presence of DNA. A small negative region spans between ~330-365 nm, and maxima exist around 410-440, 530, and <320 nm. Although it appears that Ru(I) generated by reductive quenching with ascorbate yields a spectrum with a small dip in between the maxima at 410 and 440 nm, if one considers that a small amount of Ru(III) is present (Figure 5.11A inset), this dip can be accounted for, and a spectrum resulting in the transient formed in [$\text{Ru}(\text{phen})(\text{dppz})(\text{bpy}'\text{-his})\{\text{Ru}(\text{NH}_3)_5\}^{5+}$] and [$\text{Ru}(\text{phen})(\text{dppz})(\text{bpy}'\text{-his})\}^{2+}$] at pH 5 is evident.

This spectrum we see for [$\text{Ru}(\text{phen})(\text{dppz})(\text{bpy}'\text{-his})\{\text{Ru}(\text{NH}_3)_5\}^{5+}$] in DNA is completely consistent with that of a reduced [$\text{Ru}(\text{bpy})_2(\text{bpz})\}^{2+}$] complex (bpz=2, 2'-bipyrazine) generated by pulse radiolysis [51]. It should be noted however, that the spectrum of reduced complex generated electrochemically, bears no resemblance to that generated spectroscopically [52, 53]. However, electrochemically reducing the complex

results in subsequent reductions of each ligand, leaving the metal center unaffected. Indeed, spectroelectrochemistry of $[\text{Ru}(\text{phen})(\text{dppz})(\text{bpy}'\text{-his})]^{2+}$ reduction generates an absorption profile consistent with the reduced dppz ligand (data not shown).

5.4.5 Mechanistic considerations

As shown in Figure 5.12, we propose a model in which upon excitation into its MLCT band in the presence of DNA, $[\{\text{Ru}(\text{phen})(\text{dppz})(\text{bpy}'\text{-his})\}\{\text{Ru}(\text{NH}_3)_5\}]^{5+}$ can undergo two different reaction pathways. The first pathway is the standard flash-quench route, in which the excited state is quenched by neighboring $[\text{Ru}(\text{NH}_3)_5(\text{His})]^{3+}$ to generate the powerful ground state oxidant, Ru(III). With a potential of 1.5 V, Ru(III) can oxidize guanine. As the reduced quencher is not spatially separated from the newly generated Ru(III) oxidant, back electron transfer is a dominant pathway in which Ru(III) returns to the ground state.

The second pathway occurs when the $[\{\text{Ru}(\text{phen})(\text{dppz})(\text{bpy}'\text{-his})\}\{\text{Ru}(\text{NH}_3)_5\}]^{5+}$ excited state accepts an electron from the nearby histidine thus resulting in a polarized complex in which the hole on histidine is stabilized by a nearby positive charge, forming a ligand radical coordinated to the Ru(II) center. Although $\text{RuL}^{\bullet+}$ species are good reducing agents, they are not capable of reducing the bases of DNA [51]. It is interesting to note that this phenomenon only occurs when the complex is intercalated into the DNA base pair stack; this species does not form in acetonitrile. The DNA is thus able to orient the complex in a stable polarized form, such that the ruthenium center is reduced, while the histidine moiety is oxidized.

The characterization of $[\{\text{Ru}(\text{phen})(\text{dppz})(\text{bpy}'\text{-his})\}\{\text{Ru}(\text{NH}_3)_5\}]^{5+}$ with DNA allows us to observe a variety of electron transfer pathways which can occur in the presence of DNA. Not only can this complex undergo intramolecular charge transfer between the quencher and the ruthenium (II) excited state on picosecond time scales, but a competing charge transfer event can occur between the ruthenium (II) excited state and the histidine bridge which persists on a millisecond time scale. It should be noted that it is the presence of a positive charge on, rather than the redox state of the quencher, that allows these additional pathways to occur. While systematic studies of distance dependences through DNA using this complex as a photooxidant are not feasible due to the inability to tether the complex to DNA, this system underscores the rich electron transfer chemistry of ruthenium and allows us to observe novel pathways in which electrons and holes can migrate between two metal centers.

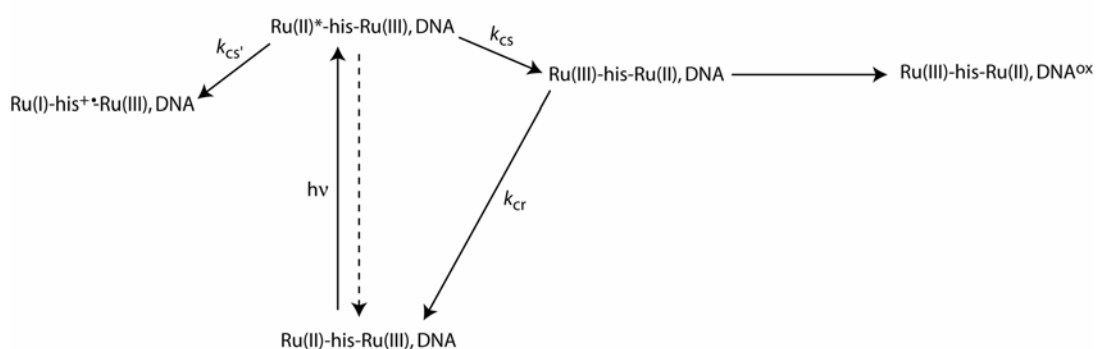


Figure 5.12. Scheme illustrating the various photophysical pathways for $[\{\text{Ru}(\text{phen})(\text{dppz})(\text{bpy}'\text{-his})\}\{\text{Ru}(\text{NH}_3)_5\}]^{5+}$ in the presence of DNA. Excitation into its MLCT results in the excited state ruthenium (II) species which can either undergo the standard flash-quench pathway resulting in the ground state oxidant Ru(III), or it can accept an electron from the nearby histidine resulting in a reduced ruthenium center and an oxidized histidine stabilized by the positive ruthenium pentaammine quencher.

5.5 References

- [1] Delaney, S.; Barton, J.K. Long-range DNA charge transport. *J. Org. Chem.* **68**, 6475-6483 (2003).
- [2] Schuster, G.B. Long-range charge transfer in DNA: transient structural distortions control the distance dependence. *Acc. Chem. Res.* **33**, 253-260 (2000).
- [3] Giese, B. Long-distance electron transfer through DNA. *Ann. Rev. Biochem.* **71**, 51-70 (2002).
- [4] Lewis, F.D.; Letsinger, R.L.; Wasielewski, M.R. Dynamics of photoinduced charge transfer and hole transport in synthetic DNA hairpins. *Acc. Chem. Res.* **34**, 159-170 (2001).
- [5] Kawai, K.; Takada, T.; Tojo, S.; Ichinose, N. ; Majima, T. Observation of hole transfer through DNA by monitoring the transient absorption of pyrene radical cation. *J. Am. Chem. Soc.* **123**, 12688-12689 (2001).
- [6] Nuñez, M.E.; Hall, D.B.; Barton, J.K. Long-range oxidative damage to DNA: effects of distance and sequence. *Chem. Biol.* **6**, 85-97 (1999).
- [7] Ly, D.; Sani, L.; Schuster, G.B. Mechanism of charge transport in DNA: internally-linked anthraquinone conjugates support phonon-assisted polaron hopping. *J. Am. Chem. Soc.* **121**, 9400-9410 (1999).
- [8] Kelly, S.O.; Barton, J.K. Radical migration through the DNA helix: chemistry at a distance. *Metal Ions Biol.* **35**, 211-249 (1999).
- [9] Wiseman, H.; Halliwell, B. Damage to DNA by reactive oxygen and nitrogen species: role in inflammatory disease and progression to cancer. *Biochem. J.* **313**, 17-29 (1996).

- [10] Ames, B.N.; Shigenaga, M.K.; Hagen, T.M. Oxidants, antioxidants, and the degenerative diseases of aging. *Proc. Natl. Acad. Sci. USA.* **90**, 7915-7922 (1993).
- [11] Steenken, S.; Jovanovic, S.V. How easily oxidizable is DNA? One-electron reduction potentials of adenosine and guanosine radicals in aqueous solution. *J. Am. Chem. Soc.* **119**, 617-618 (1997).
- [12] Burrows, C.J.; Muller, J.G. Oxidative nucleobase modifications leading to strand scission. *Chem. Rev.* **98**, 1109-1151 (1998).
- [13] Augustyn, K.E.; Shao, F.; Genereux, J.C.; Barton, J.K. Periodicities in DNA charge transport probed with N₂-cyclopropylguanine, a kinetically fast hole trap. Submitted.
- [14] Kawai, K.; Kimura, T.; Kawabata, K.; Tojo, S.; Majima, T. Excess electron transfer in DNA studied by pulse radiolysis and γ -radiolysis of naphthalimide and iodouridine modified ODN. *J. Phys. Chem. B.* **107**, 12838-12841 (2003).
- [15] Takada, T.; Kawai, K.; Tojo, S.; Majima, T. Kinetics of multistep hole transfer in DNA by monitoring the transient absorption of the pyrene radical cation. *J. Phys. Chem. B.* **107**, 4052-12057 (2003).
- [16] Lewis, F.D.; Liu, X.; Liu, J.; Miller, S.E.; Hayes, R.T.; Wasielewski, M.R. Direct measurement of hole transport dynamics in DNA. *Nature* **406**, 51-53 (2000).
- [17] Augustyn, K.E.; Pierre, V.C.; Barton, J.K. Metallointercalators as probes of DNA recognition and reaction. *Wiley Encyclopedia of Chemistry and Biology* (2007).
- [18] O'Neill, M.A.; Dohno, C.; Barton, J.K. Direct chemical evidence for charge transfer between photoexcited 2-aminopurine and guanine in duplex DNA. *J. Am. Chem. Soc.* **126**, 1316-1317 (2004).

- [19] Shao, F.; O'Neill, M.A.; Barton, J.K. Long-range oxidative damage to cytosines in duplex DNA. *Proc. Natl. Acad. Sci. USA*. **101**, 17914-17919 (2004).
- [20] Augustyn, K.E.; Genereux, J.C.; Barton, J.K. Distance-independent DNA charge transport across an adenine tract. *Angew. Chem. Int. Ed.* In press (2007).
- [21] Musa, O.M.; Horner, J.H.; Shahin, H.; Newcomb, M. A kinetic scale for dialkylaminy radical reactions. *J. Am. Chem. Soc.* **118**, 3862-3868 (1996).
- [22] Stemp, E.D.A.; Arkin, M.R.; Barton, J.K. Oxidation of guanine in DNA by $\text{Rh}(\text{phen})_2(\text{dppz})^{3+}$ using the flash-quench technique. *J. Am. Chem. Soc.* **119**, 2921-2925 (1997).
- [23] Chang, I.J.; Gray, H.B.; Winkler, J.R. High-driving force electron transfer in metalloproteins: intramolecular oxidation of ferrocyanochrome c by $\text{Ru}(2,2'\text{-bpy})_2(\text{im})(\text{His-33})^{3+}$. *J. Am. Chem. Soc.* **113**, 7056-7057 (1991).
- [24] Murphy, C.J.; Arkin, M.R.; Jenkins, Y.; Ghatlia, N.D.; Bossmann, S.H.; Turro, N.J.; Barton, J.K. Long-range photoinduced electron transfer through a DNA helix. *Science* **262**, 1025-1029 (1993).
- [25] Dunn, D.A.; Lin, V.H.; Kochevar, I.E. Base-selective oxidation and cleavage of DNA by photochemical cosensitized electron transfer. *Biochemistry* **31**, 11620-11625 (1992).
- [26] Pascaly, M.; Yoo, J.; Barton, J.K. DNA-mediated charge transport: characterization of a DNA radical localized at an artificial nucleic acid base. *J. Am. Chem. Soc.* **124**, 9083-9092 (2002).

- [27] Yoo, J.; Delaney, S.; Stemp, E.D.A.; Barton, J.K. Rapid radical formation by DNA charge transport through sequences lacking intervening guanines. *J. Am. Chem. Soc.* **125**, 6640-6641 (2003).
- [28] Fu, P.K.L.; Bradley, P.M.; van Loyen, D.; Heinz, D.; Bossmann, S.H.; Turro, C. DNA photocleavage by a supramolecular Ru(II)-viologen complex. *Inorg. Chem.* **41**, 3808-3810 (2002).
- [29] Duan, C-Y.; Lu, Z.L.; You, X-Z.; Zhou, Z-Y.; Mak, T.C.W.; Luo, Q.; Zhou, J-Y. Photoinduced intramolecular electron transfer in Schiff-base bridged ruthenium(II)-quencher molecules. *Polyhedron* **17**, 4131-4138 (1998).
- [30] Opperman, K.A.; Mecklenburg, S.L.; Meyer, T.J. Intramolecular, photoinduced electron-transfer in ruthenium(II) bipyridine-quinone complexes. *Inorg. Chem.* **33**, 5295-5301 (1994).
- [31] Strouse, G.F.; Anderson, P.A., Schoonover, J.R.; Meyer, T. J.; Keene, F.R. Synthesis of polypyridyl complexes of ruthenium(II) containing 3 different bidentate ligands. *Inorg. Chem.* **31**, 2618-2619 (1992).
- [32] Anderson, P.A.; Deacon, G.B.; Haarman, K.H.; Keene, F.R.; Meyer, T.J.; Reitsma, D.A.; Skelton, B.W.; Strouse, G.F.; Thomas, N.C.; Treadway, J.A.; White, A.H. Designed synthesis of mononuclear tris(heteroleptic) ruthenium complexes containing bidentate polypyridyl ligands. *Inorg. Chem.* **34**, 6145-6157 (1995).
- [33] Sundberg, R.J.; Gupta, G. Nitrogen-carbon linkage isomerism of histidine in ruthenium ammine complexes. *Bioinorg. Chem.* **3**, 39-48 (1973).
- [34] Yocom, K. PhD thesis, California Institute of Technology (1982).

- [35] Sambrook, J; Fritsch, E.D; Maniatis, T. *Molecular Cloning: A Laboratory Manual*. 2nd ed; Cold Spring Harbor Laboratory: New York, 1989.
- [36] Shao, F.; Augustyn, K.E.; Barton, J.K. Sequence dependence of charge transport through DNA domains. *J. Am. Chem. Soc.* **127**, 17445-17452 (2005).
- [37] Copeland, K.D.; Lueras, A.M.; Stemp, E.D.A.; Barton, J.K. DNA cross-linking with metallointercalator-peptide conjugates. *Biochemistry* **41**, 12785-12797 (2002).
- [38] Olson, E.J.C.; Hu, D.; Hormann A.; Jonkman, A.M.; Arkin, M.R.; Stemp, E.D.A.; Barton, J.K.; Barbara, P.F. First observation of the key intermediate in the “light-switch” mechanism of $[\text{Ru}(\text{phen})_2(\text{dppz})]^{2+}$. *J. Am. Chem. Soc.* **119**, 11458-11467 (1997).
- [39] Jenkins, Y.; Friedman, A.E.; Turro, N.J.; Barton, J.K. Characterization of dipyrrophenazine complexes of ruthenium (II): the light switch effect as a function of nucleic acid sequence and conformation. *Biochemistry* **31**, 10809-10816 (1992).
- [40] Hartshorn, R.M.; Barton, J.K. Novel dipyrrophenazine complexes of ruthenium(II): exploring luminescent reporters of DNA. *J. Am. Chem. Soc.* **114**, 5919-5925 (1992).
- [41] Chung, M.-H.; Kiyosawa, H.; Nishimura, S.; Kasai, H. DNA strand cleavage at 8-hydroxyguanine residues by hot piperidine treatment. *Biochem. Biophys. Res. Comm.* **188**, 1-7 (1992).
- [42] Arkin, M.R.; Stemp, E.D.A.; Pulver, S.C.; Barton, J.K. Long-range oxidation of guanine by Ru(III) in duplex DNA. *Chem. Biol.* **4**, 389-400 (1997).

- [43] Nakatani, K.; Dohno, C.; Saito, I. Design of a hole-trapping nucleobase: termination of DNA-mediated hole transport at N₂-cyclopropyldeoxyguanosine. *J. Am. Chem. Soc.* **123**, 9861-9862 (2001).
- [44] Mei, H.-Y.; Barton, J.K. A chiral probe for A-form helices of DNA and RNA: tris(tetramethylphenanthroline)ruthenium(II). *J. Am. Chem. Soc.* **108**, 7414-7416 (1986).
- [45] Mei, H.-Y.; Barton, J.K. Tris(tetramethylphenanthroline)ruthenium(II): a chiral probe that cleaves A-DNA conformations. *Proc. Natl. Acad. Sci. USA.* **85**, 1339-1343 (1988).
- [46] Lu, W.; Vicic, D.A.; Barton, J.K. Reductive and oxidative DNA damage by photoactive platinum(II) intercalators. *Inorg. Chem.* **22**, 7970-7980 (2005).
- [47] Schiemann, O.; Turro, N.J.; Barton, J.K. EPR detection of guanine radicals in a DNA duplex under biological conditions: selective base oxidation by [Ru(phen)₂(dppz)]³⁺ using the flash-quench technique. *J. Phys. Chem. B.* **104**, 7124-7220 (2000).
- [48] Yavin, E.; Boal, A.K.; Stemp, E.D.A.; Boon, E.M.; Livingston, A.L.; O'Shea, V.L.; David, S.S.; Barton, J.K. Protein-DNA charge transport: redox activation of a DNA repair protein by guanine radical. *Proc. Natl. Acad. Sci. USA.* **102**, 3546-3551 (2005).
- [49] Cullis, P.M.; Malone, M.E.; Merson-Davies, L.A. Guanine radical cations are precursors of 7,8-dihydro-8-oxo-2'-deoxyguanosine but are not precursors of immediate strand breaks in DNA. *J. Am. Chem. Soc.* **118**, 2775-2781 (1996).

- [50] Gould, I.R.; Moser, J.E.; Armitage, B.; Farid, S. Electron transfer reaction in the Marcus inverted region. Charge recombination versus charge shift reactions. *J. Am. Chem. Soc.* **111**, 1917-1919 (1989).
- [51] D'angelantonio, M.; Mulazzani, Q.G.; Venturi, M.; Ciano, M.; Hoffman, M.Z. One-electron reduction of ruthenium(II)-diimine complexes. Characterization of reduced species containing 2,2'-bipyridine, 2,2'-bipyrimidine, and 2,2'-bipyrazine in aqueous solution. *J. Phys. Chem.* **95**, 5121-5129 (1991).
- [52] Fees, J.; Ketterle, M.; Klein, A.; Fiedler, J.; Kaim, W. Electrochemical, spectroscopic and EPR study of transition metal complexes of dipyrido[3,2-a:2',3'-c]phenazine. *J. Chem. Soc. Dalton Trans.* 2595-2599 (1999).
- [53] Fees, J.; Kaim, W.; Moscherosch, M.; Matheis, W.; Klima, J.; Krejcik, M.; Zalis, S. Electronic structure of the "molecular light switch" $[\text{Ru}(\text{bpy})_2(\text{dppz})]^{2+}$ (dppz= dipyrido[3,2-a:2',3'-c]phenazine). Cyclic voltammetric, UV/Vis, and EPR/ENDOR study of multiply reduced complexes and ligands. *Inorg. Chem.* **32**, 166-174 (1993).
- [54] Arkin, M.R.; Stemp, E.D.A.; Turro, C.; Turro, N.J.; Barton, J.K. Luminescence quenching in supramolecular systems: a comparison of DNA and SDS micelle-mediated photoinduced electron transfer between metal complexes. *J. Am. Chem. Soc.* **118**, 2267-2274 (1996).